2022

Arkansas Bulletin of Water Research - Issue 2021-2022

Erin Grantz

Lillie Haddock

Brian E. Haggard

Arkansas Bulletin of Water Research

A publication of the Arkansas Water Resources Center

Issue 2021-2022

Arkansas Bulletin of Water Research

A publication of the Arkansas Water Resources Center

University of Arkansas
Don Tyson Center for Agricultural Sciences
1371 W. Altheimer Drive
Room 133
Fayetteville, AR 72704

website: awrc.uada.edu

EDITORS

Erin Grantz*
Arkansas Water Resources Center
Program Manager
egrantz@uark.edu
479-575-7192

Lillie Haddock
Arkansas Water Resources Center
Program Specialist
lmhaddoc@uada.edu

Brian E. Haggard
Arkansas Water Resources Center
Director
haggard@uark.edu
479-575-2879

**Corresponding author*

The Arkansas Bulletin of Water Research (Bulletin) is a publication of the Arkansas Water Resources Center (AWRC). We publish the Bulletin to communicate the major findings of research funded by the Water Resources Research Act Section 104(b) in Arkansas. This research is relevant to Arkansas water stakeholders, and the Bulletin provides an easily searchable and aesthetically engaging access option.

This is the fourth publication of the Bulletin. This issue contains final reports from research projects that were funded by the 104(b) program in fiscal years 2019 and 2020. The articles in this issue can be cited as an AWRC publication. Many of these projects have also appeared in peer-reviewed journal articles, which we recommend reviewing for greater detail or for updates on the findings presented here.

Please cite articles in the 2021/2022 issue of the Bulletin, as in the following example:

Dodd, A., M. Bossus, A. Mundy, L. Fowler, J. Webb, O. Echols, and E. Pollock. 2022. Assessing water quality and biological impacts of nonpoint source pollution in the Eleven Point and Lower Black River watersheds. Arkansas Water Resources Center, Fayetteville, AR, Arkansas Bulletin of Water Research, 2021/2022: 1-8.

The Bulletin is also available for outside submissions of research and investigations related to any water resources topic that is relevant for the State of Arkansas. This includes, but is not limited to, university researchers, consulting firms, watershed groups, and other agencies. Prospective authors should review the introductory material printed in earlier Bulletin issues and available at our website: **awrc.uada.edu**

The included material is based upon work supported by the U.S. Geological Survey 104(b) program under grant agreement No. G16AP00040 administered by the AWRC. The views and conclusions contained in this document are those of the authors and should not be interpreted as representing the opinions or policies of the U.S. Geological Survey.

Cover Photo: "West Fork of the White River" by Lillie Haddock

Arkansas Bulletin of Water Research

A publication of the Arkansas Water Resources Center

Issue 2021-2022

Table of Contents

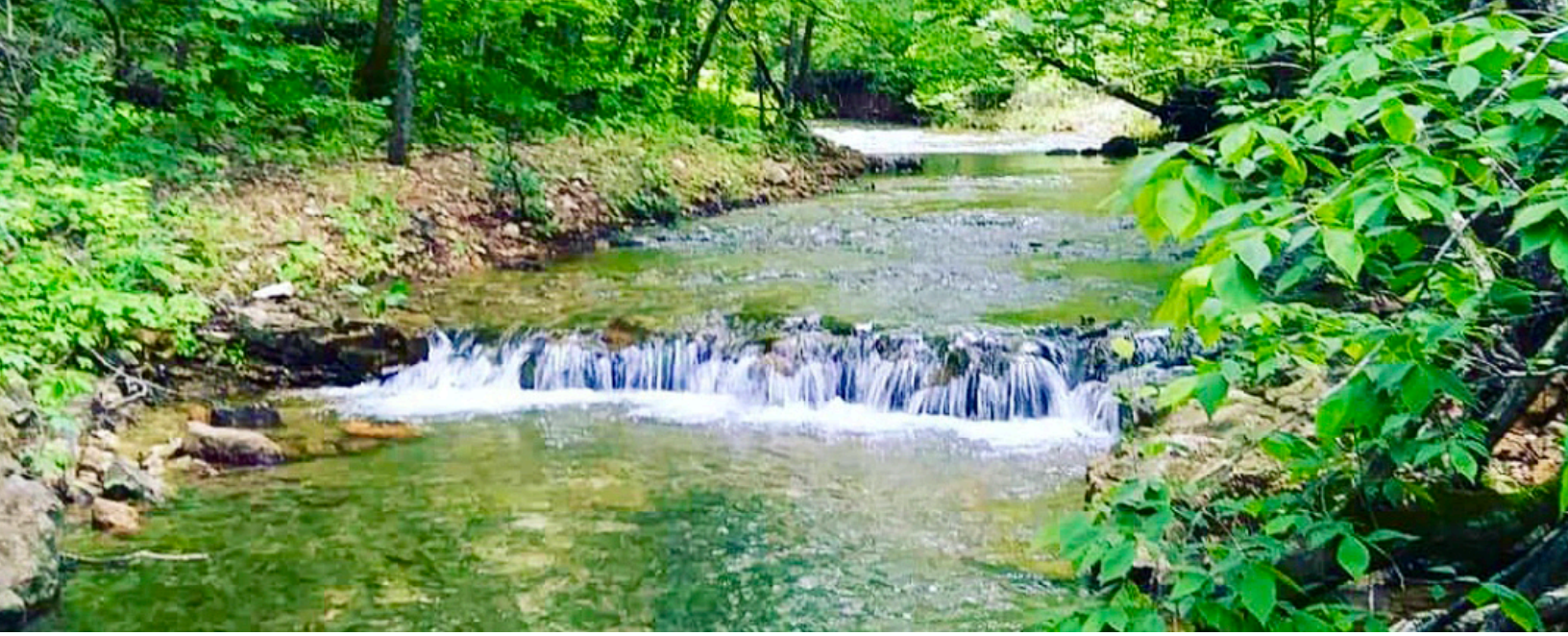

Image caption: Diles Creek. Photo courtesy of Allyn Dodd.

Assessing Water Quality and Biological Impacts of Nonpoint Source Pollution in the Eleven Point and Lower Black River Watersheds

Allyn Dodd[1]*, Maryline Bossus[1], Allison Mundy[2], Linda Fowler[2], Jordan Webb[2], Olivia Echols[2], and Erik Pollock[3]

[1]Assistant Professor, Natural Sciences Division, Lyon College, Batesville, Arkansas 72501; [2]Student, Natural Sciences Division, Lyon College, Batesville, Arkansas 72501; [3]Laboratory Manager, Stable Isotope Laboratory, University of Arkansas, Fayetteville, Arkansas, 72701
*Corresponding author, dodda@asmsa.org

Abstract: Poultry and livestock agriculture continue to expand in Northeast Arkansas, increasing the potential for nutrient enrichment and ecological degradation in critical waterways in the Mississippi Alluvial Plain. We sampled twelve tributaries of the Eleven Point and Black rivers from June 2019 to February 2020 to determine if relationships existed between poultry and livestock agriculture and water quality, periphyton abundance, presence of algal toxins, dominant water sources, and invertebrate community structure and physiology. We found no significant relationships between animal agriculture and stream nutrient levels, though preliminary results from summer 2019 suggested a positive relationship between poultry house density and phosphorus concentrations. Fewer pollution-intolerant macroinvertebrate taxa were found in tributaries closer to poultry farm operations. Our findings suggest that streams near poultry farming operations are in need of targeted mitigation to prevent further declines in sensitive invertebrate taxa. While the mechanism inducing these declines is unclear, our continued work in these watersheds may shed light on the specific habitat metrics or pollutants responsible. Additionally, the positive relationship between poultry house density and phosphorus concentrations during summer 2019 suggests a seasonal component to the impact of poultry farming on instream nutrients. These efforts to determine the impact of animal agriculture are critical as poultry agriculture continues to expand in Arkansas, potentially impacting water quality and biological condition throughout the Mississippi Alluvial Plain.

Key Points:

- We found no relationship between nutrients and animal agriculture over nine months of data collection.
- Preliminary analysis in summer 2019 revealed a positive relationship between subwatershed poultry house density and instream phosphorus concentrations, suggesting temporal variation in poultry impacts.
- Relative abundance of sensitive EPT taxa declined with increasing proximity to poultry houses.
- High nitrogen and phosphorus do not appear to impact Na^+/K^+-ATPase function in osmoregulation in a keystone crayfish species.

Introduction

Arkansas is currently the nation's second greatest producer of poultry (USDA, 2018), with poultry farming for food production expanding eastward in the state and throughout the Mississippi Alluvial Plain. The encroachment of new poultry agriculture has been especially noticeable in the Eleven Point River (EPR) and Lower Black River (LBR) watersheds; approximately 400 acres of land in these watersheds have been permitted for the construction of new poultry operations since 2016. Additionally, poultry processing facilities have been constructed or upgraded in nearby municipalities to keep pace with growing production. Currently, over half of land in the LBR and one-third of land in the EPR drainages in northeastern Arkansas is utilized for poultry or livestock production (ADEQ, 2020).

The Arkansas Natural Resource Council (ANRC) has identified two nonpoint source pollution concerns in northeastern Arkansas: nutrient loading and sedimentation from animal agriculture (ANRC, 2014). Increases in animal agriculture can affect nearby surface waters by introducing runoff high in phosphorus and nitrogen, increasing the potential for harmful algal blooms and leading to declines in invertebrate communities (Lombardo, 2000; ANRC, 2014). While the 2014 Arkansas Water Plan lists "improving water quality through nonpoint source management" as a priority issue, and poultry production continues to grow in the region (ANRC, 2014), there is currently no detailed monitoring of water quality and biological condition in the EPR and LBR drainages.

Our objective was to determine whether relationships exist between nearby animal agriculture and water quality, algal abundance, invertebrate community structure and crayfish physiology in both the EPR and LBR watersheds in Randolph, Sharp, Lawrence, and Independence counties. We also sought to determine dominant water sources, which can affect the magnitude of nonpoint source impacts. We predicted that nutrient and total suspended solid concentrations would exhibit positive relationships with subwatershed poultry house density, subwatershed pastoral land use, and flow path distance to poultry farms. Algal biomass was also expected to increase with agricultural land use metrics. Sources of channel discharge throughout both drainages were expected to be dominated by groundwater. We hypothesized that macroinvertebrate communities in the upstream portions of the EPR drainage, which had fewer surrounding poultry farms, would contain greater amounts of intolerant taxa than habitats near the EPR outlet or throughout the LBR drainage. Additionally, physiological mechanisms such as osmoregulation and respiration of invertebrate bioindicators were predicted to be negatively impacted by pollution from nearby agricultural land. Indeed, elevated nitrogen in the environment is dangerous for aquatic organisms, as it stimulates growth of nitrifying bacteria which convert it to highly toxic ammonia. Ammonia is known to disrupt ionoregulatory function in crustaceans by increasing ion permeability (Spaargaren, 1990), and exposure to ammonia is lethal at relatively low doses (Weihrauch et al., 2004). Crustaceans excrete excess ammonia mainly using their gills and antennal glands. The ammonia excretion rates are correlated with sodium absorption which is regulated by the activity of the pump Na^+/K^+-ATPase (NKA; Weihrauch et al., 2004). Increase in osmoregulation mechanisms in gills is also known to affect respiration ability in aquatic organisms (Ouattara et al., 2009). Therefore, we also assessed the impact of high nutrient concentrations in the environment on the expression and localization of NKA in a crustacean.

Methods

This study took place in 12 sites within the Eleven Point River and Lower Black River drainages (Figure 1). Sites were selected along a land use gradient of animal agriculture (e.g., pastoral livestock, poultry houses within a subwatershed, and flow path distance to poultry operations). Water quality grab sampling, in situ measurements, and periphyton sampling took place during base flow conditions monthly from June 2019 through February 2020. One storm sampling event was completed in June 2019. Total organic carbon (TOC) was determined using a Shimadzu TOC-L analyzer (Shimadzu Corporation, Kyoto, Japan). Nitrate (NO_3^-) concentrations were determined using cadmium reduction. Filtered samples were subjected to the ascorbic acid method to determine soluble reactive phosphorus (SRP) concentrations. Total suspended solids were determined by vacuum filtration of samples and determining weight of previously suspended particles on pre-weighed filters (APHA, 2005). Trace elements (Al, As, Ba, Be, B, Cd, Cs, Co, Cr, Cu, Fe, K, Li, Lu, Mn, Hg, Mo, P, Ni, Pb, Sm, Se, Ti, U, V and Zn) of source (groundwater and precipitation) and stream water samples were measured with an inductively-coupled plasma mass spectrometer (Thermo Fisher Scientific, Waltham, MA), then end-member mixing analysis was used to calculate water source mixing ratios (Rueedi et al., 2005). We collected samples for microcystin analysis on two sampling dates with highest stream temperatures that were predicted to facilitate algal toxin presence (i.e., July and August).

Water temperature, dissolved oxygen, pH, and specific conductance were measured in the field using a handheld multiparameter probe. Periphyton from benthic rocks was collected throughout each reach to determine algal biomass by ethanol extraction of chlorophyll a. Invertebrates were collected at three riffles within each stream reach in June of 2019 and identified to genus or subfamily (for Chironomidae) to determine invertebrate community structure and diversity.

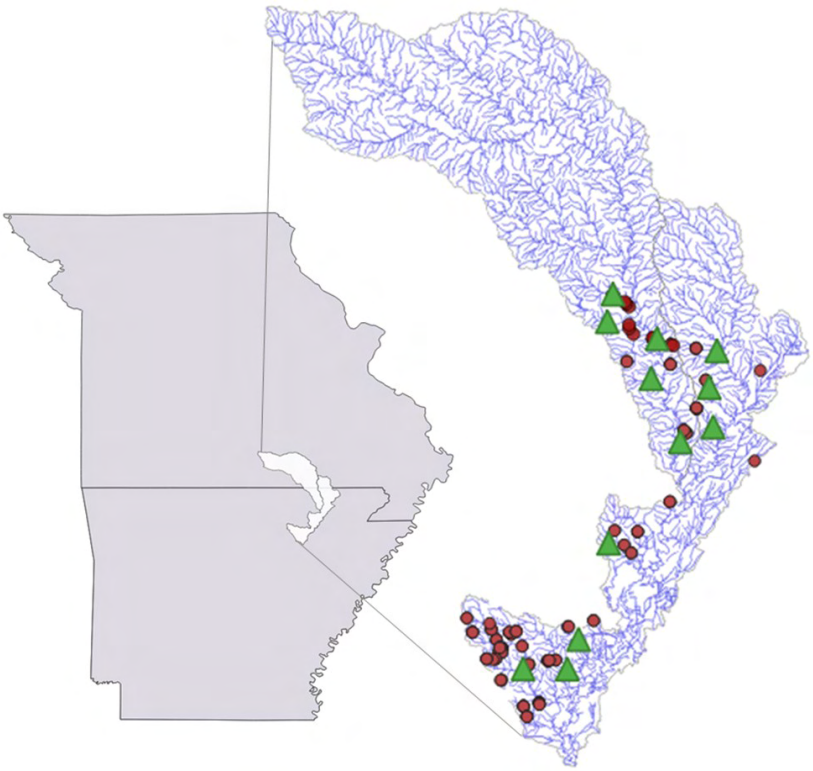

Figure 1: Map of study sites showing target watersheds. Poultry farm operations are shown as red circles while study sites are marked by green triangles.

Faxonius ozarkae specimens were sampled at each site when available in June 2019 and labeled as from polluted or non-polluted sites depending on the results from our nutrient analyses. Prior to sampling, organisms were ice-anesthetized and quickly decapitated. The three main osmoregulatory organs (gills, antennal gland, and intestine) were sampled for histology and molecular analysis. Organs from three individuals per creek were fixed using Bouin liquid (24hrs), washed with 70% alcohol and processed following the protocol from Bossus et al. (2013). Primary monoclonal mouse NKA antibody (8 µg/mL) raised against the α-5 subunit of the chicken NKA (IgG α5,Developmental Studies Hybridoma Bank; University of Iowa, USA) was used to detect NKA. The secondary antibody used at 10 µg/mL was AlexaFluor® 594 (shown in red or green) donkey anti-mouse (InvitrogenTM, Carlsbad, CA). Negative control slides were made without primary antibody and showed no staining (not shown). Slides were mounted in anti-bleaching mounting medium with dapi and visualized using a fluorescent Leica microscope and its LAS software. Organs from 10 individuals per creek were collected for molecular analysis. RNA extraction and purity check were performed following Bossus et al. (2015). The cDNA of NKA and elongation factor 1 alpha (EF1a, used as reference gene) were first amplified by PCR using Taq 2x Master mix (NEB, Ipswich, MA) and degenerate primers (Table 1) designed based on the nBLAST alignments of the gene of interest on NCBI website from several species (Table 2). PCR products were purified using Wizard® Plus SV Minipreps DNA Purification System (Promega, Madison, WI), ligated to a pXT vector (kindly provided by Dr. A. Beeser, Lyon College) using the Blunt/TA ligase master mix (NEB), and cloned into E. coli. Vectors with inserted fragments of interest were purified using PureYieldTM Plasmid Miniprep System (Promega) and sequenced by Genewiz (South Plainfild, NJ). Partial sequences for both NKA and EF1a were submitted to GenBank. Specific primers were designed using Primer3 (Table 1). cDNA synthesis and qRT-PCR followed protocol by Bossus et al. (2015) and a BioRad MiniOpticon Real-Time PCR System (Hercules, CA).

Water quality and biological data were analyzed utilizing linear regression to identify relationships between instream variables and agricultural metrics (i.e. density of subwatershed poultry houses, pastoral land use, and flow path distance from poultry operations to study streams). We employed an information theoretic approach (Burnham and Anderson, 1998) and multiple linear regression to determine what instream variables explained the greatest amount of variation in periphyton abundance and macroinvertebrate diversity across study sites. qRT-PCR data were analyzed using one-way ANOVA to compare variance of expression in transcripts between areas with low versus high nitrogen and phosphorus concentrations. Data are reported as mean + standard error.

Table 1: List of degenerated (d) primers used for cloning and sequencing (CS) and primers used for qPCR

Primer name	Nucleotide sequences (from 5' to 3')	Use
EF1a-dF1	TCGACGYDGGCCTGTTGC	CS
EF1a-dF2	AGATYGAGCGCAAGARTGG	CS
EF1a-dR1	AYTTKGGCTCDGTGCTGTCC	CS
EF1a-dR2	TCCYTGGCDGGRTCRTTCTT	CS
EF1a-F	CCCATCTCTGGCTTTAATGG	qPCR
EF1a-R	CGAAGGGGCTTGTCTGTAGG	qPCR
NKA-F6	ATGGCCTATGGTCAGATTGG	CS
NKA-dR6	GGAAGGCAGCCAGTGTRG	CS
NKA-dR7	CGRCGACACTCRTCRTAMAC	CS
NKA-F	CGTGAACAGTGGGACTCAAA	qPCR
NKA-R	AATGGAGTTACGTCGGGTCTTGC	qPCR

Table 2: List of species and GenBank Accession number of sequences used to generate degenerated primers in order to sequence NKA and EF1a

Species name	GenBank Accession number	Gene
H. sapiens	NM_000701.8	
Xenopus laevis	BC125976.1	
Anguilla marmorata	KP161606.1	NKA
Macrobrachium nipponense	MH378774.1	
Eriocheir sinensis	KC691291.1	
Portunus trituberculatus	KU361820.1	
Procambarus fallax	LC035460.1	
Drosophila melanogaster	NM_001299393.1	EF1a
Eriocheir sinensis	KY356884.1	
Penaeus monodon	MG775229.1	

Results and Discussion

We found no significant relationships between average measures of physicochemical variables at base or storm flow and subwatershed poultry house density, pastoral land use, or flow path distance (Table 3). However, we did find that the percentage of streamflow coming from groundwater was negatively related to surrounding poultry and pastoral agriculture ($R^2 = 0.70$, $p = 0.02$). This reveals that among the twelve streams in this study, those with more animal agriculture in the surrounding watershed receive greater inputs from interflow than groundwater intrusion. Streams dominated by interflow would be expected to have elevated nutrient concentrations from greater animal agriculture in the surrounding watershed, but we did not find evidence of enrichment over the year.

However, preliminary data analysis in summer 2019 showed that, after removing an outlier (Hubble Creek) with low poultry house density but high P levels, there was a positive relationship between subwatershed poultry house density and stream phosphorus concentrations ($R^2 = 0.84$, $p = 0.001$) (Figure 2). Storm samples taken in summer did not reveal relationships between instream nutrients (nitrogen and phosphorus) and surrounding poultry house density or flow path distance. Additionally, removing Hubble Creek from the regression with nine months of data did not yield a relationship. It may be that enrichment in these systems is a seasonal phenomenon, and future work in the study area will provide insight into whether phosphorus enrichment is a consistent concern during the summer months.

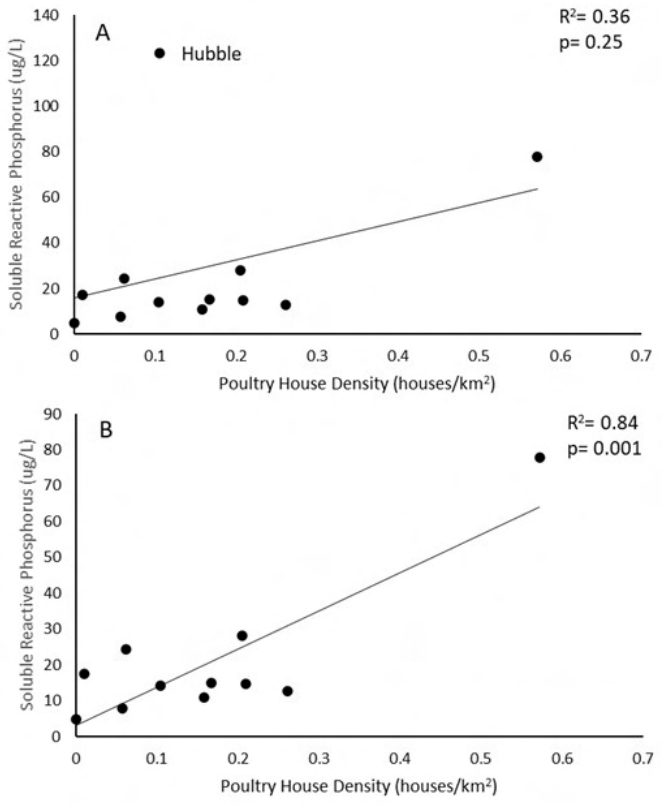

Figure 2: Relationship between summer SRP concentrations and subwatershed poultry house density with outlier due to poultry waste being stored close to the stream (Hubble) (A). Panel (B) shows relationship with outlier removed.

Soluble reactive phosphorus varied from 5 to 52 µg/L at base flow, with maximum P concentrations found in Hubble Creek, a stream with moderate surrounding poultry density but storage of poultry wastes near the stream (Dodd, personal observation). Hubble Creek had markedly greater P levels than other streams; 35 µg/L was the second-highest concentration found in the study. Phosphorus concentrations were fairly low at storm flow; however, Hubble Creek P levels were exceedingly high during storm sampling, at 186 µg/L SRP. This nutrient spike was likely caused by runoff from a nearby pile of poultry waste (within two hundred meters of the stream) washing into the channel. Measures of physicochemical variables from each stream at base flow can be found in Table 4. Table 5 shows nutrient and sediment concentrations from storm samples collected in June of 2019.

Algal biomass was not related to poultry house density, pastoral land use, and flow path distance to poultry opera-

Table 3: Results of multiple linear regression analyses between stream physicochemical variables and agricultural metrics (subwatershed poultry farm density, flow path distance from poultry operations to stream, and percent pastoral land use). Asterisks denote significant relationships.

Dependent Variable	Independent Variables	R^2	p
Total Phosphorus	Poultry Density + Percent Pasture + Flow Path Distance (for all dependent variables)	0.16	0.70
Soluble Reactive Phosphorus		0.11	0.81
Total Nitrogen		0.30	0.40
Nitrate		0.39	0.24
Total Organic Carbon		0.24	0.50
TSS		0.38	0.25

Table 4: Mean values of instream physicochemical variables and agricultural metrics at base flow. Mill-11 Pt. denote Mill Creek in the Eleven Point River watershed near Dalton, AR. Mill-Black denotes a different Mill Creek in the Lower Black watershed in Pocahontas, AR. * indicates the creeks from which F. ozarkae were sampled from, based on availability and when large enough for dissection.

Site	Poultry House Density (km^2)	Percent Pasture	Flow Path Distance (m)	Discharge (m^3/s)	Percent Groundwater	Total P (ug/L)	SRP (ug/L)	Total N (mg/L)	NO_3^- (mg/L)	TOC (mg/L)	TSS (mg/L)	Temperature (°C)	Conductivity (uS/cm)	Dissolved Oxygen (mg/L)	pH
Curia*	0.26	30.10	3017.00	3.00	47.03	16.4	5.86	0.98	0.65	2.27	16.80	13.74	240.43	6.94	7.56
Cypress*	0.21	26.90	1694.00	0.37	72.77	44.1	23.20	2.59	0.98	3.46	26.05	12.91	366.57	7.05	7.62
Diles*	0.00	26.70	6201.00	0.06	78.95	20.9	17.42	0.92	0.51	2.97	11.10	13.62	396.83	8.30	7.73
Dota*	0.57	42.90	1060.00	0.93	14.29	76.7	36.52	2.02	1.31	3.37	10.81	14.28	80.00	6.50	6.83
Eassis*	0.17	30.10	871.00	0.36	82.16	22.1	12.98	1.91	0.63	2.62	27.43	12.81	412.57	7.48	7.89
Hubble	0.11	32.40	707.00	0.34	58.67	114.2	51.91	1.39	0.83	8.10	23.53	13.69	297.50	6.86	7.82
Knotts*	0.06	30.20	1548.00	0.13	63.64	37.1	5.03	0.92	0.91	8.50	12.34	13.24	321.86	6.62	7.70
Lick	0.21	37.30	390.00	0.04	19.74	27.7	15.40	2.00	1.15	4.78	11.49	13.82	106.71	6.46	7.03
Mill-11 Pt.	0.00	42.30	996.00	1.74	58.30	13.4	10.04	2.17	1.75	2.52	24.91	13.50	403.14	8.09	7.95
Mill-Black*	0.16	51.60	1915.00	0.27	80.23	36.7	22.93	2.23	1.31	9.56	11.90	14.21	295.67	7.56	7.57
Tennessee*	0.06	35.20	163.00	1.01	73.50	57.9	35.68	2.60	1.33	3.22	41.63	13.69	370.14	6.99	7.64
Upshaw*	0.10	28.20	531.00	0.20	85.71	16.5	10.92	1.42	1.09	1.87	20.14	12.83	430.00	7.79	7.72

Table 5: Mean values of soluble reactive phosphorus (SRP), nitrate (NO_3^-), and total suspended solids (TSS) from storm samples collected in June 2019.

Site	Storm SRP (ug/L)	Storm NO_3^- (mg/L)	Storm TSS (mg/L)
Curia	8.83	1.44	54.25
Cypress	26.50	3.38	31.29
Diles	19.42	1.31	56.50
Dota	38.84	2.21	4.60
Eassis	17.07	2.61	57.75
Hubble	238.59	2.97	71.75
Knotts	80.26	2.08	46.25
Lick	19.18	2.33	5.29
Mill-11 Pt.	40.42	3.57	44.25
Mill-Black	62.18	3.84	215.25
Tennessee	92.84	3.57	50.50
Upshaw	16.31	1.71	79.50

tions ($R^2 = 0.38$, $p = 0.25$) (Table 6). Algal biomass was also not related to any other instream variable, including phosphorus and nitrogen concentrations. Chlorophyll a was low across most sites (Table 7), and lowest at Hubble Creek (1.9 μg Chl a/cm^2), though algae were potentially constrained by noticeable shading of the stream channel, as nutrient limitation was unlikely given the high phosphate and nitrate concentrations found at that site.

The percentage of Ephemeroptera, Plecoptera, and Trichoptera (EPT) taxa decreased when poultry operations were closer to a stream ($p = 0.01$) (Figure 3), confirming our hypothesis that poultry agriculture would reduce the presence of sensitive invertebrates. Proximity to poultry agriculture appears to be negatively impacting sensitive taxa, even though we found no discernible mechanistic relationship between instream variables and physicochemical conditions. In the future, we will be measuring substrate size and embeddedness in these streams as we continue sampling to determine whether poultry houses are influencing habitat metrics rather than nutrient and sediment inputs. EPT taxa richness was greatest in Diles Creek (73%), the stream with the lowest subwatershed poultry house density and greatest distance to poultry operations. EPT richness was lowest in Upshaw Creek (5%), which was in a subwatershed with low poultry house density but was directly adjacent to a poultry farm.

We found no relationships between Shannon's diversity index, macroinvertebrate abundance, and any instream variable or surrounding animal agriculture (Shannon's: $R^2 = 0.24$, $p = 0.67$; Abundance: $R^2 = 0.13$, $p = 0.77$) (Table 6). Shannon's diversity varied from 0.87 to 1.95, with the lowest diversity as well as the lowest abundance of invertebrates found at Hubble Creek. The benthos of Hubble Creek is dominated by sand with only small patches of cobbles in addition to the high nutrient levels and nearby application of poultry waste. The habitat itself was not conducive to colonization, but it was difficult for us to determine whether habitat or poultry waste runoff was the dominant metric keeping macroinvertebrate diversity and abundance low, or if perhaps some combination of the two factors were discouraging macroinvertebrate colonization and/or secondary production. Future sampling events and collection of habitat data may provide greater insight into the primary impact affecting macroinvertebrates at Hubble Creek. Surprisingly, abundance was greatest at Upshaw, which was next to a poultry farm; Upshaw had the lowest amount of EPT taxa, and most of invertebrates found there were chironomids.

Table 6: Results of multiple linear regression analyses between algal biomass, macroinvertebrate indices (Shannon's diversity, abundance, and percent EPT taxa), and their respective candidate models. Asterisks denote significant models. Italicized independent variables under a candidate model show individual p-values for each model parameter to illustrate primary drivers explaining variation in the dependent variable.

Dependent Variable	Independent Variables	R^2	p
Chlorophyll a	Poultry Density + Percent Pasture + Flow Path Distance	0.38	0.25
	SRP + NO3- + TSS + TOC + Discharge	0.77	0.06
Shannon's Diversity	Poultry Density + Percent Pasture + Flow Path Distance	0.67	0.24
	SRP + NO3- + TSS + TOC + Discharge	0.51	0.4
	Chlorophyll a	0.09	0.66
Abundance	Poultry Density + Percent Pasture + Flow Path Distance	0.13	0.77
	SRP + NO3- + TSS + TOC + Discharge	0.42	0.55
	Chlorophyll a	0.15	0.22
Percent EPT Taxa	Poultry Density + Percent Pasture + Flow Path Distance	0.65	0.03*
	Poultry Density		0.75
	Percent Pasture		0.71
	Flow Path Distance		0.01*
	SRP + NO3- + TSS + TOC + Discharge	0.55	0.33
	Chlorophyll a	0.04	0.54

Table 7: Mean values of algal biomass sampled from June 2019 to February 2020. Microcystin was measured in July and August 2019. Macroinvertebrates were sampled in June 2019.

Site	Microcystin (ug/L)	Chlorophyll a (ug/cm^2)	Shannon's Diversity	Abundance	Percent EPT Taxa
Curia	0.026	4.25	1.87	261	55.29
Cypress	0.016	3.30	1.75	184	6.82
Diles	0.029	3.16	1.68	852	73.40
Dota	0.009	4.39	1.72	254	23.56
Eassis	0.022	4.89	1.86	533	47.52
Hubble	0.020	1.91	0.87	33	30.05
Knotts	0.023	2.39	1.77	486	26.20
Lick	0.018	3.26	1.59	336	6.95
Mill-11 Pt.	0.015	11.40	1.74	696	21.95
Mill-Black	0.035	1.93	1.95	346	42.80
Tennessee	0.049	4.23	1.16	875	5.98
Upshaw	0.035	6.33	1.20	2530	4.71

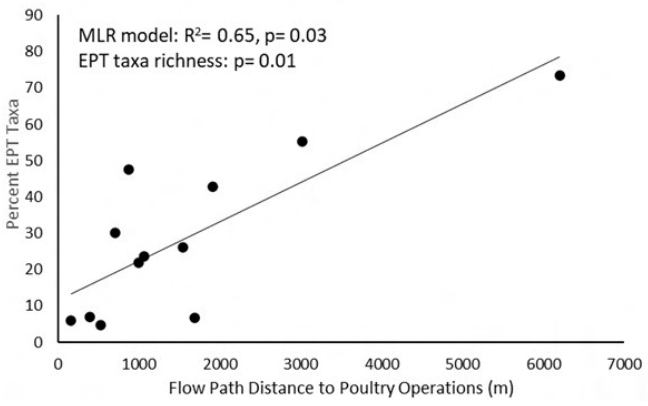

Figure 3: Percent EPT taxa versus flow path distance in meters from poultry operations. Omnibus multiple linear regression statistics and percent EPT taxa richness significance within the MLR model are shown at top left.

Relative abundance of taxa compared to poultry house density and flow path distance to poultry are shown in Figure 4.

The most common crayfish observed in the area was F. ozarkae (personal observation). This species was sampled from the creeks indicated by * in Table 4. Three creeks from which crayfish samples were analyzed first were selected based on summer N and P level data: Diles Creek was our non-polluted creek; Tennessee and Mill-Black creeks were our polluted samples. The partial sequence of NKA in F. ozarkae showed a significantly high level of identity (99.35%) with another crayfish Procambarus clarkii (QDE54942.1) and at least 96.75% similar to several other decapods, indicating a high level of conservation of this gene in this Order. The transcript expression of NKA in gills and intestine (Figure 5) shows no significant difference among the 3 creeks (p = 0.77 in gills and p = 0.55 in intestine). Results in the antennal gland are in progress. These results are consistent with the similar localization and observed staining intensity of NKA in gills, intestine and antennal gland in crayfish from Diles, Mill-Black, and Tennessee creeks (Figure 6). In the gills, about half of the lamellae had NKA localized in the cells' basolateral membrane indicating their role in osmoregulation, while the other half showed little to no NKA, suggesting rather a role in gas exchange (Figure 6, A,A'). NKA basolateral localization was also found in the enterocytes

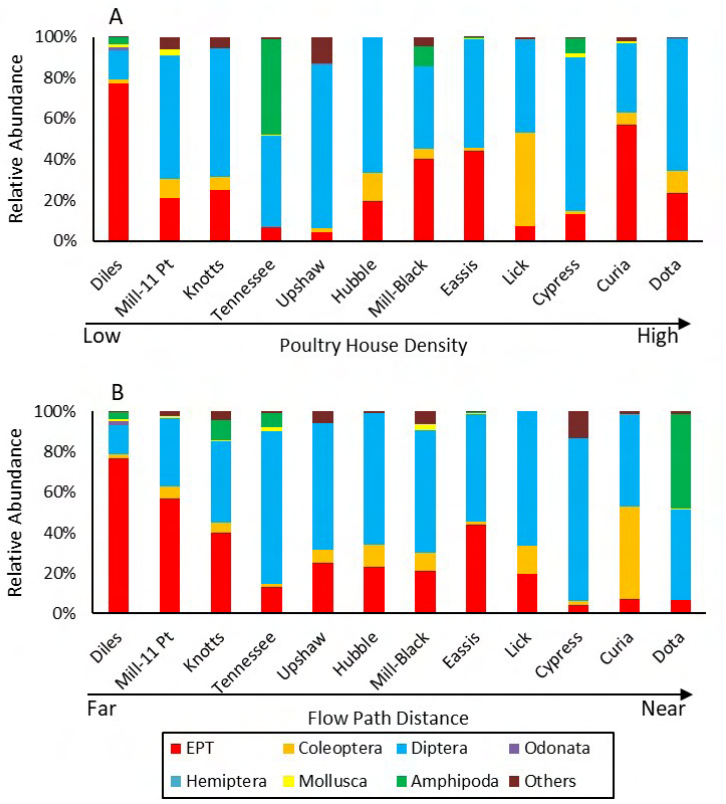

Figure 4. Relative abundance of macroinvertebrate taxa from low to high poultry house density (a) and low to high flow path distance from poultry operations (b).

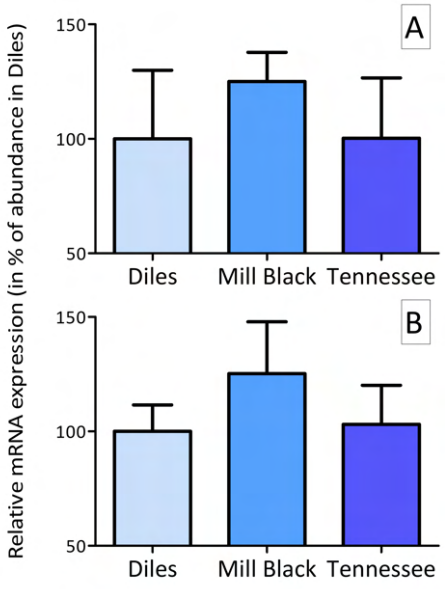

Figure 5: NKA transcript abundance in gills and intestine from the Ozark crayfish in non-polluted creek (Diles) and two polluted creeks (Mill-Black and Tennessee). The expression of NKA is expressed in % of NKA abundance in Diles. Bars represent the mean value + s.e.m. (N = 6 to 9). Expression levels were normalized against a reference gene, EF1a. No significant difference in expression between creeks was found (p = 0.7732 in gills and p = 0.5469 in intestine).

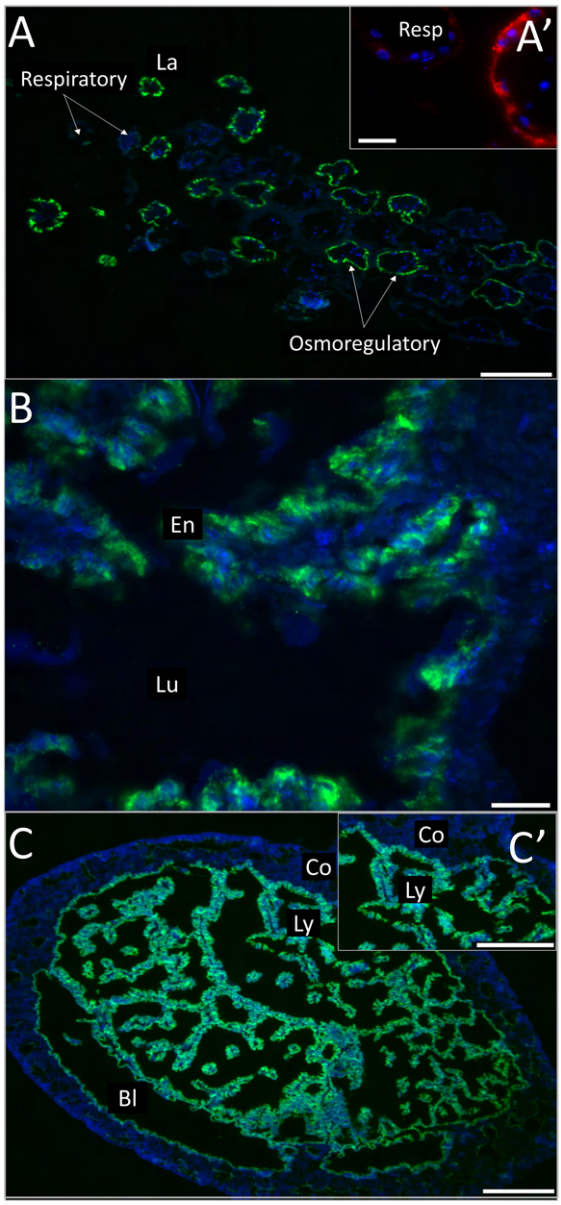

Figure 6: Cross sections of gill (A,A'), intestine (B) and antennal gland (C,C') from F. ozarkae immunostained with monoclonal NKA antibody (green or red) and nuclei stained with dapi. The gill apparatus consists of lamellae (La) made of a thin layer of respiratory (Respiration/Resp) or osmoregulatory (osmoregulation) epithelium, covered with a thin cuticle. The osmoregulatory lamellae (A,A') and the enterocytes of the intestine (B) showed a basolateral NKA immunostaining. The antennal gland (C,C') was stained with NKA antibody in the basolateral membrane of the cells forming the epithelium of the labyrinth (Ly) and bladder (Bl) but absent in the coelomosac (Co). Immunostaining and morphology were similar in all three organs of organisms sampled from polluted and non-polluted creeks (N = 3). Lu: lumen of the intestine. Scales: 100 µm in A, C and C', 20 µm in A' and B'.

(Figure 6, B) and the cells forming the epithelium of the labyrinth and bladder in the antennal gland (Figure 6, C,C'), but was absent in the coelomosac. No change in morphology of those organs was observed between crayfish of non- and polluted creeks. The lack of significant differences in organ morphology and NKA expression and localization in osmoregulatory organs indicates that neither respiration nor osmoregulation seem to be impacted by an increase in nitrogen and phosphorus at the levels detected in our study. However, to confirm this result, we will look at potential differences in NKA activity levels as well as the impact on expression of the other proteins involved in ammonia excretion (Na^+/NH_4^+ exchanger, Na^+/H^+-antiport, V-Type H^+-ATPase).

Conclusions

Animal agriculture is affecting sensitive macroinvertebrate taxa in tributaries of the Lower Black and Eleven Point Rivers despite having no significant relationships with nutrient and sediment concentrations. While we found evidence of poultry farms increasing phosphorus in the summer of 2019, no effect was detected over the rest of the study. Sensitive EPT taxa are not as abundant in streams with nearby chicken houses, though we are still working to determine the mechanism by which intolerant taxa are being excluded. No effect of pollution was shown on NKA expression which might indicate that the observed nutrient concentrations found do not affect crayfish osmoregulation. These findings benefit Arkansas water resource managers by revealing a decline in sensitive invertebrates, which are often considered sentinel species, in streams with nearby poultry operations. This research assists the USGS in addressing pressing water issues by demonstrating that proximity to farming operations is a critical consideration in the conservation of water quality and macroinvertebrate communities.

Acknowledgements

This material is based upon work supported by the United States Geological Survey under grant agreement No. G16AP00040 and administered by the Arkansas Water Resources Center. The views and conclusions contained in this document are those of the authors and should not be interpreted as representing the opinions or policies of the U.S. Geological Survey.

References

Arkansas Division of Environmental Quality (ADEQ). 2020. Final General Stormwater NPDES Permits Database. Accessed December 28, 2020.

Arkansas Natural Resource Commission (ANRC). 2014. Arkansas Water Plan: 2014 Update. Little Rock, AR.

Arkansas Pollution Control & Ecology Commission (APC&EC). 2007. Regulation 2: Regulation Establishing Water Quality Standards for Surface Waters of the State of Arkansas. #014.00-002.

American Public Health Association (APHA). 2005. Standard methods for the examination of water and wastewater, 21st ed., Washington, DC.

Boehler, K. E. 2010. Poultry growers in Arkansas: Agents or independent contractors. Arkansas Law Review 63: 849-82.

Bossus, M., Charmantier, G., Blondeau-Bidet, E., Valletta, B., Boulo, V., Lorin-Nebel, C. 2013. The ClC-3 Chloride channel and Osmoregulation in the European Sea Bass, Dicentrarchus labrax. Journal of Comparative Physiology, Part B, 183, 5, 641-662.

Bossus, M.C., Madsen, S.S., Tipsmark, C.K., 2015. Functional dynamics of claudin expression in Japanese medaka (Oryzias latipes): response to environmental salinity. Comparative Biochemistry and Physiology, Part A, 187, 74-85.

Burnham, K.P. and D.R. Anderson. 1998. Practical use of the information-theoretic approach. In Model selection and inference pp. 75-117. Springer, New York, NY.

Lombardo, L.A., G.L. Grabow, J. Spooner, D.E. Line, D.L. Osmond, and G.D. Jennings. 2000. Section 319 Nonpoint Source National Monitoring Program Successes and Recommendations. NCSU Water Quality Group, Biological and Agricultural Engineering Department, NC State University, Raleigh, North Carolina.

Ouattara, N., Bodinier, C., Negre-Sadargues, G., D'Cotta, H., Messad, S., Charmantier, G., Panfili, J., Baroiller, J.F. 2009. Changes in gill ionocyte morphology and function following transfer from fresh to hypersaline waters in the tilapia Sarotherodon melanotheron. Aquaculture, 290, 155-164.

Rueedi, J., R. Purschert, U. Beyerle, C. Alberich, R. Kipfer. 2005. Estimating groundwater mixing ratios and their uncertainties using a statistical multi parameter approach. Journal of Hydrology 305: 1-14.

Spaargaren, D.H. 1990. The effect of environmental ammonia concentrations on the ion-exchange of shore crabs, Carcinus maenas (L.). Comparative Biochemistry and Physiology part C 97, 87-91.

United States Department of Agriculture (USDA), National Agricultural Statistics Service. 2018. Poultry: Production and Value- 2018 Summary. https://www.nass.usda.gov/Publications/Todays_Reports/reports/plva0418.pdf

Weihrauch, D., Morris, S., Towle, D.W. 2004. Ammonia excretion in aquatic and terrestrial crabs. The Journal of Experimental Biology, 207, 4491-4504.

Image caption: Sunflower (left) and pea shoot (right) microgreens growing on Biostrate mats. After harvest, the Biostrate mats with remaining roots were evaluated as a potential carbon source for the treatment of spent hydroponic nutrient solution. Photo courtesy of Kristen Gibson.

Utilization of Biodegradable Hydroponic Growth Media as a Carbon Source for Greenhouse Wastewater Denitrification

Gina M. Misra[1] and Kristen E. Gibson[2]*

[1]M.S. student (graduated), Food Science, University of Arkansas, Fayetteville, Arkansas 72701; [2]Associate Professor, Food Science, University of Arkansas, Fayetteville, Arkansas 72701
*Corresponding author, keg005@uark.edu

Abstract: Denitrification of spent hydroponic nutrient solution discharged from greenhouses poses a potential environmental hazard. Aerobic denitrification requires a source of organic carbon, which can be costly for treating large volumes of wastewater. This study proposes the use of spent biodegradable hydroponic grow mats as a source of organic carbon. We compared various anaerobic conditions for the digestion of spent organic growth substrate as a source of organic carbon for the potential treatment of hydroponic wastewater. Grow mats in tap water demonstrated the greatest concentration of organic carbon produced during anaerobic digestion. Anaerobic digestion of grow mats resulted in peak levels of organic carbon after 7 days and decreased thereafter. Leaf waste in addition to Biostrate (type of grow mat) and tap water is capable of producing 5 liters of 5454 mg/L (ppm) total organic carbon. Based on the above results, approximately 12.5 L of nutrient solution (2.5:1 C:N ratio) containing 218 mg/L N can potentially be treated. Our findings provide are the first steps in a sustainable and cost-effective treatment for hydroponic wastewater through utilization of another waste stream (i.e. spent, organic grow mats).

Key Points:

- Nutrient concentrations in hydroponic wastewater can be much greater than typical agricultural wastewater.
- Organic grow mats used in hydroponic cultivation can be a source of organic carbon for treatment of hydroponic wastewater.
- Under anaerobic conditions, digestion of grow mats resulted in peak levels of organic carbon after 7 days and decreased thereafter.

Introduction

For the cultivation of horticultural and food crops in hydroponic systems, nitrogen and phosphorus must be added in excess of what is needed (Sonneveld, 1981). Hydroponic nutrient water cannot be used indefinitely due to risk of plant pathogen accumulation and nutrient depletion. As a result, spent hydroponic wastewater rich in nitrogen and phosphorus is often released directly into the environment. The nutrient levels in hydroponic wastewater can potentially be much higher even than that of typical agricultural wastewater, landfill leachate, and municipal sewage (Yamamoto-Ikemoto, 2000). Combined with other wastewater streams and non-point sources of pollution, the water quality of proximal waterbodies can become compromised.

Researchers have explored various treatments to reduce nitrogen and phosphorus levels in hydroponic and greenhouse wastewater to concentrations that are safe for the environment. These technologies include high performance ultrafiltration membranes (Liu et al., 1999; Seo et al., 2010), mineral treatments (Yi et al., 2003, 2005; Seo et al., 2008; Dunets et al., 2014), bioreactors (Yamamoto et al., 2000; Park et al., 2008, 2009; Seo et al., 2008), absorbers (Dunets et al., 2014), and constructed wetlands (Prystay et al., 2001; Seo et al., 2008, 2010; Gruyer et al., 2013). A major limiting factor in the removal efficiency of biological methods (e.g., bioreactors or constructed wetlands) is an abundant, inexpensive carbon source for denitrifying bacteria to use when reducing NO_3-to N_2. Although rich in nitrogen, hydroponic wastewater typically has very little organic carbon available.

Many hydroponic systems use inorganic substrates such as rockwool, perlite, expanded clay, gravel, or simply suspend plant roots directly in nutrient water. However, some systems, particularly those that grow microgreens, will use fibrous mats made of biodegradable materials such as hemp (Dannehl et al., 2015), felt (Van Quy et al., 2016), or wood (Weber et al., 2016). While inorganic substrates can be washed and reused, organic substrates cannot be reused and present a significant disposal challenge (personal communication), which undermines sustainability goals of these systems. In the present study, we used spent organic growth substrate as a source of organic carbon for hydroponic wastewater treatment and to enhance reusability of the growth substrate waste stream. Therefore, the objectives of this study were to: 1) Characterize hydroponic wastewater from a large commercial hydroponics facility in Northwest Arkansas as well as two small research systems at University of Arkansas to determine volume and nitrogen concentrations to be treated, 2) Determine concentrations of bioavailable carbon that can be obtained from soaking or digesting several types of organic growth mats, and 3) Compare nitrogen removal efficiency in both the commercial and the research system as well as a control "synthetic" wastewater mix using carbon from digested mats. Based on the above objectives, we hypothesized that extraction of bioavailable carbon from spent growth mats for treatment of hydroponic wastewater will reduce nitrogen concentrations to levels equivalent to currently utilized technologies. We also hypothesized that bioavailable carbon and time to extract the carbon will vary based on the material type.

Methods

Bucket digestors for organic carbon generation

To obtain organic carbon from anaerobic digestion, three 20-L polyethylene Nalgene buckets were used to hold the treatments. Spent grow mats and wastewater were collected at a commercial scale nutrient film technique (NFT) hydroponic lettuce system in Winslow, Arkansas. Spent Biostrate™ mats used to grow microgreens were prepared by first removing all of the remaining leaves and stems from the harvested crop and setting them aside. The collected mats were cut into 1 in^2 pieces. Each of three independent digestions lasted 4 weeks. All experiments were conducted at ambient temperature of 20 to 22°C. Water samples were tested for Nitrate-N, Nitrite-N, Ammonium-N, and Total Organic Carbon (TOC) (EPA 412.1). All water samples were analyzed in the Arkansas Water Resources Center. The pH of each treatment was recorded on a weekly basis.

First digestion (aerobic versus anaerobic)

Two treatments were set up as a proof of concept. One treatment included 750 g of Biostrate mat pieces and 250 g of microgreen leaf waste in 8 L of autoclaved tap water. The second treatment included 750 g of Biostrate™ mat pieces and 250 g of microgreen leaf waste in 8 L of wastewater drawn from the waste valve of the hydroponic farm. Wastewater was poured directly into a 20-L bucket on-site and closed for transport back to the lab. One 50 mL sample from each bucket was collected every 7 days and stored at -20°C until processing. An identical set of buckets were set up but included an air bubbler to inject oxygen to compare an aerobic versus anaerobic process. The oxygen levels were maintained at 83-87% dissolved oxygen (DO) and measured using a DO meter. At the end of the 4-week period, all of the samples were processed and analyzed for Total Nitrogen (TN) and Total Organic Carbon (TOC). The TOC samples were not acidified prior to storage at 4°C. The samples were not filtered prior to submission; however, 1:10 and 1:100 dilutions were prepared for TOC analysis.

Second digestion (anaerobic)

The second digestion was set up to determine if a different type of growing mat made from hemp could be an alternate source of organic carbon. Four treatment conditions were set up in 20-L Nalgene buckets under anaerobic con-

ditions: 1) 750 g of Biostrate mats plus 250 g of microgreen leaf waste in 8 L of hydroponic wastewater; 2) 8 L of just hydroponic wastewater; 3) 750 g of hemp mats plus 250 g of microgreen leaf waste in autoclaved distilled water; and 4) 750 g of Biostrate mats plus 250 g of microgreen leaf waste in distilled water. The samples were collected and processed for TN and TOC on the same day each week. The TOC samples were acidified with 40 uL of HCl in 40 mL of sample prior to processing. Samples were collected in duplicate.

Third digestion (anaerobic)

Three treatment conditions were set up in 20-L Nalgene buckets: 1) 8 L of autoclave tap water to serve as a control; 2) 8 L of autoclaved tap water, 750 g of spent BioStrate™ mats, and 250 g of previously removed leaf and stem waste; and 3) 8 L of autoclaved tap water and 750 g of spent BioStrate™ mats only. The mixtures were then left to anaerobically digest (i.e., no air bubbler was included) for 30 days. Triplicate samples (50 mL) were collected from each bucket on a weekly basis and duplicate samples were processed for TN and TOC on the same day each week. The TOC samples were acidified as described previously.

Impact of pH on anaerobic digestion of Biostrate™ mats

In order to determine the optimal pH for anaerobic digestion of Biostrate™ grow mats, 5 phosphate buffers at different pH levels were prepared (Table 1).

Following buffer preparation, 20 g of Biostrate™ grow mats were cut into four equal sections (~5 g each) and then each section was cut into small pieces. The small pieces from each section were placed in individual 1 L glass bottles. Each bottle was filled with the appropriate buffer (pH 5.4, 5.8, 6.2, 6.6). An additional control treatment at pH 7.4 was also prepared. Bottles were capped and sealed with parafilm to maintain anaerobic conditions and held under ambient conditions (20-22°C). Samples (5 mL) from each bottle were collected weekly in duplicate over 28 days as well as a final sample collected on day 56. The 5 mL samples were added to 45 mL of Millipore water in a 50 mL conical tube for a final 1:10 dilution. The TOC samples were acidified. Actual TOC values were recorded by multiplying the reported TOC values by 10 due to the dilution factor.

Analysis of grow mat composition

BioStrate™ mats and hemp mats were analyzed at the Fayetteville Agricultural Diagnostic Laboratory to characterize the material. Parameters measured included percent neutral detergent fiber (hemicellulose, cellulose, and lignin) and acid detergent fiber (cellulose and lignin) in the mats (AOAC 1990a,b) as well as percent nitrogen, percent carbon, and pH. A saturation analysis was also performed on the grow mats to obtain electrical conductivity, nitrate, phosphorus, potassium, calcium, magnesium, sulfur, sodium, iron, manganese, zinc, copper, and boron.

Anaerobic denitrification (bucket, non-pumped system)

While generating organic carbon for the aerobic denitrification experiment, an unexpected result occurred. Denitrification of residual nitrogen in greenhouse-derived wastewater occurred in a low oxygen environment using undigested Biostrate™ mats (see Results). Thus, we decided it was necessary to determine if anaerobic digestion of the grow mats to yield organic carbon was necessary prior to denitrification, or if using the mats directly was feasible. Three 20-L Nalgene buckets were set up for anaerobic denitrification (Figure 1). The following conditions were prepared: 1) synthetic wastewater-only control; 2) spent grow mats with synthetic wastewater; and 3) organic carbon liquid generated by anaerobic digestion of the spent grow mats and synthetic wastewater. Duplicate sampling was conducted weekly.

Table 1: Phosphate buffer formulations.[1]

pH	Na_2HPO_4-$7H_2O$ (mw: 268.07 g/mol)	Molarity	NaH_2PO_4-H_2O (mw: 137.99 g/mol)	Molarity
5.4	0 g	0 M	1.557 g	0.0110 M
5.8	0.131 g	0.0005 M	1.313 g	0.0095 M
6.2	0.603 g	0.0023 M	1.069 g	0.0077 M
6.6	1.076 g	0.0040 M	0.826 g	0.0060 M
7.4 (Control)	2.021 g	0.0075 M	0.339 g	0.0025 M

[1]Recipe calculator: https://www.aatbio.com/resources/buffer-preparations-and-recipes/phosphate-buffer-ph-5-8-to-7-4

Figure 1: Example of the pump-included hydroponic wastewater system.

Data Analysis

The changes in total organic carbon (TOC), total nitrogen (TN), Nitrate-N and Nitrite-N (N+N), and ammonia-N and ammonium-N(A+A) were plotted against the experiment time for each treatment. Furthermore, the pH of the treatments was plotted against time. Basic description statistics such as mean and standard deviation were also determined.

Results and Discussion

Anaerobic digestion of grow mats

First Digestion

In the tap water (TW) treatment, TN increased slightly relative to the increase in TOC, from 0.79 mg/L to 121.34 mg/L after 4 weeks. The increase in TOC was dramatic, from 0.49 mg/L to 545.44 mg/L in 4 weeks. In the hydroponic wastewater treatment, a significant concentration of nitrogen was present at the start of the experiment (214.76 mg/L) due to residual from the nutrients added for lettuce production. The TN decreased from 214.67 mg/L to 81.7 mg/L by the end of the 4 weeks. The level of TOC increased from 19.48 mg/L to only 78.36 mg/L. No replicates were taken for this experiment, so it is unknown if the differences between treatments were statistically significant. The aerobic digestion resulted in no change in TN or TOC and was deemed an ineffective strategy for generating TOC from Biostrate (data not shown).

Second Digestion

For all treatments, the TOC levels peaked at week 1 and declined thereafter (Figure 2). The total nitrogen increased slightly for each treatment.

The starting nitrogen concentration for distilled water and wastewater were similar, indicating that the day we collected the wastewater, it was more "spent" than on the collection day from the first digestion (i.e., more nitrogen had been used up by the microgreens). There appeared to be no difference between hemp and Biostrate as an organic carbon source; however, the anaerobic digestion also yielded no usable organic carbon by the end of the 4-week period.

Third Digestion

In the TW control treatment, TOC remained consistent, ranging from 0.91 to 1.71 (Figure 3). The TOC in both TW+Biostrate™ and TW+Biostrate+LW treatments increased from 69.65 and 114.76 mg/L with in the first week, respectively. After Week 1, the TOC concentrations decreased to 15 mg/L for the TW+Biostrate treatment and 50.89 mg/L in the TW+Biostrate+LW treatment.

When comparing TN across treatments, the TW control treatment remained consistent and ranged from 0.82 to 1.06 mg/L (Figure 4). TN increased in the TW+Biostrate treatment from 41.05 to 49.76 mg/L from Week 0 to Week 3, and then decreased to 41.25. In the TW+Biostrate+LW treatment, TN increased throughout the experiment, starting at 61.48 mg/L and ending at 85.00 mg/L.

As for N+N, the TW control and TW+Biostrate+LW treatment remained consistent throughout the experiment, ranging from 0.64 to 0.67 and 0.008 to 0.05 mg/L respectively (Figure 5). The N+N for the TW+Biostrate treatment remained consistent from Week 0 until Week 3 where the N+N concentration increased from 0.023 to 2.88 mg/L on Week 4. Like other previous parameters, A+A for the TW control treatment remained consistent, ranging from 0.01 to 0.046 mg/L across the experiment (Figure 6). The A+A in

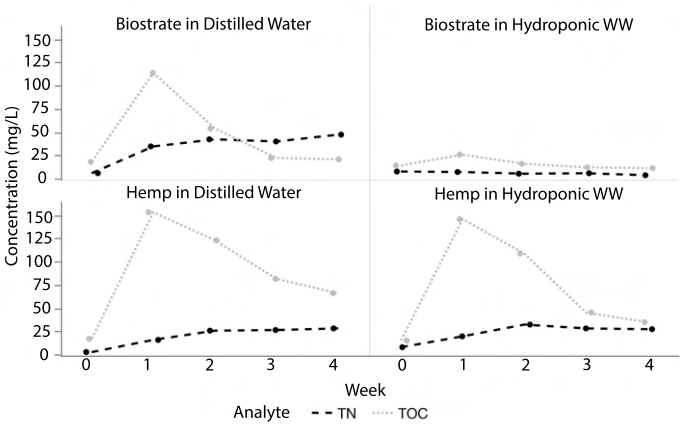

Figure 2: Impact of anaerobic digestion conditions on total nitrogen (TN) and total organic carbon (TOC) over time. WW=wastewater

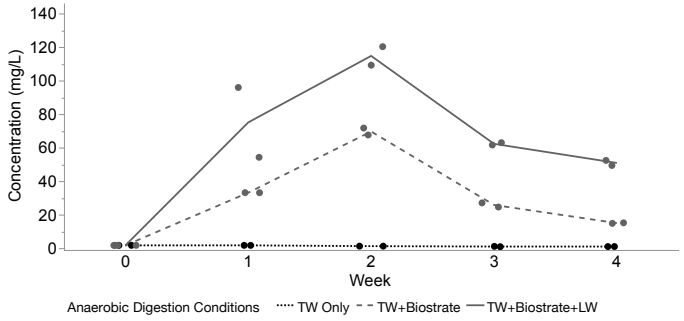

Figure 3: Concentration of total organic carbon (TOC) by anaerobic digestion of condition over time.

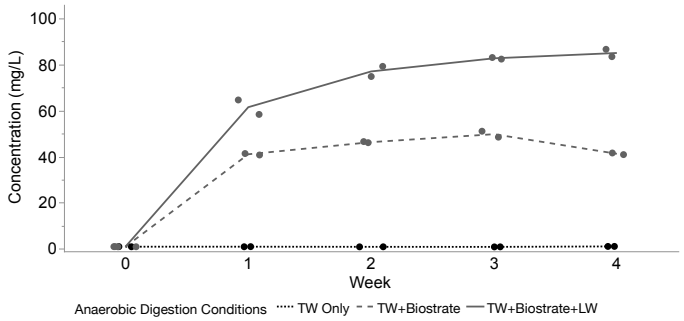

Figure 4: Concentration of total nitrogen (TN) by anaerobic digestion condition over time.

the TW+Biostrate treatment increased from 23.10 mg/L on Week 0 to 30.93 mg/L on Week 3, then decreased to 25.71 mg/L on Week 4. The TW+Biostrate+LW treatment's A+A increased from Week 0 until Week 1. From Week 1 to Week 2 A+A then decreased slightly, then increased from Week 3 to Week 4. Table 2 summarizes the results and C:N ratios of these experiments, wherein only the first was successful at generating sufficient organic carbon for denitrification.

The pH of the treatments followed a similar trend from Week 0 to Week 2 where the pH decreased and then increased (Figure 7). After Week 2, the pH of the TW control treatment continued to decrease and the pH of the TWB and TWB+L treatments increased until Week 3. The pH of the TW+Biostrate treatment then decreased in Week 4 where the TW+Biostrate+LW treatment increased.

Impact of pH on total organic carbon during anaerobic digestion of grow mats.

To assess the impact of pH level on TOC over time during anaerobic digestion of Biostrate™ mats, five pH levels were selected, and TOC was assessed. Overall, the mean level of TOC was 3.66 mg/L (Table 3) with the peak level at 7.99 mg/L for sample pH 5.4 on day 56, whereas 0.95 mg/L was the lowest TOC recovered in the pH 7.4 sample on day 54 (data not shown). The general trend of TOC values over time are presented in Figure 8. For all samples, the mean peak recovery occurred on day 28 then TOC levels declined by day 56 (Figure 9). The pH from day 0 to day 7 increased then dipped down at week 14 for all samples (Figure 10).

Grow Mat Analysis

The BioStrate™ mats had a greater proportion of neutral detergent fiber of 94.82% compared to the hemp mats which were 86.12% (Table 4) (Van Soest et al., 1991; AOAC, 1990). The percent nitrogen was highest in the hemp mats at 0.31% and least in the BioStrate™ mats at 0.09% (AOAC, 1990). The pH of a water extract of the hemp mats was 5.9 and the pH of BioStrate™ mats using the same technique was 6.3 (Cataldo et al., 1975). Table 5 shows the extraction analysis results for Biostrate™ and hemp which indicate low nutrient content overall for these grow mats.

Table 2. Summary of C:N ratios and effectiveness of anaerobic digestion after 4 weeks

Condition	Carbon (mg/L)	Nitrogen (mg/L)	C:N Ratio	TOC (mg/L)
TW	0.49	0.79	0.62	545
TW + Biostrate	18.15	5.96	3.04	20.09
TW + Biostrate + LW	75.09	61.48	1.22	50.89

TW=tap water; LW = leaf waste; TOC=total organic carbon

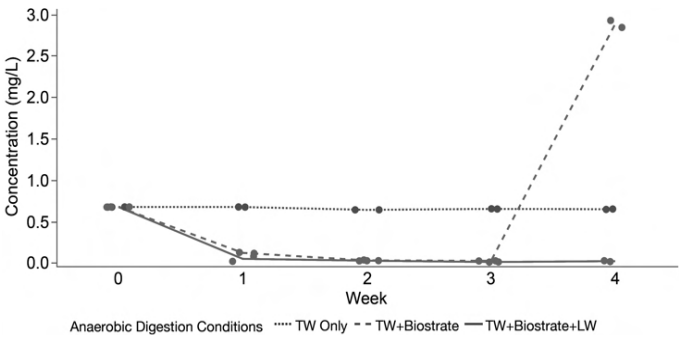

Figure 5: Concentration of nitrate-nitrite by anaerobic digestion condition over time.

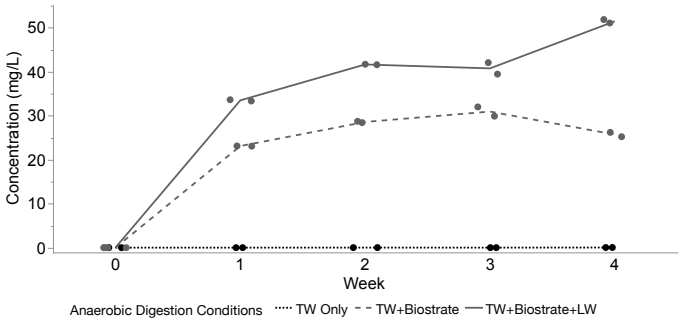

Figure 6: Concentration of ammonia + ammonium (A+A) by anaerobic digestion condition over time.

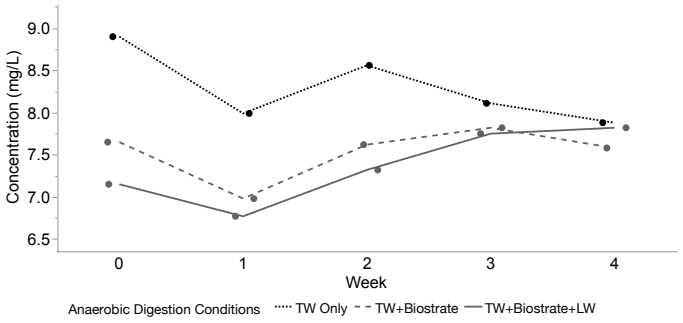

Figure 7: pH by anaerobic digestion condition over time.

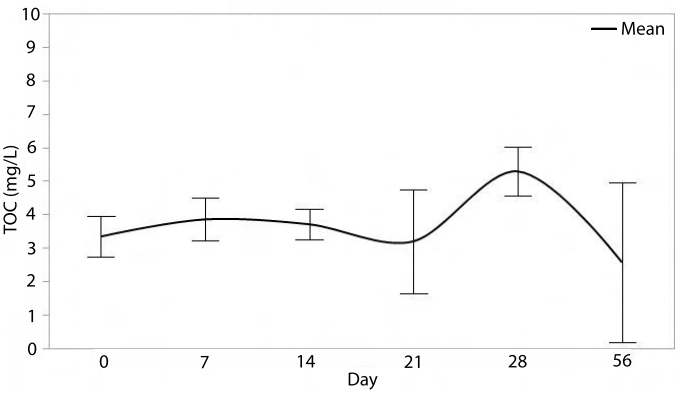

Figure 8: The mean TOC (mg/L) over time. Each error bar is constructed using 1 standard deviation from the mean.

Table 3: Comparison of mean TOC (mg/L) values by pH over time

	Mean TOC (mg/L) (±SD) by Day					
Sample	0	7	14	21	28	56
pH 5.4	3.53 (0.85)	3.61 (0.54)	3.50 (0.47)	3.77 (1.35)	4.63 (0.70)	4.00 (3.30)
pH 5.8	3.73 (0.39)	3.70 (0.88)	3.87 (0.53)	2.29 (1.14)	5.37 (0.52)	1.40 (0.14)
pH 6.2	2.92 (0.62)	4.05 (0.62)	3.82 (0.51)	2.96 (1.39)	5.15 (0.49)	4.27 (3.41)
pH 6.6	3.31 (0.37)	3.85 (0.49)	3.68 (0.62)	4.02 (2.49)	5.82 (0.94)	2.05 (1.20)
pH 7.4	3.21 (0.69)	4.06 (0.78)	3.66 (0.19)	2.96 (1.18)	5.47 (0.61)	1.13 (0.33)
Average	3.66					

SD = Standard Deviation

Table 4: The composition analysis of biostrate and hemp

Parameter	Biostrate	Hemp
Acid detergent fiber (%)	91.97	75.91
Neutral detergent fiber (%)	94.82	86.12
Nitrogen (%)	0.09	0.31
Carbon (%)	48.94	42.99
pH	6.3	5.9

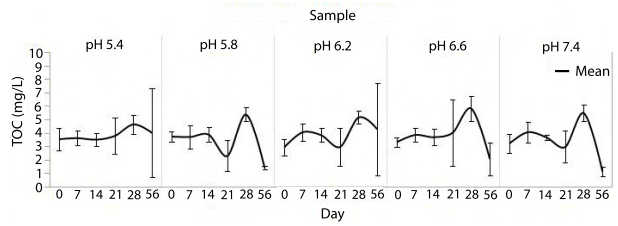

Figure 9: The TOC (mg/L) over time by pH level. Each error bar is constructed using 1 standard deviation from the mean.

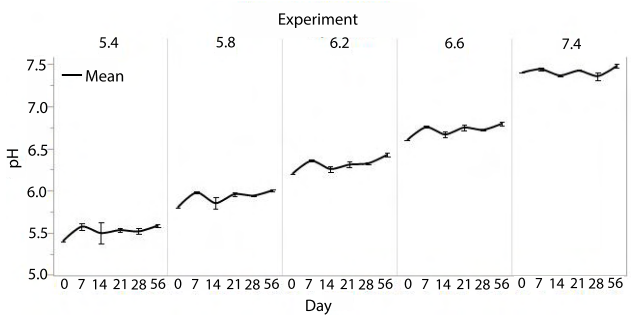

Figure 10: The change in pH over time. Each error bar is constructed using 1 standard deviation from the mean.

Wastewater Treatment System

The wastewater treatment system was only created within this study. Future experiments aim to observe the denitrification potential of the aerated, pump-included system compared to aerated, pump-less system, and an anaerobic denitrification system.

Discussion

The primary purpose of this experiment was to determine the amount of organic carbon that could be extracted from the anaerobic digestion of the BioStrate™ mats and leafy green waste, and if either tap water or hydroponic wastewater was a more appropriate digestion medium. In the first digestion, TOC production occurred in tap water but not in hydroponic wastewater. However, denitrification unexpectedly occurred in the hydroponic wastewater bucket containing Biostrate™, where total nitrogen decreased by 62% over 4 weeks. As previously stated, the organic carbon in subsequent experiments increased initially (Figure 1), then began to steadily decline. This could be due to the increased concentrations of nitrogen and carbon present in the water at the start of the experiment. Increased initial concentrations of nitrogen and carbon could have favored dissimilatory nitrate reduction to ammonium (DNRA) since A+A concentrations increased in the BioStrate™ and BioStrate™ + leafy green waste treatments from Week 0 to Week 4 (see Second Digestion). DNRA is assumed to occur when nitrate is the limiting nutrient compared to organic carbon (Cole and Brown, 1980).

With the increase in ammonium from the anaerobic degradation of organic matter, a different approach may be used to remove nitrogen from the system. Under anoxic conditions, anaerobic ammonium oxidation (anammox) bacteria form nitrogen gas (N_2) from nitrite and ammonium (Jetten et al., 2005). Anammox bacteria have been detected in most aquatic habitats that contain anoxic zone (Dong et al., 2009; Jetten et al., 2005). The chemolithoautotrophic anammox pathway is preferred in habitats that are oxygen-depleted and that are limited in organic matter. As organic matter decomposes anaerobically, ammonification occurs producing ammonium. Furthermore, DNRA can also produce ammonium for the anammox bacteria. Nitrite can be produced by aerobic nitrifying bacteria that inhabit the surface of the water where the oxic and anoxic habitats interact (Hao et al., 2002). Moreover, anammox bacteria were observed to reduce nitrate to nitrite through the oxidation of organic compounds (Guven et al., 2005).

Another possible explanation of the continual loss of TOC in the BioStrate™ treatments is that the anaerobic digestion process continued further than desired. In anaerobic digestion, there are four steps: (1) hydrolysis, (2) fermentation or acidogenesis, (3) acetogenesis, and (4) methanogenesis (Gould, 2015). Step 1 is hydrolysis where large organic polymers including proteins, fats, and carbohydrates, are broken down into smaller polymers including amino acids, fatty acids, and simple sugars. The goal of the anaerobic digestion in this study was to create the simple sugars for the bacteria. While all steps occur simultaneously, step 2 of fermentation or acidogenesis may have outpaced step 1. In step 2, the small polymers previously mentioned

Table 5: The saturation extract analysis biostrate and hemp

Parameter	Biostrate	Hemp
EC (μmhos/cm)	32	96
NO_3-N (mg/L)	0.3	0.1
P (mg/L)	1.0	1.7
K (mg/L)	2.1	3.7
Ca (mg/L)	0.5	4.2
Mg (mg/L)	0.3	1.4
S (mg/L)	0.3	5.7
Na (mg/L)	2.0	7.2
Fe (mg/L)	0.1	0.3
Mn (mg/L)	0.001	0.07
Zn (mg/L)	0.002	0.16
Cu (mg/L)	0.02	0.02
B (mg/L)	0.02	0.02

are broken down further. As fermentative bacteria break down the polymers, an acidic environment and ammonia is created. The increased ammonia content can be observed in Figure 5.

Conclusions

A clear understanding of the carbon and nitrogen cycles are necessary to produce organic carbon for denitrification. Factors including environmental conditions, the concentrations of different nitrogen and carbon molecules, and bacteria present can influence the biochemical reactions within the system. In this study, the first objective was to decompose spent organic substrates to produce organic carbon for denitrification. Future research would be necessary to explain the differences in organic carbon production between the three digestion scenarios. One experiment would be to observe organic carbon production when organic carbon is the limiting nutrient compared to total nitrogen. This may encourage the decomposition of the substrates in the system. Furthermore, a different approach such as using anaerobic ammonium oxidation may be used as another process to produce atmospheric nitrogen for nitrogen removal. As the hydroponic industry continues to grow, organic materials such as the spent substrates and wastewater will be produced. A sustainable and cost-effective method of treatment will become more pertinent to prevent the release of nutrients into soil, with the potential to cause eutrophication within proximal surface waters.

Acknowledgements

This material is based upon work supported by the United States Geological Survey under grant agreement No. G16AP00040 and administered by the Arkansas Water Resources Center. The views and conclusions contained in this document are those of the authors and should not be interpreted as representing the opinions or policies of the U.S. Geological Survey.

References

Association of Official Analytical Chemists (AOAC). 1990a. Method 973.18: Fiber (Acid Detergent) and Lignin in Animal Feed. 15th ed. Association of Official Analytical Chemists. Arlington, VA. ANKOM Technology Method 5 – Acid Detergent Fiber in Feeds – Filter Bag Technique for A200.

Association of Official Analytical Chemists (AOAC). 1990b. Method 990.03 Protein (crude) in Animal Feed. 15th ed. Association of Official Analytical Chemists. Arlington, VA. ANKOM Technology Method 6 – Neutral Detergent Fiber in Feeds – Filter Bag Technique for A200.

Cataldo, D.A., M. Maroon, L.E. Schrader, and V.L. Youngs. 1975. Rapid colorimetric determination of nitrate in plant tissue by nitration of salicylic acid. Commun. Soil Sci. Plant Anal. 6:71-80. 10.1080/00103627509366547.

Cole, J.A., and C.M. Brown. 1980. Nitrate reduction to ammonia by fermentative bacteria - short circuit in the biological nitrogen cycle. FEMS Microbiology Letters. 136: 1-11.

Dannehl, D., J. Suhl, C. Ulrichs, and U. Schmidt. 2015. Evaluation of Substitutes for RockWool as Growing Substrate for Hydroponic Tomato Production. Journal of Applied Botany and Food Quality. 88: 68–77.

Dong, L.F., C.J. Smith, S. Papaspyrou, A. Stott, A.M. Osborn, and D.B. Nedwell. 2009. Changes in benthic denitrification, nitrate ammonification, and anammox process rates and nitrate and nitrite reductase gene abundances along an estuarine nutrient gradient (the Colne Estuary, United Kingdom). Applied and Environmental Microbiology. 75:3171-3179.

Dunets, S. and Y. Zheng. 2014. Removal of phosphate from greenhouse wastewater using hydrated lime. Environmental Technology. 35:2852-2862, DOI: 10.1080/09593330.2014.924567

Gould, C.M. 2015. Bioenergy and anaerobic digestion. Bioenergy: biomass to biofuels. 297-317.

Gruyer, N., M. Dorais, B.W. Alsanius, and G.J. Zagury. 2013. Simultaneous Removal of Nitrate and Sulfate from Greenhouse Wastewater by Constructed Wetlands. Journal of Environment Quality 42: 1256-1266.

Guven, D., A. Dapena, B. Kartal, M.C. Schmid, B. Maas, K. van de Pas-Schoonen, S. Sozen, R. Mendez, H.J.M. Op den Camp, M.S.M. Jetten, M. Strous, and I. Schmidt. 2005. Propionate oxidation by and methanol inhibition of anaerobic ammonium-oxidizing bacteria. Applied and Environmental Microbiology. 71:1066-1071.

Hagopian, D.S., and J.G. Riley. 1998. A closer look at the bacteriology of nitrification. Aquacultural Engineering. 18:(4):223–244.

Hao, A., J.J. Heijnen, and M.C.M. Van Loosdrecht. 2002. Model-based evaluation of temperature and inflow variations on a partial nitrification-ANAMMOX biofilm process. Water Research. 36:4839-4849.

Jetten, M.S.M., I. Cirpus, B. Kartal, L. van Niftrik, K.T. van de Pas-Schoonen, O. Sliekers, S. Haaijer, W. van der Star, M. Schmid, J. van de Vossenberg, I. Schmidt, H. Harhangi, M. van Loosdrecht, J.G. Kuenen, H.O. den Camp, and M. Strous. 2005. 1994-2004: 10 years of research on the anaerobic oxidation of ammonium. Biochemistry Society Transactions. 33:119-123.

Park, J.B.K., R.J. Craggs, and J.P.S. Sukias. 2008. Treatment of hydroponic wastewater by denitrification filters using plant prunings as the organic carbon source. Bioresource Technology. 99(8):2711–16.

Park, J.B.K., R.J. Craggs, and J.P.S. Sukias. 2009. Removal of Nitrate and Phosphorus from Hydroponic Wastewater Using a Hybrid Denitrification Filter (HDF). Bioresource Technology. 100:3175–3179.

Prystay, W., and K.V. Lo. 2001. Treatment of Greenhouse Wastewater Using Constructed Wetlands. Journal of Environmental Science and Health, Part B. 36: 341–353.

Seo, D.C., W.Y. Park, J.S. Lim, and S.K. Park. 2008. Optimum configuration, filter media depth and wastewater load of small-scale constructed wetlands for treating the hydroponic waste solution in greenhouses. Korean Journal of Environmental Agriculture. 27:217-224.

Seo, D.C., J.H. Park, Y.S. Cheon, S.K. Park, A.R. Kim, W.G. Lee, S.W. Lee, S.T. Lee, J.S. Cho, and J.S. Heo. 2010. Treatment Efficiency of Pollutants in Constructed Wetlands under Different Hydroponic Wastewater Injection Methods and Characteristic of Filter Media. Korean Journal of Environmental Agriculture. 29(2): 146–51.

Sonneveld, C. 1981. Items for application of macro-elements in soilless culture. Acta Horticulturae. 126:187–195.

Van Soest, P.J., J.B. Robertson, and B., A. Lewis. 1991. Methods for dietary fiber, neutral detergent fiber, and non-starch polysaccharides in relation to animal nutrition. Journal of Dairy Science. 74:3583-3597.

Weber, C.F. 2016. Nutrient Content of Cabbage and Lettuce Microgreens Grown on Vermicompost and Hydroponic Growing Pads. Journal of Horticulture. 03 (04).

Yamamoto-Ikemoto, R., T. Komori, M. Nomuri, Y. Ide, and T. Matsukami. 2000. Nitrogen removal from hydroponic culture wastewater by autotrophic denitrification using thiosulfate. Water Science and Technology. 42(3-4): 369-376.

Yi, Q., L. Chaoxiang, D. Chunhong, L. Fengming, H. Hongying, H. Xia, and S. Hangchang. 2003. Study on Ability of Nitrification in a Subsurface Constructed Wetland System Treating Sewage. Huan jing ke xue= Huanjing kexue. 24(1):80-83.

Yi, W., K.V. Lo, D.S. Mavinic, P.H. Liao, and F. Koch. 2005. The Effects of Magnesium and Ammonium Additions on Phosphate Recovery from Greenhouse Wastewater. Journal of Environmental Science and Health -Part B Pesticides, Food Contaminants, and Agricultural Wastes. 40(2): 363–74.

Image caption: Water holding pools at a drinking water plant. Photo from iStock.

Nitroxyl – The Missing Link in NDMA Formation in Chloramine Systems

Huong T. Pham[1] and Julian Fairey[2]*

[1]Graduate Student, Department of Civil Engineering, University of Arkansas, Fayetteville, Arkansas 72701; [2]Associate Professor, Department of Civil Engineering, University of Arkansas, Fayetteville, Arkansas 72701
*Corresponding author, julianf@uark.edu

Abstract: The NDMA formation pathway in chloraminated drinking water remains unresolved. The goal for this project was to investigate the role of nitroxyl and peroxynitrite, both hypothesized chloramine decay intermediates and RNS, in the NDMA formation pathway in drinking water systems. Profiles of dichloramine decomposition, nitrous oxide formation, and dissolved oxygen consumption indicated the formation of nitroxyl and peroxynitrite, both RNS, from dichloramine hydrolysis. Experiments with of uric acid, a peroxynitrite scavenger, implicated peroxynitrite as a central node in the N-nitrosodimethylamine (NDMA) formation pathway. Revised unified chloramine kinetic model with nitroxyl as the heretofore unidentified intermediate (*I*) of dichloramine hydrolysis accurately simulated kinetic profiles of dichloramine, monochloramine, dissolved oxygen, and NDMA between pH 7 and 10, the pH range of interest in chloramine systems. The State of Arkansas has twelve public water systems using chloramines, serving a total approximately 100,000 people. These facilities are located throughout the state and have limited resources to dedicate to NDMA control strategies. An accurate understanding of the NDMA formation pathway during chloramination would facilitate development of strategies to curb NDMA formation and promote monochloramine stability. The main findings of the project were published in the journal *Environmental Science & Technology* (Pham, Wahman, & Fairey, 2021).

Key Points:

- Dichloramine, nitrous oxide, and dissolved oxygen profiles indicated the formation of nitroxyl and peroxynitrite, both reactive nitrogen species (RNS), from dichloramine decomposition.
- Experiments with uric acid, a peroxynitrite scavenger, implicated peroxynitrite as a central node in the N-nitrosodimethylamine (NDMA) formation pathway.
- Revised unified chloramine kinetic model with nitroxyl as the heretofore unidentified intermediate (*I*) of dichloramine hydrolysis accurately simulated kinetic profiles of dichloramine, monochloramine, dissolved oxygen, and NDMA between pH 7 and 10, the pH range of interest in chloramine systems.

Introduction

The USEPA Technical Fact Sheet for *N*-nitrosodimethylamine (NDMA) issued in November 2017 states that NDMA is a priority pollutant, classified as a B2 probable human carcinogen, and is a significant concern as a drinking water contaminant. Although industrial production of NDMA no longer occurs in the United States, NDMA still forms as an unintended by product of drinking water disinfection.

NDMA forms through various reaction pathways, and yields are largely dependent on the type of disinfectant with chloramines > ozone = chlorine dioxide > free chlorine (Pham, Wahman, Zhang, & Fairey, 2019). In Northwest Arkansas, the Carroll Boone Water District uses chloramines, which provides drinking water to approximately 13,000 customers in Harrison, Green Forest, Berryville and Eureka Springs. There are twelve public water systems in Arkansas that use chloramines, including Magnolia, Texarkana, and Waldron. Many rural water systems use chloramines to help meet the Stage 2 Disinfectants/Disinfection Byproduct rule and hence may experience elevated levels of NDMA. An accurate understanding of the NDMA formation pathway may lead to strategies to minimize its formation in chloramine systems.

The goal of this project was *to investigate the role of nitroxyl and peroxynitrite, both hypothesized chloramine decay intermediates, in the formation of NDMA in drinking water systems*. The widely accepted reaction mechanism for NDMA formation involves a nucleophilic substitution between dichloramine and unprotonated amine-based precursors to form an unsymmetrical dimethylhydrazine (UDMH), which then reacts with dissolved oxygen to form NDMA (Schreiber & Mitch, 2006). However, this latter reaction is spin-forbidden, meaning is likely kinetically unfavorable and therefore is unlikely to occur rapidly. This runs counter to our preliminary data which show rapid formation of NDMA at pH 10. This could have important implications for NDMA control strategies and other nitrogen-containing disinfection byproducts. A recent study also showed that nitrification in storage facilities and distribution systems can lead to elevated NDMA levels (Zeng & Mitch, 2016) but the underlying reaction mechanism was not determined. In this research, an NDMA formation pathway was investigated that involved RNS generated from the decomposition of dichloramine.

The research hypothesis was that nitroxyl (HNO/NO^-) was the key intermediate in NDMA formation, shown in Figure 1. Nitroxyl is known to react with dissolved oxygen to form peroxynitrite (Smulik et al., 2014), which is a known nitrosating agent, followed by the reaction with dimethylamine (DMA) to form NDMA.

Nitroxyl may form through at least four pathways, which are (1) abiotic pathway from the breakdown of dichloramine ($NHCl_2$), (2) biotic pathway in which monochloramine (NH_2Cl) reacts with hydroxylamine generated by nitrifying bacteria, (3) abiotic pathway through the reaction of hydroxide ion with monochloramine to form hydroxylamine, which then reacts with NH_2Cl and (4) free chlorine reaction with hydroxylamine generated through nitrification. In this project report, Pathway #1 was investigated.

Methods

Batch kinetic experiments were conducted using DMA, a model NDMA precursor, and dichloramine at pH 7, 8, 9, 10. All NDMA formation kinetic experiments were performed headspace free in 25 mL amber glass vials sealed with PTFE-lined screw top lids. DMA solutions were diluted with Milli-Q water to 25 µM DMA in a volumetric flask and adjusted with 40 mM buffer to the desired pH, along with peroxynitrite scavenger (uric acid) in certain experiments. Buffers used were bicarbonate for pH 10, borate for pH 9, and phosphate for pH 8 and 7. Monochloramine

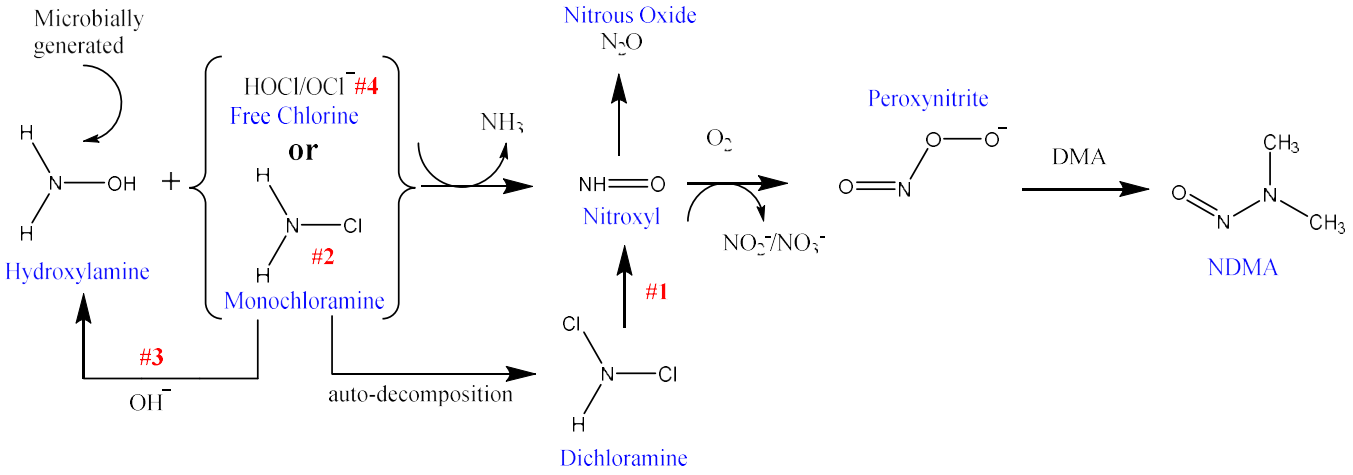

Figure 1: Proposed NDMA formation pathways (#1, #2, #3 and #4) with nitroxyl as the intermediate.

solutions at 2 mM were freshly prepared before each experiment following the procedure developed by Do, Chimka, and Fairey (2015) then adjusted to pH 3.7 with 2 N sulfuric acid and aged for 1 hour to make dichloramine. The pH of the dichloramine was not adjusted before mixing with DMA stock solution due to its fast decomposition at these conditions. Precisely 5 mL of the dichloramine solution was added to 10 mL of 25 µM DMA at the same pH and 5 mL of the corresponding buffer at 200 mM. Nitrous oxide (N_2O) and dissolved oxygen (DO) microelectrodes (Unisense) were used to quantify concentrations of these species kinetically.

Following the desired reaction time (up to 4 hours unless stated otherwise), 20 mL aliquots were quenched of chloramines with 0.5 g dry quenching mix containing 1.8 g ascorbic acid, 1 g KH_2PO_4 and 39 g Na_2HPO_4 (12.5 mM ascorbic acid in solution). After quenching, 10 mL samples were immediately extracted with dichloromethane at a 10:1 water:dichloromethane volume ratio using a back-and-forth shaker table at high speed for 15 minutes. Following a 5-minute quiescent settling period, dichloromethane was extracted with a Pasteur pipette and stored for NDMA analysis.

Monochloramine was kinetically quantified using Hach Method 10171 and total chlorine was quantified by DPD Method 8167. The difference between the total chlorine and monochloramine was assumed to be dichloramine.

NDMA was identified and quantified using gas chromatography–mass spectrometry (GC-MS). Splitless injections of 5 µL were used with an injector temperature was 250 °C. The separation column used was a RESTEK 12497 FAME-WAX with a length of 30 m, inner diameter 0.25 mm, with a stationary phase film thickness of 0.25 µm. Helium carrier gas was used with constant flow rate at 1.0 mL/min. The oven program was 45 °C for 3 minutes followed by a ramp of 25 °C/min to 130 °C and then 12 °C/min to 230 °C hold for 1 minute. The full scan and selected ion monitoring (SIM) mode were simultaneously. Six-point NDMA standard curves (10 – 1000 µg-L^{-1}) were used to quantify the concentrations of the unknown samples ($R^2 > 0.999$). Blanks and check standards were run after at least every ten injections. Standard solutions are prepared following the same procedure as samples.

The data were used for model validation because the key reactants (dichloramine and dissolved oxygen), stable intermediates (nitrous oxide) and products (NDMA) were kinetically quantified. The model was composed of i) the unified model of chloramine chemistry developed by Jafvert and Valentine (1992) ii) the nitroxyl kinetic reactions measured by Lymar and Shafirovich (2007) iii) the decomposition of peroxynitrite developed by Kirsch, Korth, Wensing, Sustmann, and de Groot (2003), and iv) the hypothesized NDMA formation reactions stemming from peroxynitrite. The three underlying models - Jafvert and Valentine (1992), Lymar and Shafirovich (2007) and Kirsch et al. (2003) – were previously validated. However, this work is the first to combine the unified model with the nitroxyl and peroxynitrite models and, as such, adjustments to the empirically derived RNS rate expressions were expected.

Results and Discussion

Figure 2 shows the impact of uric acid on NDMA formation at pH 7 – 10. A dose of uric acid at 200 µM and higher changed the dichloramine profiles and therefore, the upper limit was set at 160 µM. NDMA formation at pH 7, 8, and 9 had a dose-response relationship with uric acid. At pH 10, a decrease in NDMA formation was observed only after the uric acid concentration increase from 140 µM to 170 µM. The NDMA concentration decreased by about 50% with 120 µM uric acid at pH 9, 80% with 160 µM uric acid at pH 8, and 100% with 140 µM uric acid at pH 7.

Uric acid is a known scavenger for peroxynitrite and its decomposition products, such as $NO_2^{\bullet}$ and $CO_3^{\bullet-}$ radicals (Hooper et al., 2000; Hooper et al., 1998). While uric acid is non-selective and can also scavenge reactive oxygen species such as hydroxyl and superoxide radicals, Schreiber and Mitch (2006) ruled out the role of these species in the NDMA formation pathway by conducting scavenging experiments using tert-butanol and superoxide dismutase. Therefore, Figure 2 supported that (i) the majority of the NDMA formation occur through a peroxynitrite mediated pathway and (ii) peroxynitrite was associated with $NHCl_2$ decomposition.

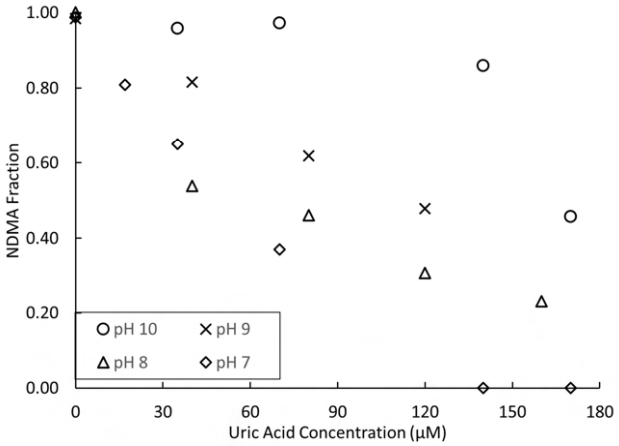

Figure 2: NDMA formation at 4 hours versus uric acid does in waters amended with 10 µM DMA, ca. 800 µeq Cl_2/L $NHCl_2$ and 40 mM corresponding buffer at pH 7, 8, 9 and 10.

Dichloramine hydrolysis was hypothesized to form nitroxyl, which can react with itself to form nitrous oxide (N_2O), a stable end-product. In a competing reaction, nitroxyl can also react with dissolved oxygen (DO) to form peroxynitrite. Therefore, detection of N_2O formation and DO consumption during dichloramine decomposition served as a nitroxyl formation marker. Figure 3 shows di-

chloramine, N_2O, NDMA, and DO kinetic profiles at pH 7 – 10. N_2O, NDMA and DO profiles track with $NHCl_2$ decomposition, indicating their linkage to $NHCl_2$ decomposition.

To assess the NDMA formation pathway through nitroxyl, a kinetic model, referred as UF+RNS model, was implemented in AQUASIM. The model was composed of the i) unified model of chloramine chemistry developed by Jafvert and Valentine (1992), ii) nitroxyl kinetic reactions in water measured by Lymar and Shafirovich (2007), iii) decomposition of peroxynitrite developed by Kirsch et al. (2003), and iv) NDMA formation through a direct reaction between DMA and dichloramine developed by Schreiber and Mitch (2006) along with v) the hypothesized formation of NDMA through peroxynitrite.

Table 1 shows the revised rate constants along with the corresponding standard errors. The reactions that needed revisions were (1) the hydrolysis of dichloramine, proposed to form nitroxyl, (2) nitroxyl and dichloramine, and (3) the reaction between DMA and dichloramine. The rate constants for these reactions were empirical, formulated to match chloramine species and NDMA formation only. Therefore, they were considered for re-estimation in the current project. The revised UF+RNS captured the kinetic

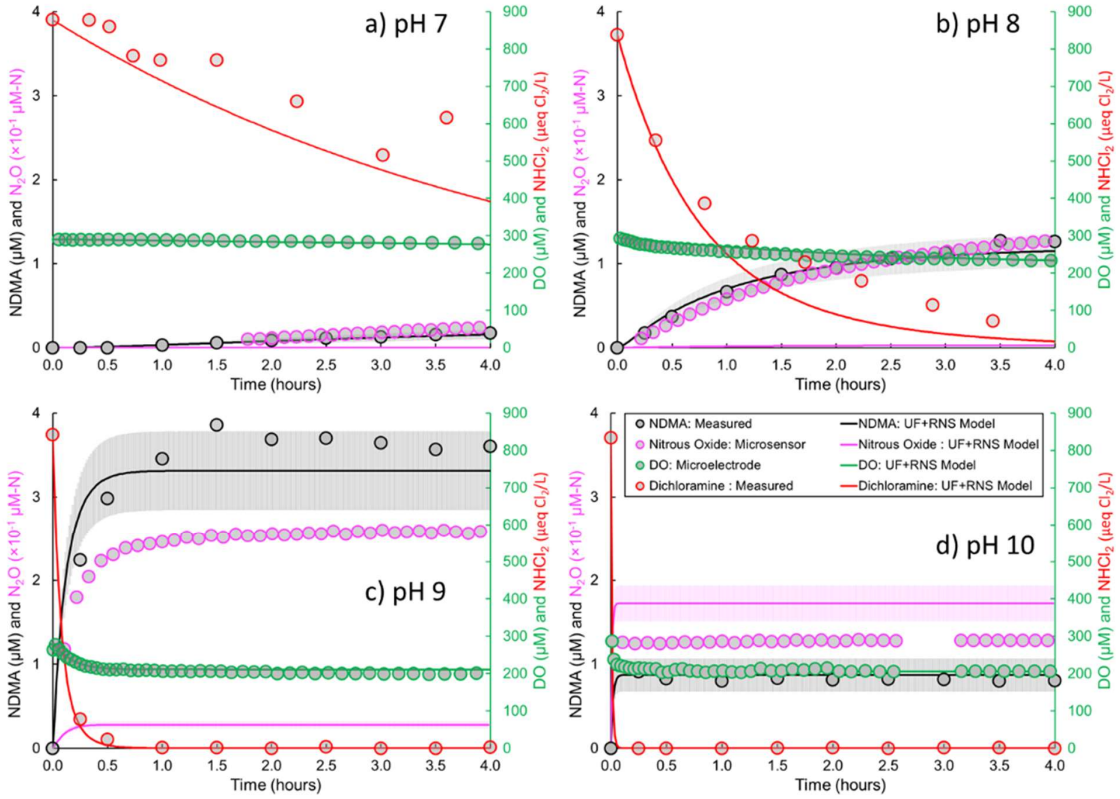

Figure 3: NDMA (black, primary y-axis), Nitrous Oxide (N_2O, magenta, primary y-axis), DO (green, secondary y axis) and Dichloramine ($NHCl_2$, red, secondary y-axis) profiles in waters dosed with ca. 800 μeq Cl_2/L $NHCl_2$ and containing 10 μM DMA buffered at (a) pH 7, (b) pH 8, (c) pH 9 and (d) pH 10. Points are measured values, lines are UF+RNS model simulations, and shaded areas are simulations encompassing one standard error in the estimated parameters (see Table 1).

Table 1. Revised reactions and rate constants implemented in the UF+RNS model. Estimated rate constants provided with their standard error.

		Rate Constant (M^{-1} s^{-1}, unless state otherwise)	
#	Reaction	Published	This work
U7	$NHCl_2 + H_2O \xrightarrow{k_{u7}} HNO + 2H^+ + 2Cl^-$	110	186 ± 6
U8	$HNO + NHCl_2 \xrightarrow{k_{u8}} HOCl$ + products	2.7×10^4	$(8.2 \pm 0.8) \times 10^4$
P5	$NHCl_2 + (CH_3)_2NH \xrightarrow{k_{p5}} (CH_3)_2NNHCl + H^+ + Cl^-$	52	28 ± 8
R7	$ONOOH + (CH_3)_2NH \xrightarrow{k_{r7}} (CH_3)_2NNO$ + products	NA	$k_{r7}=k_{r7A}\,[\exp(-k_{r7B}/[H^+])]$ $k_{r7A} = (2.1 \pm 0.4) \times 10^7$ M^{-1} s^{-1} $k_{r7B} = (4.4 \pm 0.3) \times 10^{-10}$ M
R8	$ONOOH + (CH_3)_2NNHCl \xrightarrow{k_{r8}} (CH_3)_2NNO$ + products	NA	$(1.3 \pm 0.8) \times 10^7$

profiles and yields of $NHCl_2$, DO, and NDMA at pH 7-10 (see Figure 3). Notably, at pH 9 and 10, the simulated DO and NDMA profiles matched the measured data in terms of kinetics and yields throughout the 4-hour time-course.

For additional discussion, please refer to Pham et al. (2021).

Conclusions

This project presented multiple lines of evidence to support that $NHCl_2$ hydrolysis resulted in HNO formation, heretofore referred as a unidentified reactive intermediate in the Jafvert and Valentine (1992) model. Once formed, nitroxyl reacted with dissolved oxygen to produce peroxynitrite, both RNS. Peroxynitrite and/or its decomposition products then reacted with unprotonated amine to form NDMA in the presence of DMA. Therefore, scavenging RNS such as nitroxyl and/or peroxynitrite may curb NDMA formation in chloramine systems.

Further research should consider additional nitroxyl formation pathways independent of $NHCl_2$ (Figure 1, pathway #3 and #4). The reaction of NH_2Cl with NH_2OH implicated nitroxyl and peroxynitrite formation (Wahman, Speitel, & Machavaram, 2014), providing a potential mechanism to evaluate and explanation of enhanced NDMA formation during nitrification episodes (Zeng & Mitch, 2016).

Acknowledgements

This material is based upon work supported by the United States Geological Survey under grant agreement No. G16AP00040 and administered by the Arkansas Water Resources Center. The views and conclusions contained in this document are those of the authors and should not be interpreted as representing the opinions or policies of the U.S. Geological Survey.

References

Do, T. D., Chimka, J. R., & Fairey, J. L. (2015). Improved (and Singular) Disinfectant Protocol for Indirectly Assessing Organic Precursor Concentrations of Trihalomethanes and Dihaloacetonitriles. Environ Sci Technol, 49(16), 9858-9865 doi:10.1021/acs.est.5b01304

Hooper, D. C., Scott, G. S., Zborek, A., Mikheeva, T., Kean, R. B., Koprowski, H., & Spitsin, S. V. (2000). Uric acid, a peroxynitrite scavenger, inhibits CNS inflammation, blood–CNS barrier permeability changes, and tissue damage in a mouse model of multiple sclerosis. The FASEB Journal, 14(5), 691-698 doi:https://doi.org/10.1096/fasebj.14.5.691

Hooper, D. C., Spitsin, S., Kean, R. B., Champion, J. M., Dickson, G. M., Chaudhry, I., & Koprowski, H. (1998). Uric acid, a natural scavenger of peroxynitrite, in experimental allergic encephalomyelitis and multiple sclerosis. Proceedings of the National Academy of Sciences of the United States of America, 95(2), 675-680 doi:10.1073/pnas.95.2.675

Jafvert, C. T., & Valentine, R. L. (1992). Reaction Scheme for the Chlorination of Ammoniacal Water. Environ Sci Technol, 26(3), 577-586 doi:Doi 10.1021/Es00027a022

Kirsch, M., Korth, H. G., Wensing, A., Sustmann, R., & de Groot, H. (2003). Product formation and kinetic simulations in the pH range 1-14 account for a free-radical mechanism of peroxynitrite decomposition. Archives of Biochemistry and Biophysics, 418(2), 133-150 doi:10.1016/j.abb.2003.07.002

Lymar, S. V., & Shafirovich, V. (2007). Photoinduced release of nitroxyl and nitric oxide from diazeniumdiolates. Journal of Physical Chemistry B, 111(24), 6861-6867 doi:10.1021/jp070959+

Pham, H. T., Wahman, D. G., & Fairey, J. L. (2021). Updated Reaction Pathway for Dichloramine Decomposition: Formation of Reactive Nitrogen Species and N-Nitrosodimethylamine. Environ Sci Technol doi:10.1021/acs.est.0c06456

Pham, H. T., Wahman, D. G., Zhang, W., & Fairey, J. L. (2019). N-Nitrosodimethylamine (NDMA) Formation Mechanisms in Drinking Water Systems. Encyclopedia of Water, 1-14 doi:doi:10.1002/9781119300762.wsts0037

Schreiber, I. M., & Mitch, W. A. (2006). Nitrosamine formation pathway revisited: the importance of chloramine speciation and dissolved oxygen. Environ Sci Technol, 40(19), 6007-6014 doi:10.1021/es060978h

Smulik, R., Debski, D., Zielonka, J., Michalowski, B., Adamus, J., Marcinek, A., . . . Sikora, A. (2014). Nitroxyl (HNO) Reacts with Molecular Oxygen and Forms Peroxynitrite at Physiological pH Biological Implications. Journal of Biological Chemistry, 289(51), 35570-35581 doi:10.1074/jbc.M114.597740

Wahman, D. G., Speitel, G. E., Jr., & Machavaram, M. V. (2014). A proposed abiotic reaction scheme for hydroxylamine and monochloramine under chloramination relevant drinking water conditions. Water Res, 60, 218-227 doi:10.1016/j.watres.2014.04.051

Zeng, T., & Mitch, W. A. (2016). Impact of Nitrification on the Formation of N-Nitrosamines and Halogenated Disinfection Byproducts within Distribution System Storage Facilities. Environ Sci Technol, 50(6), 2964-2973 doi:10.1021/acs.est.5b05668

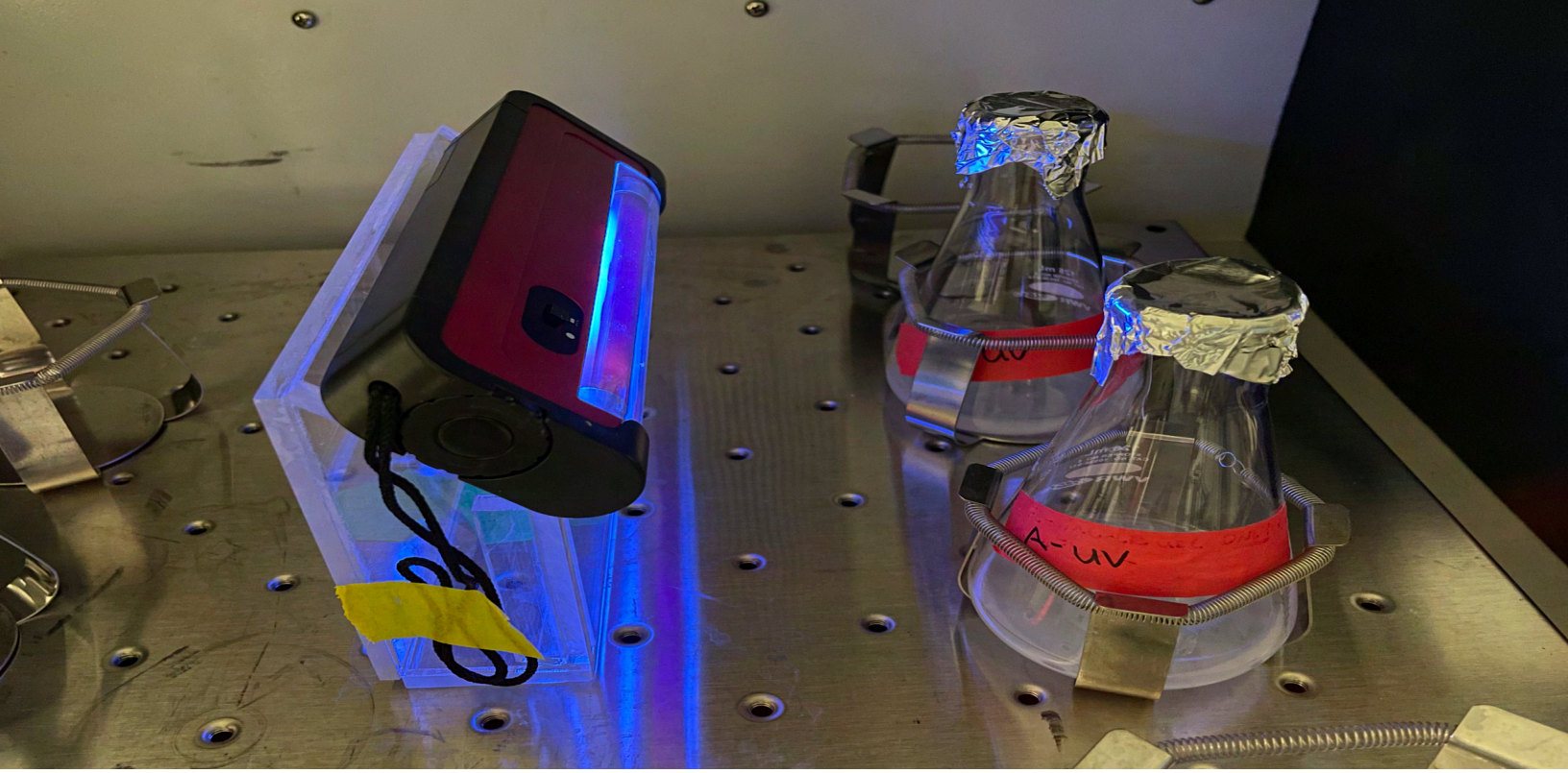

Image caption: A glimpse into the general experimental setup utilized. Flasks containing MC-LR, TiO_2, and DI water are exposed to UV light while being mixed. Normally, this is covered as to not allow outside light to interfere with the UV treatment. Photo courtesy of Zane Wood.

In Situ Cyanotoxin Mitigation: Net Design to Enhance Photocatalytic Degradation Mechanisms

Dr. Lauren Greenlee[1] and Dr. Wen Zhang[2]*

[1]Associate Professor, Ralph E. Martin Department of Chemical Engineering, University of Arkansas, Fayetteville, Arkansas 72701; [2]Associate Professor, Department of Civil Engineering, University of Arkansas, Fayetteville, Arkansas 72701
*Corresponding author, wenzhang@uark.edu

Abstract: Harmful algal blooms (HABs) and their associated cyanotoxins cause negative environmental, water quality, and human health impacts, however, no in situ treatment approach currently exists that can treat both HAB cyanobacteria and cyanotoxins. This study investigated the dispersed and immobilized photocatalytic titanium dioxide (TiO_2) nanoparticles for the removal of microcystin-LR (MC-LR) cyanotoxin in water. MC-LR adsorption testing on uncoated and 5x coated TiO_2 nets resulted in 0% and 13% adsorption, respectively. The 5x coated TiO_2 net removed MC-LR by 96%, 64%, and 10% for UV, indirect UV, and no UV exposure over 2 hours. MC-LR removal by 5x coated TiO_2 nets fit pseudo first-order kinetics, where the rate constant was k=0.0264 min-1 for 5x coated TiO_2 nets. Overall, the study indicated TiO_2 photocatalysts coated on nylon supports provide an immobilization approach for in-situ MC-LR removal by TiO_2 nanoparticles. Given the prevalence and importance of surface waters in the state of Arkansas for human recreation, environmental health, fresh water supply, and municipal/industrial development, the occurrence of HABs has a direct impact on Arkansas state economic vibrancy and environmental health. This work will benefit environmental quality for the State of Arkansas and the broader Mississippi River Basin by providing a feasible in situ treatment of cyanotoxin caused by HAB.

Key Points:

- A TiO_2 spray-coated nylon mesh achieves 96% MC-LR removal in water.
- Pseudo first-order kinetics were established for degrading microcystin-LR with immobilized TiO_2 nanoparticles.
- This study demonstrates the feasibility of in situ treatment of cyanotoxins.

Introduction

Harmful algal blooms (HABs) have been recognized as global phenomenon that can have devastating consequences: they produce cyanotoxins or accumulate biomass that alter the food web dynamics, adversely impacting the health of humans, livestock and wildlife (Anderson et al., 2002). As a result, it is a national interest to prevent, control and mitigate HABs. Currently there are no effective treatment methods for *in situ* and simultaneous treatment of cyanobacteria and cyanotoxin. As eutrophication worsens in water bodies due to excessive nutrients discharge from anthropogenic activities, it is imperative to develop an effective *in situ* treatment method that can inactivate cyanobacteria and degrade cyanotoxins simultaneously, without deleterious impacts on the aquatic ecosystem.

In our initial collaborative work together, we have demonstrated a novel treatment approach that would allow mitigation of both HABs and their cyanotoxins in the water source; our approach is innovative in that it uses the concept of a reusable and retrievable fishing net to apply a catalytic environment locally to an HAB The local application of a net at the HAB/cyanotoxin source prevents the spread of HAB/cyanotoxin and minimizes unwanted catalytic reactions, resulting in point-source treatment with few negative side effects. Our preliminary results suggest that HAB cyanobacteria can be removed via physical coagulation. As a result, the goal of this research is to design a TiO_2 nanoparticle-net configuration that enables optimized cyanotoxin degradation. The cyanotoxin compound, microcystin-LR, was tested as representative of the ten cyanotoxins on the Fourth Unregulated Contaminant Monitoring Rule established by the Environmental Protection Agency (EPA).

Methods

Spray Coated TiO_2 Net Preparation

A 1:6 mass ratio Nafion to TiO_2 methanol solution was made by diluting and mixing concentrated TiO_2 nanoparticles and concentrated Nafion ionomer with methanol. Woven, 100 μm hole nylon mesh was cut into 4 cm by 4 cm squares and encased in aluminum foil on all sides but the front. Airbrush tubing was connected to an air supply, which was turned on to a constant and consistent airflow. A 250 μL volume of 1:6 mass ratio Nafion to TiO_2 methanol solution was added to the fluid cup, and a coat of the solution was applied evenly onto the surface of the nylon net. Additional spray coats of solution were applied once a previous coat dried for approximately 2 minutes and was dry to the touch. Nylon nets were spray coated 2, 5, and 8 times with TiO_2 and Nafion solution. Spray coated nets were left overnight in a hood to dry completely before analysis and experiments.

Spray Coated TiO_2 Net Analysis

SEM and EDX were utilized to observe net surfaces and to confirm TiO_2 attachment, and SEM and LA-ICP-MS were used to analyze net stability in a water environment that mimicked MC-LR experimental conditions (e.g., 100 rpm mixing of deionized water on an orbital shaker) for 0, 24, and 72 hours. Prior to SEM and EDX, all nets were sputter coated with gold for 1 minute to ensure charge for imaging and mapping. EDX mapping utilized titanium and carbon elements, which were acquired for 3 minutes. LA-ICP-MS utilized 10-line scans per net to obtain average count rates of Ti47, which was used as the reference material for titanium detection. Since laser ablation is destructive, new net samples were made for all repeats.

Spray Coated TiO_2 Net Experiments

Once thawed overnight, stock MC-LR was mixed then diluted and used for all samples within a batch. Concentrated MC-LR was pipetted into a 100 mL fused quartz Erlenmeyer flask filled with water to reach a 200 ppb starting concentration. The flask was stirred by hand for no more than 20 seconds to ensure complete mixing of MC-LR in water. Once stirred, an initial t=0 min time sample was taken and added to a centrifuge tube. An uncoated or spray coated TiO_2 nanoparticle net was added to the appropriate flask. Once a net was added to the flask, the solution and net were stirred by hand for an additional 20 seconds, and a second t=0 min time sample was taken and added to a centrifuge tube. The flask was capped with a rubber stopper and placed on an orbital shaker rotating at 100 rpm for 60 minutes, and a t=60 min sample was taken to observe possible MC-LR adsorption to net surfaces either free of or spray coated with nanoparticles. Following 60-minute adsorption tests, experimental solutions were exposed to UV light (365 nm wavelength and 230 $\mu W/cm^2$ intensity at 3 inches), indirect UV light (365 nm wavelength and <230 $\mu W/cm^2$ intensity), or no UV light using an angled UV lamp. For experiments using UV light with a spray coated net, samples were taken at 10-minute intervals for 30 minutes followed by 15-minute intervals for 90 minutes and added to centrifuge tubes. For experiments using uncoated nets as well as for experiments without UV light, samples were taken 60 minutes and 120 minutes after the initial 60-minute interval and added to centrifuge tubes. All samples were centrifuged at 7800 rpm for no more than 20 minutes. Sample solutions were transferred from centrifuge tubes to glass autosampler vials and analyzed using LC-MS. MC-LR standards (0, 10, 50, 100, 150, 200 ppb) were used for LC-MS analysis, and the multiple reaction monitoring (MRM) peak values for standards were used to create a standard curve. Sample MRM peak values were compared to the standard curve to obtain a MC-LR concentration profile for each experimental set. All experiments were performed in triplicate.

Results and Discussion

TiO_2 Attachment on Nylon Nets

TiO_2 solution was sprayed onto nylon nets one time (1x), twice (2x), five times (5x), and eight times (8x). With each spray application, the nanoparticles appear agglomerated, where agglomeration is more evident as a function of increased spray coats. To confirm TiO_2 solution attachment to nylon nets, uncoated and TiO2 coated nets were assessed using EDX mapping. In Figure 1, EDX images for a 5x spray coated TiO_2 net are shown at 300 µm, 50 µm, and 10 µm. Significant amounts of agglomerated titanium contrast carbon in the images at all scales, and the net is largely covered in TiO_2. Note that EDX is a qualitative tool, and the goal of EDX mapping images is to indicate relative TiO_2 attachment rather than quantitative results. The EDX for uncoated and 2x spray coated nets demonstrates limited or minimal titanium spectral intensity, which indicates a lack of significant TiO_2 attachment onto the net surface. As a result, 5x spray coated nets were used in the cyanotoxin degradation experiments.

MC-LR Adsorption onto Spray Coated TiO_2 Nets

The theoretical TiO_2 particle mass loadings were 2.5 mg, 6.25 mg, and 10 mg, respectively, for the 2x, 5x, and 8x spray nets, and the theoretical mass loading for 0.25 g/L dispersed TiO_2 was 6.25 mg. Therefore, the amount of TiO_2 present on 5 spray net surfaces was comparable to the amount of TiO_2 present for dispersed 0.25 g/L TiO_2 experiments when volume is taken into account. Experimental batches that utilized uncoated and 5x coated TiO_2 nets underwent a 1-hour adsorption test prior to incorporating UV exposure. For uncoated nets and 5x coated TiO_2 nets, the average adsorption percentages were -3% and 13%, respectively. The -3% adsorption value for the uncoated net implies an average 0% adsorption, which is expected since no TiO_2 nanoparticles are present on the nets for adsorption of MC-LR onto TiO_2 to occur. The 13% adsorption percentage for TiO_2 falls within the average calculated standard deviations and is most likely due to experimental losses and fluctuations with MC-LR, such as attachment onto experimental containers or detection using LC-MS instrumentation. The 13% value is not significant enough to signify that adsorption is predominant.

LC-MS data for MC-LR degradation using 5x spray coated and uncoated nets over 2 hours are shown in Figure 2, where 5x coated TiO_2 net and uncoated net experiments are represented in Figure 2a and Figure 2b, respectively. In Figure 2a, the decrease in MC-LR concentration for no UV, indirect UV, and UV exposure using 5x coated TiO_2 nets was 10%, 64%, and 96%, respectively, from 0 minutes to 120 minutes. The indirect UV experiments utilized a less intense light source compared to the UV light experiments, and a MC-LR degradation trend that fell between direct UV and no UV results was observed. For direct UV exposure, results show rapidly decreased MC-LR concentration as a function of time, which indicates significant MC-LR degradation over the 120-minute time period. The average starting concentration was 175 ppb MC-LR, and after 2 hours under direct UV conditions with the 5x spray coated net, the MC-LR concentration decreased to 8 ppb on average. For the 5x spray coated net with UV, error spread decreased as time progressed. Larger spread is observed between 0 minutes and 75 minutes, and minimal error spread occurred for 90, 105, and 120 minutes. Although there is more variability up to 75 minutes, the 5x spray coated net consistently degrades MC-LR below 25 ppb after 75 minutes. Results for uncoated net exposure to no UV, indirect UV, and UV conditions

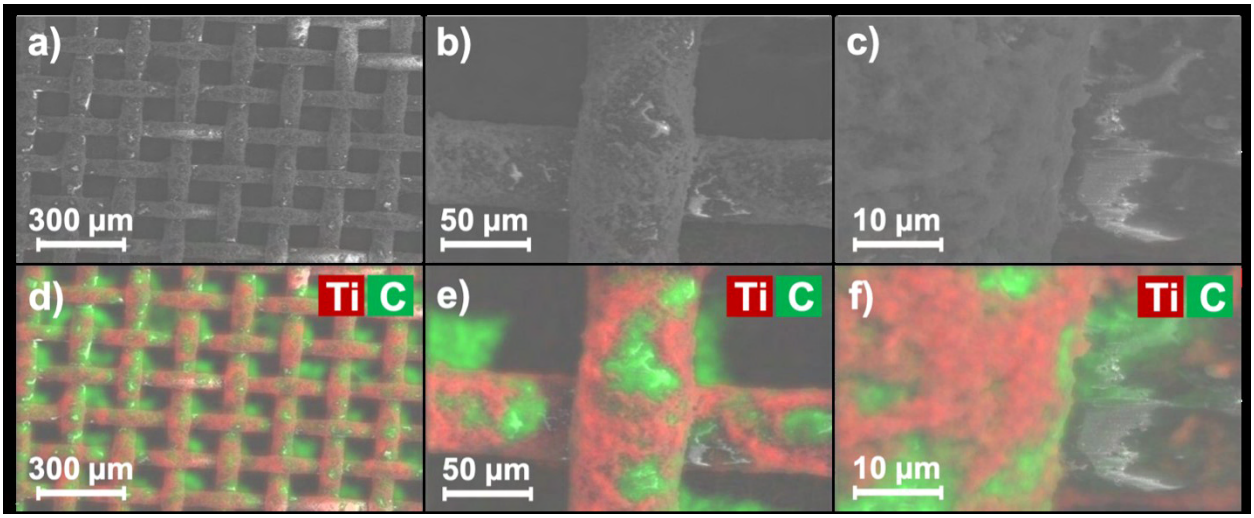

Figure 1: EDX mapping for 5x spray coated TiO_2 net, consisting of 1:6 mass ratio Nafion ionomer to TiO_2 nanoparticles on nylon netting. Mapping was acquired for roughly 3 min per image. The mapping images show the 5x spray coated TiO_2 net at (a) 300 µm, (b) 50 µm, and (c) 10 µm scales. All samples were sputter coated with gold for roughly 1 min prior to EDX mapping.

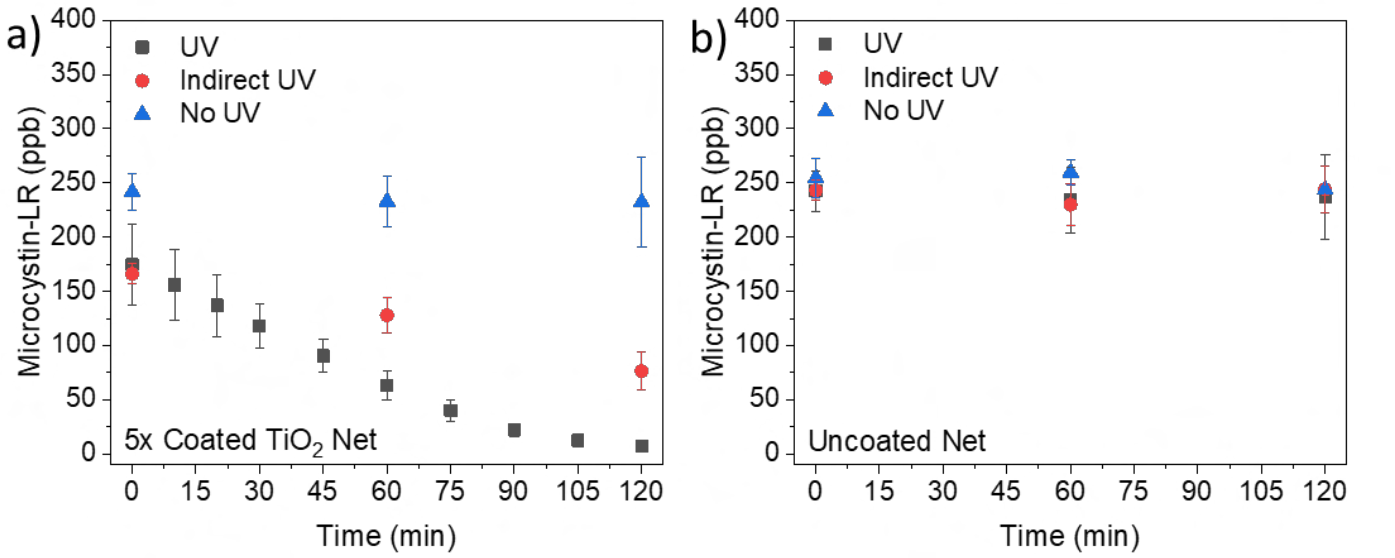

Figure 2: LC-MS data show MC-LR degradation using a MC-LR theoretical starting concentration of 200 ppb and a (a) 5x coated TiO_2 net or (b) uncoated nylon net with UV light (365 nm wavelength with 230 μW/cm² intensity at 3 inches), indirect UV light (365 nm wavelength with <230 μW/cm² intensity), or no UV light exposure. All experiments were done in triplicate.

are shown in Figure 2b. While slight variations in average MC-LR concentrations occur over the 2-hour time period, MC-LR consistently remains at about 250 ppb, where calculated standard deviations for each time point are ≤ ±8%. No photocatalytic nanoparticles were present on the surface of uncoated nets, so no MC-LR degradation was expected.

Although systems used between authors are variable, studies have repeatedly shown and proven the ability of dispersed TiO_2 nanoparticles to degrade MC-LR under UV conditions. Pinho et al. utilized a pilot scale solar photoreactor to degrade 100 μg/L MC-LR with 200 mg/L TiO_2 in roughly 32 minutes (Pinho et al., 2015). Lawton et al. observed rapidly degraded MC-LR, where 200 μg/mL MC-LR was degraded to nearly zero after 20 minutes of UV light exposure in the presence of TiO_2 catalyst (1% m/v) (Lawton et al., 1999). In addition to further showing the ability of dispersed TiO_2 to degrade MC-LR under light conditions, the work presented in this study solidifies the capability of spray coated nanoparticle nets to perform equivalently to dispersed nanoparticles.

Kinetic Analysis

Data representing MC-LR degradation by 5x coated TiO_2 nets were fitted to pseudo zeroth, first, and second order kinetics. First order kinetics have the correlation coefficient (i.e., R^2 value) closest to 1 (i.e., 0.965) compared to zeroth and second order. Using pseudo first-order kinetics, the rate constant (k) was 0.0264 min^{-1} for 5x coated nets. Shephard et al. utilized a photoreactor using immobilized TiO_2 on a fiber glass sheet to degrade 55 g/mL MC-LR with TiO_2 ranging from 0.2-1 g/L and fit degradation data to first order kinetics, where the rate constant was 0.117 min^{-1} (Shephard et al., 2002). Feng et al. fit 20 μg/L MC-LR degradation data using nano-TiO_2 thin film to pseudo first-order kinetics and obtained a rate constant of 0.0157 min^{-1} (Feng et al., 2006). This work demonstrates that the rate constant for 5x coated TiO_2 nets is similar to dispersed TiO_2 data in literature studies.

Conclusions

This study investigated the development and performance of immobilized TiO_2 nets utilizing nylon mesh supports for direct microcystin-LR degradation in comparison to dispersed TiO_2. Nets spray coated with a 6.25 mg (5x spray coats) theoretical mass loading were observed to be more homogeneous and evenly coated with TiO_2 solution compared to nets with 2.5 mg (2x spray coats) and 10 mg (8x spray coats) particle loading. 5x spray coated TiO_2 nets were tested under various UV exposure conditions, where 96% and 64% MC-LR removal was observed for 5x coated nets with direct (230 μW/cm²) and indirect (<230 μW/cm²) UV over a 2-hour time period. MC-LR removal was not indicated for uncoated nets under varying UV and 5x coated TiO_2 nets with no UV applied. The final MC-LR concentration was 8 ppb after degradation. The study has shown that the degradation of MC-LR followed pseudo first-order reaction kinetics for 5x coated TiO_2 nets. Overall, 5x coated nets are capable of degrading MC-LR similarly to dispersed TiO_2 nanoparticles under UV conditions, suggesting that immobilized TiO_2 does not hinder degradation ability for MC-LR. In addition, varying UV conditions and UV intensity

play crucial roles in MC-LR degradation, where sufficient UV light intensity and TiO_2 nanoparticle concentrations are necessary to effectively degrade MC-LR over time.

The feasibility of utilizing TiO_2-immobilized nets in a water environment for the treatment of MC-LR cyanotoxins has implications for both natural and engineered water systems. Direct, in-situ MC-LR treatment using retrievable TiO_2 immobilized netting could degrade toxins in natural surface waters (e.g., lakes and ponds). Direct treatment could help alleviate cyanotoxin level spikes in recreational water over blooming periods, making water safer. Additionally, since water treatment facilities struggle with treating cyanotoxin-rich waters, direct treatment method could aid in decreasing microcystin toxins prior to transport and processing at facilities.

Acknowledgements

This material is based upon work supported by the United States Geological Survey under grant agreement No. G16AP00040 and administered by the Arkansas Water Resources Center. The views and conclusions contained in this document are those of the authors and should not be interpreted as representing the opinions or policies of the U.S. Geological Survey.

References

Anderson, Donald M, Patricia M Glibert, and Joann M Burkholder. 2002. Harmful algal blooms and eutrophication: nutrient sources, composition, and consequences, Estuaries, 25: 704-26.

Feng, Xiaogang, Fei Rong, Degang Fu, Chunwei Yuan, and Yan Hu. 2006. Photocatalytic degradation of trace-level of microcystin-LR by nano-film of titanium dioxide, Chinese Science Bulletin, 51: 1191-98.

Lawton, Linda A, Peter KJ Robertson, Benjamin JPA Cornish, and Marcel Jaspars. 1999. Detoxification of microcystins (cyanobacterial hepatotoxins) using TiO_2 photocatalytic oxidation, Environmental science & technology, 33: 771-75.

Pinho, Livia X, Joana Azevedo, Angela Brito, Arlete Santos, Paula Tamagnini, Vitor JP Vilar, Vítor M Vasconcelos, and Rui AR Boaventura. 2015. Effect of TiO_2 photocatalysis on the destruction of *Microcystis aeruginosa* cells and degradation of cyanotoxins microcystin-LR and cylindrospermopsin, Chemical Engineering Journal, 268: 144-52.

Shephard, Gordon S, Sonja Stockenström, David de Villiers, Willem J Engelbrecht, and Gabriël FS Wessels. 2002. Degradation of microcystin toxins in a falling film photocatalytic reactor with immobilized titanium dioxide catalyst, Water Research, 36: 140-46.

Image caption: Produced water collected from a hydraulic fracturing facility in Texas, USA. Photo courtesy of Mahmood Jebur.

Integrated Electrocoagulation/Ultrafiltration-Membrane Distillation-Crystallization for Treating Hydraulic Fracturing Produced Water

Mahmood Jebur[1], Yelyzaveta Bachynska[2], and Ranil Wickramasinghe[3]*

[1]PhD student, Department of Chemical Engineering, University of Arkansas, Fayetteville, Arkansas 72701; [2]Undergraduate Student, Department of Chemical Engineering, University of Arkansas, Fayetteville, Arkansas 72701; [3]Professor, Department of Chemical Engineering, University of Arkansas, Fayetteville, Arkansas 72701
*Corresponding author, swickram@uark.edu

Abstract: In this work, produced water (PW) generated from hydraulic fracturing was treated using an integrated electrocoagulation/ultrafiltration, membrane distillation and crystallization processes (EC/UF-MDC). The focus of this work was to determine the feasibility of this integrated process for increasing water recovery. The results of this work suggest that optimizing the various unit operations in this integrated process could be used to recover PW. All membrane based separation processes suffer from membrane fouling. Pretreatment of the feed is essential to suppress fouling of the membrane. Here electrocoagulation (EC) followed by ultrafiltration (UF) was used to achieve high removal efficiency of both total suspended solids (TSS) and total organic carbon (TOC). Dissolved organic compounds are known to foul the hydrophobic membrane used in MD. In this study, a significant reduction in membrane fouling was obtained, which can lead to a long-term durability of MD system. In addition, the use of membrane distillation crystallization (MDC) can help mitigate the scale formation. Crystallization in the feed tank was used to suppress scale formation on the MD membrane. The integrated EC/UF-MDC process can have a potential impact on Water Resources/Oil & Gas Companies. By treating and reusing PW, preservation of surface and groundwater forming 80% of the water utilized in hydraulic fracturing could be achieved. In addition, treating PW will reduce the amount of PW directly disposed in Class II disposal wells, which further address the main cause of earthquakes.

Key Points:

- A high TOC removal efficiency was obtained using the combined EC/UF system by reducing the TOC concentration from 395 to 23.3 mg/L.
- Applying crystallization after MD (described as MDC) can lead to an increase in water recovery and reduce scale formation caused by inorganic compounds.
- A long-term MDC experiment with regeneration showed that the polyvinylidene fluoride (PVDF) membrane can be totally recovered with more than 95% membrane regeneration by simply running DI water on both sides of the membrane for 1 hour.

Introduction

Currently, unconventional shale gas and oil is the fastest growing sector for U.S. energy supply. Hydraulic fracturing combined with horizontal drilling is a technology used to enable the exploitation of abundant oil and gas resources that were previously unreachable (Warpinski et al., 2008). The extraction of shale gas using this advanced technique has increased from 14 % of the U.S. natural gas production in 2004 to 97 % in 2018. A drastic increase in water usage for hydraulic fracturing has been observed due to this increase in shale gas production (Perrin, 2019; Vidic et al., 2013). In hydraulic fracturing, water is mixed with chemicals and pumped at high pressure through the well bore to fracture tight rock formations. Then, the pressure is reduced, and the water flows back to the surface as flowback and PW. The amount of PW generated during the extraction period of each well is around 15 to 23 million liters (Malakoff, 2014). In general, approximately 116 billion liters of PW are produced in U.S. annually (Rosenblum et al., 2016). In the Fayetteville shale, about 20.06 million liters of water was used per well (A. Kondash & Vengosh, 2015).

Due to the increase in water demand, PW needs to be treated and reused. Treating PW is very challenging because it contains a wide range of contaminants including high total dissolved solids (TDS) concentration, high total suspended solids (TSS), polar and non-polar organic compounds, and low surface tension dissolved species (Luek & Gonsior, 2017; Orem et al., 2014). Deep well injection is the current accepted practice to manage PW. Deep well injection practices have several drawbacks such as the limitation of available deep well injection sites, the cost of transporting PW to the available sites, and the effects of deep well injection practices on enhancing earthquakes. There are few options available to treat PW. Distillation based technologies such as multistage flash distillation or integrating evaporation, crystallization, and spray drying is an option to treat PW (Baig et al., 2011). Even though these techniques can treat high TDS brines with significant recovery, they still suffer from some drawbacks, such as high cost, large footprint, and the use of chemicals (Morillo et al., 2014).

Membrane technology is another option used to treat high TDS brines, such as reverse osmosis (RO). Brines with a TDS below 50,000 mg/L can be successfully treated using RO. However, at a high TDS (> 50,000 mg/L) RO cannot be used because the applied pressure on the feed side is less than the osmotic pressure (Duong et al., 2015; Pérez-González et al., 2012). Membrane distillation (MD) is a promising technique that can be used to treat high TDS PW. In MD, a microporous hydrophobic membrane is used as a barrier between the feed and permeate streams. Due to the vapour pressure difference resulting from the temperature difference between the feed and permeate, the water vapour molecules will transport from the feed stream (warm brines) to the permeate (cold) stream. The advantage of using MD instead of other known membrane techniques is that the feed TDS concentration has little effect on the separation process, which means MD is relatively insensitive to the feed salinity so it can be used to treat a high TDS brine (Deshmukh et al., 2018; Yun et al., 2006). In direct contact membrane distillation, which is used in this study, the feed and permeate streams are in direct contact with the two surfaces of the membrane (Lin et al., 2014).

However, MD like all other membrane technologies still suffers from fouling and wetting propensity of the membrane, which affect its long-term performance (Kafuku & Mbarawa, 2013). While development of new high performance membranes is essential, our focus here is on development of an integrated process that maximizes water recovery. Consequently, we use commercially available polyvinylidene fluoride (PVDF) membranes. Here, we evaluated the feasibility of using the integrated EC/UF-MDC to address the issues of both scaling and wetting and maximize water recovery. The integrated EC/UF-MDC system could be used to successfully treat PW and overcome most of the drawbacks faced by using other techniques. Using the integrated EC/UF-MDC operation can provide several advantages such as low cost, small footprint, treating high TDS brines, and mitigating the membrane wetting and scaling.

Our preliminary results showed that using the electrocoagulation (EC) as a pretreatment step is essential to mitigate fouling and wetting. In fouling, a deposition of suspended or dissolved substances on the membrane surface and/or within its pores will occur resulting in a decrease of the membrane permeability. However, in wetting, the water will starts flowing into the membrane pores causing a deterioration of permeate quality (Sardari et al., 2018). In electrocoagulation a sacrificial electrode (anode) is frequently used. By applying an electrical current, metal ions are released into the solution to generate a variety of metal hydroxides as shown in the following reactions $M_{(s)} \rightarrow M^{n+}_{(aq)} + ne^-$ (at anode) and $2H_2O + 2e^- \rightarrow 2OH^- + H_2$ (at cathode), where M is often Al or Fe (Fayad, 2018). Various metal complexes form; such as $M(OH)^{(n-1)+}$, $M(OH)_2^{(n-2)+}$ and $M_6(OH)_{15}^{(6n-15)+}$, and can contribute in neutralizing the negatively charged organic species and suspended solids. These metal complexes can convert to amorphous $M(OH)_{n(s)}$ particles as the solution ages. Organic compounds and suspended solids can easily be adsorbed and trapped by $M(OH)_{n(s)}$ particles, which eventually are deposited as floc (Gamage & Chellam, 2014). The EC unit was directly followed by Ultrafiltration (UF) unit to remove all formed particulate matter more quickly than by sedimentation of the floc particles.

Employing crystallization after EC/UF-MD can mitigate membrane fouling and scaling by reducing the formation of crystal nuclei in the bulk feed, specifically when using

PW having a high TDS concentration, which is more likely causing scale formation. The EC/UF-MDC technology can also offer a potential solution to the high TDS brine disposal by recovering both water and minerals at high rates, which can lead to a nearly zero liquid discharge (G. Chen et al., 2014; Edwie & Chung, 2013). In this research, we did test the optimized operating conditions in the EC/UF-MDC system. This research evaluated the feasibility of using EC/UF-MDC system to recover water and minerals from shale gas PW. This technology can have a potential impact on Water Resources/Oil & Gas Companies because surface water and groundwater form about 80% of the water utilized in hydraulic fracturing (H. Chen & Carter, 2016). Further about 95% of the collected PW is directly disposed in Class II disposal well (A. J. Kondash et al., 2017). Using deep well injection may not be always available due to the new regulations that may be issued in the future. Some studies show that there is a strong connection between deep well injection of PW and earthquakes, which could be the main reason to apply new regulations to minimize or eliminate the deep well injection of PW (Rubinstein, n.d.). To preserve water resources, reduce the cause of earthquakes and manage fracturing wastewater, treating and reusing PW is very essential. The EC/UF-MDC could be an effective technology to treat and reuse PW to obtain high water recovery.

The overall objective of this research is to achieve high recovery rates of water and minerals from shale gas PW. Integrating EC/UF-MDC is essential to address the problem of scaling and wetting in MD. EC unit can provide high removal efficiency of TSS and total organic carbon (TOC). This can mitigate the wetting problems and providing a long-term durability of the membrane in MD system. Crystallization unit can reduce scaling in the membrane cell by decreasing the formation of crystal nuclei in the feed bulk. This can provide an attractive technical advancement capable for treating shale gas PW. Figure 1 shows the concept of a combined EC/UF-MDC processes for PW treatment.

Methods

PW Characterization

Two types of PW (A and B) collected from a hydraulic fracturing facility in Texas, USA was analyzed at the Arkansas Water Resources Center, University of Arkansas (Fayetteville, AR, USA). The EPA standard methods 160.1, 160.2, 415.1 and 180.1 were used to measure TDS, TSS, turbidity and TOC (Metcalf et al., 1991) , respectively. In addition, the EPA methods 200.7 and 300.0 were also used to measure cations and anions, respectively. Conductivity was measured using conductivity meter (VWR, Radnor, PA).

Membrane characterization

The membrane static water contact angles were measured using a sessile drop contact angle goniometer (Model 100, Rame-Hart Instrument Company, Netcong, NJ, USA). The DI water droplet volume used in water contact angle was 2 µL introduced at a rate of 0.5 µL/s. In water contact angles, the measurements were applied after allowing the droplet to stabilize for 10 sec. For each membrane, the average value of three contact angle measurements obtained at three different locations was reported and used in this study.

For each membrane before and after MD or MDC, both the surface morphology and elemental analysis were obtained using scanning electron microscopy (SEM) and energy-dispersive X-ray (EDX) spectroscopy, respectively, using Nova Nanolab 200 Duo-Beam Workstation (FEI, Hillsboro, OR, USA).

EC/UF pretreatment

Figure 2 shows a diagram of the EC/UF system. In this work, the custom-built polycarbonate continuous reactor having a total volume of 1078 cm^3 (dimensions of 7 cm x 11 cm x 14 cm) was designed and fabricated, which was used to conduct all the continuous EC experiments. Five aluminum electrodes were fitted vertically inside the reactor with a 10 mm inter-electrode spacing. A DC power supply (Hewlett Packard, Palo Alto, CA, USA) was connected to a reverse

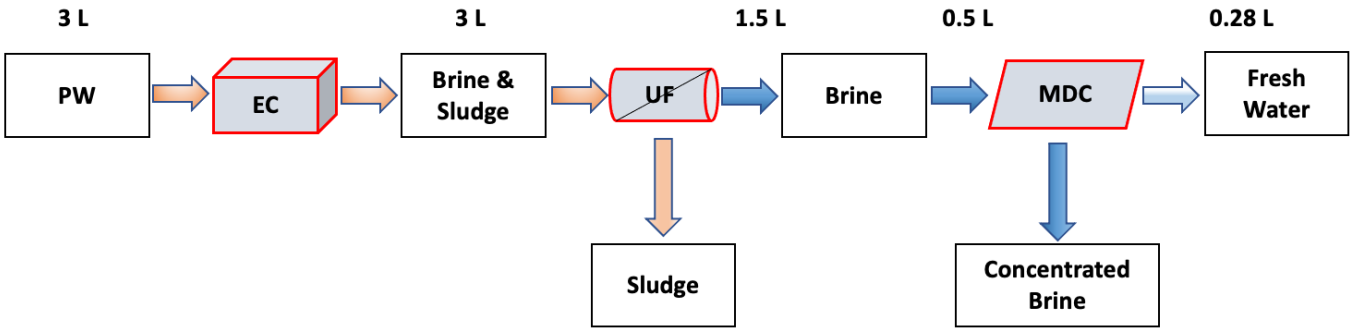

Figure 1: Diagram of the combined EC/UF-MDC process investigated in this work.

polarity switch which enabled the direction of the current to alternate every 30 sec. This is essential to prevent formation of a passivation layer on the electrode which would suppress further reactions (Cañizares et al., 2007; Timmes et al., 2010).

UF was conducted immediately after EC using a UF ceramic membranes cell purchased from CeraMem® (Waltham. MA, USA). Honeycomb-like ceramic membrane module having a nominal average pore size of 10 nm with active membrane area of 0.13 m^2 was used in crossflow mode. The entire 3 L of EC treated PW was placed in the UF feed tank. Initially, the feed was recirculated through the membrane module by means of a diaphragm pump (P800, King-Kong, Taiwan) while the permeate outlet was closed. The permeate side pressure was essentially at atmospheric pressure, while the feed pressure was 70 kPa at a feed flow rate of 2.5 L/min. The permeate outlet was opened once steady state had been reached. Then, the permeate water was collected in the permeate tank, which was placed on a computer-connected analytical balance (Mettler Toledo, Columbus, OH). The permeate flux was calculated based on the rate of permeate collection in the permeate tank. About 50% of the EC treated water was recovered. After each experiment, the membrane was cleaned by circulating hot DI water for 1 hour prior to starting a new experiment.

MDC treatment

Figure 3 shows the diagram of the direct contact membrane distillation (MD) system used in this work. The MD module is a custom-made acrylic membrane cell with 2 mm deep channels and 40 cm^2 effective membrane area. For mechanical support and mixing, PTFE spacers (ET 8700, Industrial Netting, Minneapolis, MN, USA) were applied in the membrane module. By using two peristaltic pumps (Masterflex I/P, Cole Parmer, Vernon Hills, IL), the feed and permeate streams were pumped on opposite sides of the membrane at 0.5 L/min in counter current flow. A computer-connected analytical balance (Mettler Toledo, Columbus, OH, USA) was used to measure and record the weight of the permeate. The temperature of the permeate and feed tanks was maintained at 20°C and 60°C using an external chiller and heater, respectively (PolyScience, Niles, IL, USA).

In crystallization, the feed tank was placed in a water bath after recovering 10% of the feed volume to maintain the temperature at 20°C for 5 min and induce precipitation in the feed tank to suppress scale formation on the membrane surface due to supersaturation of the feed. Then, the feed water was filtered using a paper filter (10 µm) to remove the formed salt crystals in the feed water. In this way, we may help increasing water recovery and limit scale formation on the membrane surface. After that, the feed water was returned to the MD system and pumped through a heat exchanger to increase the temperature of the feed entering the MD module to 60 °C.

Based on the weight change of the permeate tank, the water flux was calculated and normalized using the initial average flux during the first 15 min of operation. The permeate conductivity was continuously monitored using a conductivity meter (VWR, Radnor, PA, USA). Each MD or MDC experiment was conducted using 500 ml of real or pretreated EC/UF PW. A membrane regeneration cycle was conducted during the long-term MDC experiment once 40% of the feed volume was recovered or there was no weight increase of the permeate for 20 min. Regeneration of the membrane involved pumping DI water on both sides of the membrane at 0.5 L/min for 1 hour. A commercial superhydrophobic PVDF membrane having a pore size of 0.65 µm was used in all the MD and MDC experiments conducted in this study. The PVDF membrane was purchased from MilliporeSigma (Billerica, MA, USA).

Results and Discussion

Wastewater characterization

Two types of PW (A and B) were treated with chlorine dioxide at the hydraulic fracturing facility to remove bacteria and iron prior to receival. The water quality parameters of both PW A and B as received from the hydraulic fractur-

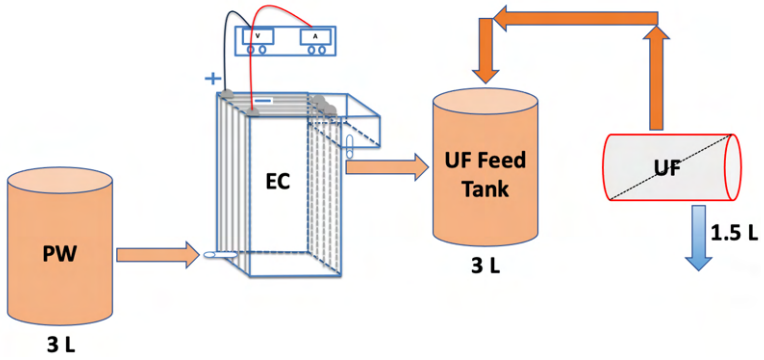

Figure 2: Diagram showing the EC/UF system investigated here.

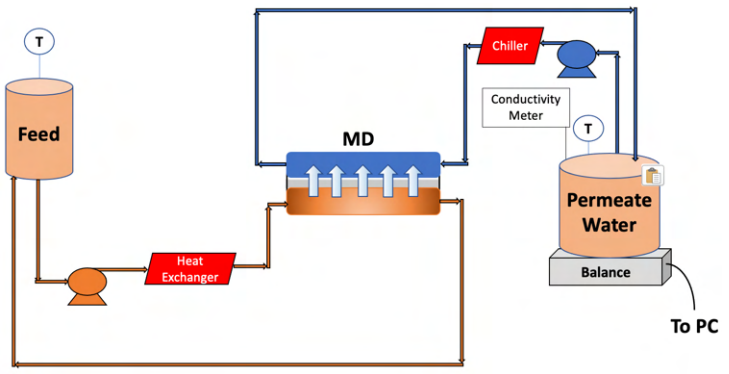

Figure 3: Diagram of MD system used in this study.

ing facility as well as after the pretreatment step of EC/UF are shown in Table 1. The TDS is very high, being about 4 times and 7 times more than seawater for PW A and PW B, respectively. Chlorine, calcium, magnesium potassium and sodium are the majority of the inorganic ions present in PW. Membrane scaling can be caused by a high concentration of calcium ions due to the precipitation of calcium sulfate (Sardari et al., 2019). The TOC and TSS are also high about 395 mg/L and 187 mg/L, respectively for PW A. The quality of the PW in general is highly variable, which affects the efficiency of the treatment operations.

Table 1: Water quality analysis for PW received from the hydraulic fracturing facility and after the EC/UF pretreatment operation.

Parameter	Unit	PW A*	EC/UF PW A**	PW B*	EC/UF PW A**
TDS	mg/L	137247	121037	245300	239760
TOC	mg/L	395	23.3	120	44
TSS	mg/L	187	76.4	131	48
Turbidity	NTU's	147	0.6	6	0.3
pH	-----	7.4	7.3	6.7	3.9
Chloride	mg/L	83117	94350	156820	166170
Sulfate	mg/L	545	786	478	430
Aluminum	mg/L	0	0	0	64
Iron	mg/L	0.7	0	0.2	0.7
Calcium	mg/L	2396	N/A	30500	31700
Magnesium	mg/L	383	419	5454	5335
Potassium	mg/L	1089	906	4331	4680
Sodium	mg/L	55902	44308	63600	68100
Conductivity	µS/cm	166300	312000	323400	229000
Total Phosphorus	mg/L as P	4.9	7.3	0.015	N/A

Note: * is real produced water received from the hydraulic fracturing facility; ** is pretreated produced water using electrocoagulation followed by ultrafiltration.

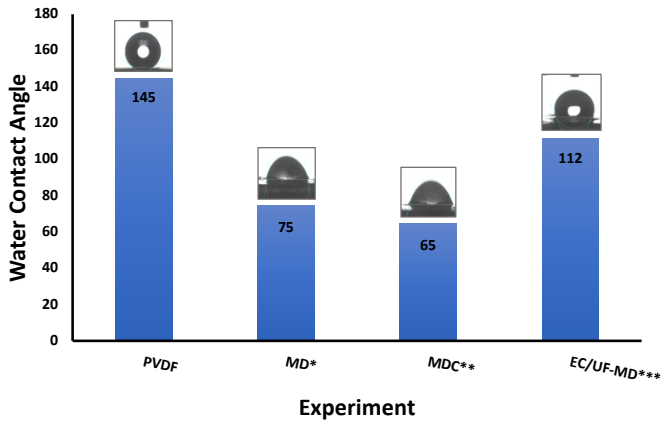

Figure 4: The water contact angle measurements of PVDF membranes before and after MD or MDC experiment.
Note: PVDF is a fresh membrane before MD or MDC experiment; * is PVDF membrane after membrane distillation of real PW A; ** is PVDF membrane after membrane distillation crystallization of real PW A; *** is PVDF membrane after membrane distillation crystallization of EC/UF pretreated real PW A.

Membrane characterization

The water contact angle of PVDF membranes before and after MD and MDC experiments is shown in Figure 4. As can be seen the PVDF fresh membrane before MD and MDC has a large water contact angle of 145 indicating a superhydrophobic membrane. This is essential for MD as only water vapor should pass through the membrane pores. The membrane should be resistant to wetting by water. However, Figure 4 shows that the adsorption of dissolved organic compounds on the membrane surface could lead to a significant decrease in the water contact angle as obtained in PVDF membranes after MD (water contact angle of 75) and MDC (water contact angle of 65) of real PW A. These compounds could lead to scale deposition on the layer of adsorbed organic compounds if they are polar (Sardari et al., 2018). Therefore, applying a pretreatment step using EC/UF to remove most of the organic compounds and suspended solids can help in mitigating the decrease in contact angle as shown in Figure 4. The PVDF membrane after MD of EC/UF pretreated real PW A has a high water contact angle of 112.

Figure 5 shows the SEM images of all the PVDF membranes before and after MD and MDC. Table 2 shows a list of the MD and MDC experiments. In this study, we did focus on presenting the MD and MDC results using PW A at 0.5 L/min flow rate. The SEM images of unused PVDF membrane as well as membranes after, MD, MDC, EC/UF-MD, and EC/UF-MDC are given in Figure 5A, 5B, 5C, 5D, and 5E, respectively. As can be seen some deposition (highlighted with circle) on the membrane surface is observed after MD, while very minimum deposition is observed after MDC and specifically MDC of EC/UF pretreated PW A. This means that applying a pretreatment step using EC/UF followed by MD and then crystallization can successfully suppress scale formation on the membrane surface due to supersaturation of the feed and scale deposition on the layer of adsorbed organic compounds.

The elemental analysis of all PVDF membranes used in this study was obtained using energy-dispersive X-ray (EDX). The average elemental ratios of carbon/fluorine (C/F) and oxygen/fluo-

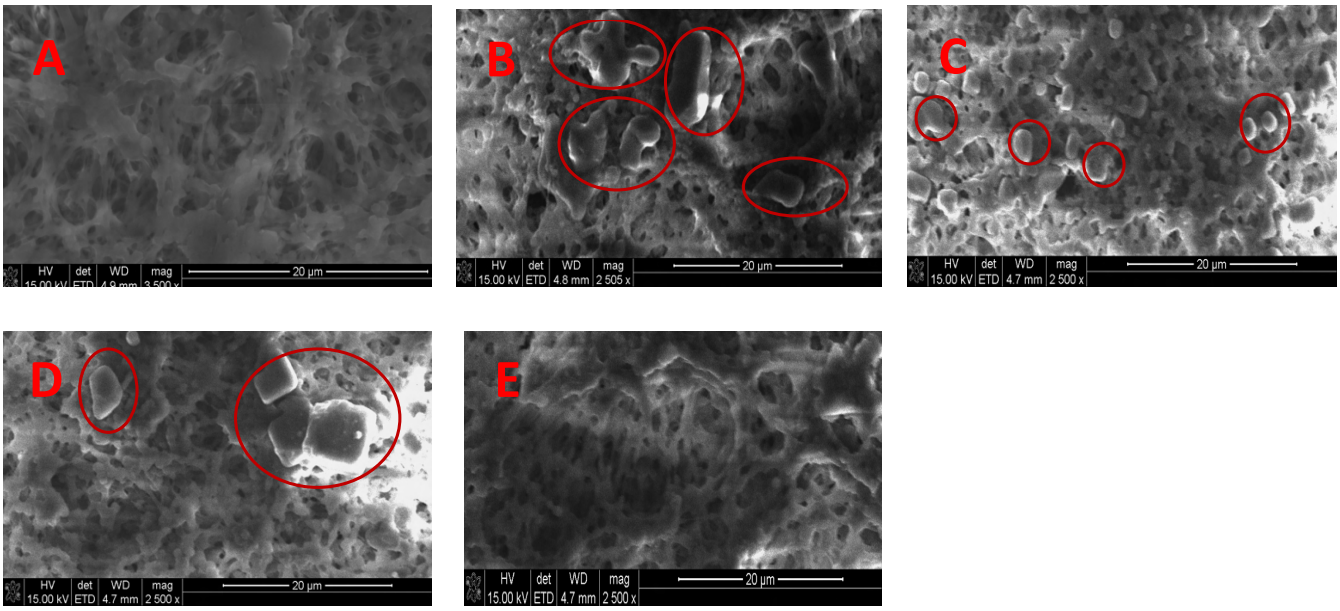

Figure 5: SEM images of the membrane surface before (fresh PVDF) and after MD or MDC: 5A is fresh PVDF membrane; 5B is PVDF membrane after MD of real PW A; 5C is PVDF membrane after MDC of real PW A; 5D is PVDF membrane after MD of pretreated EC/UF PW A; and 5E is PVDF membrane after MDC of pretreated EC/UF PW A.

Table 2: Lists of the MD and MDC experiments conducted here.

#	Experiment Type	PW Type	Flux	XRD	SEM/ EDX	Whole Analysis
1	MD of real PW at 0.5 L/min flow rate*	A	Done	Done	Done	
2	MDC of real PW at 0.5 L/min flow rate*	A	Done	Done	Done	
3	EC/MF-MD of real PW at 0.5 L/min flow rate*	A	Done	Done	Done	Done
4	EC/MF-MDC of real PW at 0.5 L/min flow rate*	A	Done	Done	Done	
5	MD of real PW at 0.14 L/min flow rate	A	Done		Done	
6	MDC of real PW at 0.14 L/min flow rate	A	Done		Done	
7	Regeneration MDC of real PW at 0.5 L/min flow rate*	A	Done			
8	MD of real PW at 0.14 L/min flow rate	B	Done	Done	Done	
9	MDC of real PW at 0.14 L/min flow rate	B	Done	Done	Done	
10	EC/MF-MD of real PW at 0.14 L/min flow rate	B	Done	Done	Done	Done
11	EC/MF-MDC of real PW at 0.14 L/min flow rate	B	Done	Done	Done	
12	Regeneration MDC of real PW at 0.5 L/min flow rate*	B	Done			

Note: * means the experiments that are used in this report

rine (O/F) for PVDF membranes after MD and MDC are given in Table 3. As can be seen the C/F and O/F ratios are high for PVDF membranes after MD and MDC of real PW A with no pretreatment, which is mainly due to the organic fouling. However, the C/F and O/F ratios are low for PVDF membranes used in MDC of EC/UF pretreated PW A due to the high removal efficiency of organic compounds achieved by EC followed by UF.

EC performance

In EC, the reduction of water takes place at the cathode forming hydroxide ions, while aluminum ions are generated continuously at the anode. A variety of aluminum hydroxides are produced in the solution when coagulating ions (aluminum and/or hydroxide ions) undergo hydrolysis in water. Introducing aluminum hydroxides can help destabilize suspended, emulsified, and dissolved contaminants, which can further aggregate and precipitate as sludge or lift up to the surface as flocs. The aggregated aluminum hydroxides will adsorb soluble organic compounds. This adsorption phenomenon is a result of the liquid-solid intermolecular attraction forces between the adsorbable solute in the solution and the large surface area of the porous floc that form.

In this work, only the first and last electrodes are con-

Table 3: The C/F and O/F atomic percent ratios for PVDF membranes after MD and MDC of both real PW A and pretreated EC/UF PW A.

Membranes	C/F atom percental ratio	O/F atom percental ratio
PVDF after MD*	2.4	0.37
PVDF after MDC*	1.8	0.23
PVDF after MD**	1.7	0.19
PVDF after MDC**	1.6	0.12

Note: * is PVDF for MD or MDC of real PW A; ** is PVDF for MD or MDC of EC/UF pretreated real PW A.

nected to the power supply in a bipolar series (BPS) configuration to simplify the electrical connections. Also, the BPS configuration was used in previous studies, which show an enhancement in the TOC removal. In our previous work, several batch EC experiments were conducted to determine the appropriate EC current and reaction time. A range of currents (1 to 3 A) and a reaction time of 5 min were studied in this work. Each EC experiment was conducted continuously using 3 L of real PW A. After EC, treated water was removed from the sludge and settled floc. The recovered pretreated water samples were analyzed and the TOC removal for the recovered water was defined as, TOC removal (%) $=((X_{pw}-X_{rw})/X_{pw}) \times 100$. Where, X_{pw} and X_{rw} are the TOC in the PW A and recovered water after EC, respectively.

Table 4 describes the TOC removal at different applied current using EC in continuous mode. As can be seen, the TOC removal increases from 65 % to 74 % as the current increases from 1 to 3 A. To obtain higher TOC removal, higher current and longer reaction time were required. A long continuous EC experiment was also conducted at 3 A current and 5 min reaction time to evaluate the feasibility of EC in obtaining a consistent TOC removal. Figure 6 shows that a consistent TOC removal (> 70%) was achieved when conducting EC in continuous mode even after 100 min. The TOC in the treated PW A that was the feed for UF and MD was 102 mg/L and 23.3 mg/L, respectively.

UF performance

The variation of permeate flux with time is shown in Figure 7. First, the ceramic membrane was tested with DI water to determine the initial DI flux of 270 L m^{-2} h^{-1} bar^{-1}. Then, the ceramic membrane was used to filter an EC pretreated PW A. The flux gradually decreased to 71 L m^{-2} h^{-1} bar^{-1} and stabilized at 70 L m^{-2} h^{-1} bar^{-1} even after 100 min. The decrease in flux with time is due to the deposition of flocs on the membrane surface. The membrane was regenerated after 50% recovery by simply recirculating the hot water for 1 hour and tested with DI water. The DI water flux shows a similar initial flux value. The initial flux was about 300 L m^{-2} h^{-1} bar^{-1}. The result suggests that EC was effective at flocculating the dissolved organic compounds and particle matter that could plug the pores of the UF ceramic membrane. Also, regenerating the UF membrane by circulating hot water is sufficient to remove flocs from the membrane surface resulting in a minimal irreversible fouling.

Table 4: The TOC removal of PW A treated using EC in continuous mode at different operating conditions current (1, 2, and 3), 5 min reaction time and using 5 Al electrodes in BPS configuration.

No.	Sample Name	TOC ppm	RE of TOC %
1	EC continuous, PW A at 1A current	140	65
2	EC continuous, PW A at 2A current	124	68
3	EC continuous, PW A at 3A current	102	74

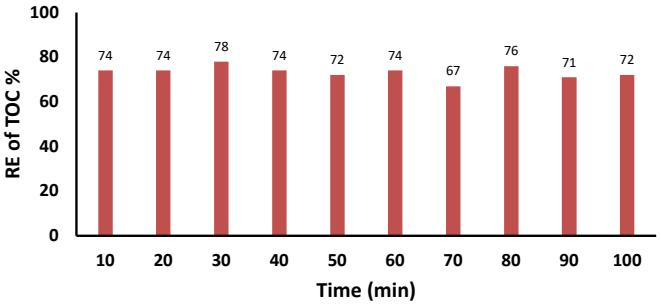

Figure 6: Total organic carbon (TOC) removal efficiency of EC treated PW A in continuous mode at 3 A current and 5 min reaction time (Long-term continuous EC experiment).

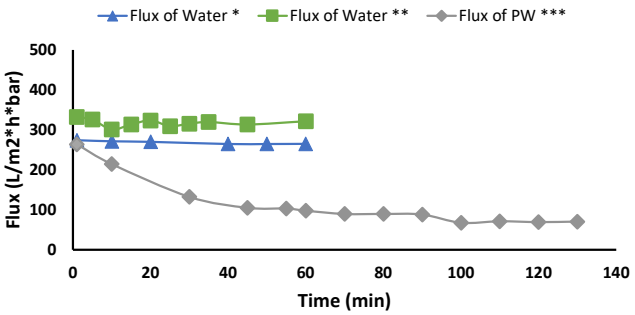

Figure 7: UF flux of water and EC treated PW A. Note: * is water flux before using EC pretreated PW A; ** is water flux after using EC pretreated PW A and cleaning with hot water; *** is the permeate flux of using EC pretreated PW A to recover about 50% of the feed volume.

MD and MDC performance

In MDC, the experiment was conducted in several runs. Each run was stopped after recovering 10% of the feed volume. Then, the feed tank was placed in water bath and maintained at 20°C for 5 min, which is considered as a crystallization step. After that the feed water was filtered to remove any formed crystal before starting the next run. To maximize the water recovery and membrane life, we would like to promote precipitation in the feed reservoir during crystallization, not on the membrane surface. The normal-

ized flux versus time for commercial PVDF membranes used in MD and MDC of real PW A with no pretreatment is shown in Figure 8. For real PW A, applying MDC can enhance the water recovery resulting in more stabilized flux as shown in Figure 8. The conductivity of the permeate samples collected from both MD and MDC experiments gradually increased due to transporting volatile inorganic compounds such as ammonium chloride from the feed stream to the permeate stream. The concentration of ammonium in the permeate samples was in the range of 10 to 18 mg/L. Table 5 summarizes the volume of the feed water recovered as well as the salts produced. Here, the use of MDC minimized the risk of supersaturation and precipitation on the membrane surface. During crystallization, precipitation was observed in the feed tank.

Figure 9 shows the normalized flux versus time for commercial PVDF membranes using MD and MDC of EC/UF pretreated real PW A. A similar flux profile was observed when using MD and MDC of EC/UF pretreated PW A. The combined EC/UF pretreatment step reduced the TOC in PW A to around 23.3 mg/L, which can help mitigating the deposition of polar organic compounds on the membrane surface and further decreasing the likelihood of precipitation of dissolved salts on the layer of adsorbed organic species

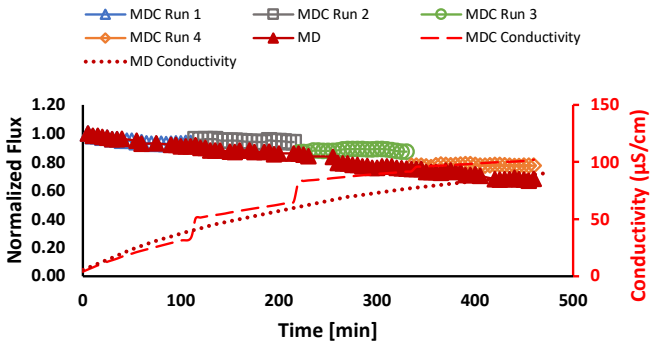

Figure 8: Normalized flux versus time for commercial PVDF membrane using MD and MDC of real PW A at 0.5 L/min flow.
Note: In each MDC Run, 10 % of the feed volume was recovered.

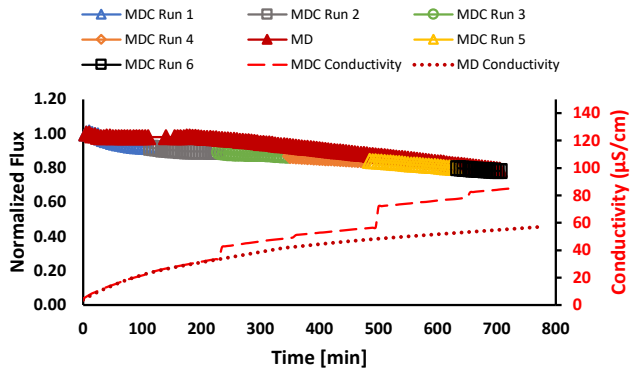

Figure 9: Normalized flux versus time for commercial PVDF membranes using MD and MDC of EC/UF treated PW A at 0.5 L/min flow. Note: In each MDC Run, 10 % of the feed volume was recovered or there was no weight increase of the permeate for 20 min.

resulting in a very similar membrane performance between MD and MDC. Crystallization showed no significant differences in membrane performance when comparing MDC and MD of EC/UF pretreated PW A, which is mainly due to first reducing the layer of adsorbed organic species, which further decreasing the likelihood of precipitation of dissolved salts on the membrane surface, and second not reaching the supersaturation limit after recovering about 55% of the feed volume.

A salt recovery of 42 kg/m^3 was obtained during the MDC of PW A by cooling the feed water after each run at 20 °C for 5 min. The X-ray diffraction (XRD) analysis was conducted to identify the purity of the salts produced via MDC. Figure 10 shows the XRD patterns of crystals produced during MDC of PW A. The results indicate that the main salts formed is halite (sodium chloride), a monovalent ion of low crystallinity, as shown in Figure 10.

A high water recovery was obtained when using MDC with regeneration as shown in Table 5 indicating that 198 ml of permeate removed in the first cycle for the commercial PVDF membrane after 4 runs. Then the membrane was regenerated by simply running DI water on both sides of the membrane for 1 hour. The normalized flux for the second cycle shown in Figure 11 was similar to first cycle indicating that most of the adsorbed species were removed by simply flushing the membrane with water. During the second cycle, a desired total permeate volume of 201 ml was recovered. This means that the commercial PVDF membrane using MDC could be regenerated and reused to recover more water.

In addition, the MDC experiment with regeneration was conducted using PW B as shown in Figure 12. The first cycle was conducted for 3 runs resulting in a water recovery of 118 ml with a decrease in the normalized flux in 1st cycle run 3. However, after cleaning with water, the normalized flux increased and stabilized for two runs resulting in a water recovery of 100 ml. The conductivity of the permeate water after MDC of PW B was not high indicating that there are no volatile inorganic compounds such as ammonium chloride moved from the feed stream to the permeate stream.

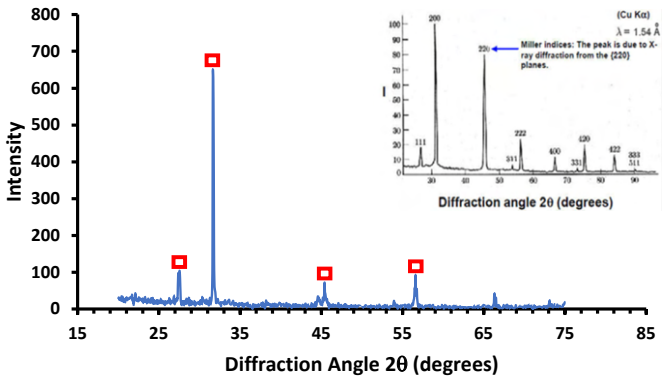

Figure 10: XRD spectra of salts produced in MDC of PW A spectra as well as XRD spectra of NaCl as standard shown in inset.

Table 5: Summary of water and salt recovery using PVDF membranes after MD and MDC of real PW

Experiment	Water Recovery (ml)	Salt Recovery (kg/m^3)
MD PW A (high flow 0.5 L/min)	183	N/A
MDC PW A (high flow 0.5 L/min)	205	42
MD EC/UF PW A (high flow 0.5 L/min)	281	N/A
MDC EC/UF PW A (high flow 0.5 L/min)	277	N/A
MDC PW A with regeneration (high flow 0.5 L/min) 1st Cycle	198	N/A
MDC PW A with regeneration (high flow 0.5 L/min) 2nd Cycle	201	N/A

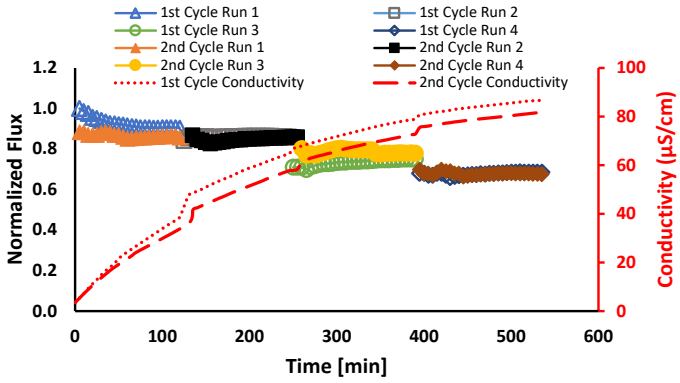

Figure 11: Normalized flux versus time for commercial PVDF membranes usng MDC of real PW A at 0.5 L/min flow (long experiment with regeneration). Note: 1st Cycle was obtained by conducting MDC for 4 runs resulting in 40% water recovery; 2nd Cycle was conducted for 4 runs after cleaning the membrane.

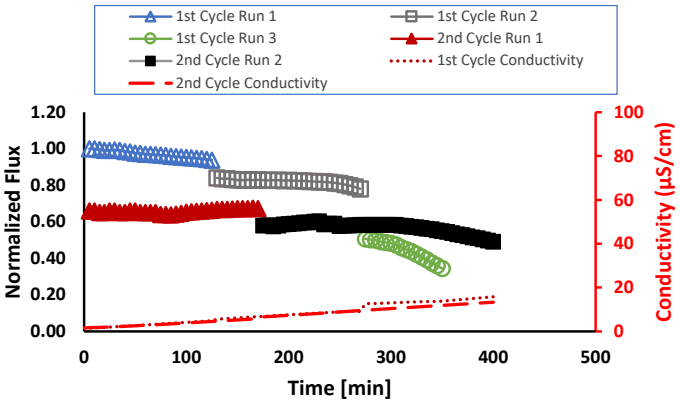

Figure 12: Normalized flux versus time for commercial PVDF membranes using MDC of real PW B at 0.5 L/min flow (long experiment with regeneration). Note: 1st Cycle was obtained by conducting MDC for 3 runs; 2nd Cycle was conducted for 2 runs after cleaning the membrane.

Conclusions

The combined EC/UF-MDC process was investigated for treating hydraulic fracturing PW. The PW investigated here had a high TDS, TSS, and TOC. Nevertheless, 55% of the feed volume was recovered using the process developed here. By applying crystallization after MD, precipitation on the membrane is suppressed when treating real PW. We found that an adequate reduction in the PW TOC can be achieved using EC, and UF can efficiently remove the particulate matter. The stability of the MDC membrane is critical and requires a membrane with high flux at high TDS and resistant to breakthrough. It is likely that the TDS and other properties of the PW will determine what train of treatment is required to achieve high water and mineral recovery.

The EC/UF-MDC technology can have a potential impact on Water Resources/Oil & Gas Companies because surface water and groundwater form about 80% of the water utilized in hydraulic fracturing. This process could be effectively used to treat and reuse PW in order to obtain about a high recovery of water. The data collected from treating real PW can be used to evaluate the integrated EC/UF-MDC system, which can further lead to the next step of establishing a pilot scale process.

Acknowledgements

This material is based upon work supported by the United States Geological Survey under grant agreement No. G16AP00040 and administered by the Arkansas Water Resources Center. The views and conclusions contained in this document are those of the authors and should not be interpreted as representing the opinions or policies of the U.S. Geological Survey.

References

Baig, H., Antar, M. A., & Zubair, S. M. (2011). Performance evaluation of a once-through multi-stage flash distillation system: Impact of brine heater fouling. Energy Conversion and Management, 52(2), 1414–1425. https://doi.org/10.1016/j.enconman.2010.10.004

Cañizares, P., Jiménez, C., Martínez, F., Sáez, C., & Rodrigo, M. A. (2007). Study of the electrocoagulation process using aluminum and iron electrodes. Industrial and Engineering Chemistry Research, 46(19), 6189–6195. https://doi.org/10.1021/ie070059f

Chen, G., Lu, Y., Krantz, W. B., Wang, R., & Fane, A. G. (2014). Optimization of operating conditions for a continuous membrane distillation crystallization process with zero salty water discharge. Journal of Membrane Science, 450, 1–11. https://doi.org/10.1016/j.memsci.2013.08.034

Chen, H., & Carter, K. E. (2016). Water usage for natural gas production through hydraulic fracturing in the United States from 2008 to 2014. Journal of Environmental Management, 170, 152–159. https://doi.org/10.1016/j.jenvman.2016.01.023

Deshmukh, A., Boo, C., Karanikola, V., Lin, S., Straub, A. P., Tong, T., Warsinger, D. M., & Elimelech, M. (2018). Membrane distillation at the water-energy nexus: Limits, opportunities, and challenges. Energy and Environmental Science, 11(5), 1177–1196. https://doi.org/10.1039/c8ee00291f

Duong, H. C., Chivas, A. R., Nelemans, B., Duke, M., Gray, S., Cath, T. Y., & Nghiem, L. D. (2015). Treatment of RO brine from CSG produced water by spiral-wound air gap membrane distillation - A pilot study. Desalination, 366, 121–129. https://doi.org/10.1016/j.desal.2014.10.026

Edwie, F., & Chung, T. S. (2013). Development of simultaneous membrane distillation-crystallization (SMDC) technology for treatment of saturated brine. Chemical Engineering Science, 98, 160–172. https://doi.org/10.1016/j.ces.2013.05.008

Fayad, N. (2018). The application of electrocoagulation process for wastewater treatment and for the separation and To cite this version :

Gamage, N. P., & Chellam, S. (2014). Mechanisms of physically irreversible fouling during surface water microfiltration and mitigation by aluminum electroflotation pretreatment. Environmental Science and Technology, 48(2), 1148–1157. https://doi.org/10.1021/es405080g

Kafuku, G., & Mbarawa, M. (2013). Influence of Fatty Acid Profiles during Supercritical Transesterification of Conventional and Non-Conventional Feedstocks: A Review. American Journal of Analytical Chemistry, 04(09), 469–475. https://doi.org/10.4236/ajac.2013.49060

Kondash, A. J., Albright, E., & Vengosh, A. (2017). Quantity of flowback and produced waters from unconventional oil and gas exploration. Science of the Total Environment, 574, 314–321. https://doi.org/10.1016/j.scitotenv.2016.09.069

Kondash, A., & Vengosh, A. (2015). Water Footprint of Hydraulic Fracturing. Environmental Science and Technology Letters, 2(10), 276–280. https://doi.org/10.1021/acs.estlett.5b00211

Lin, S., Yip, N. Y., & Elimelech, M. (2014). Direct contact membrane distillation with heat recovery: Thermodynamic insights from module scale modeling. Journal of Membrane Science, 453, 498–515. https://doi.org/10.1016/j.memsci.2013.11.016

Luek, J. L., & Gonsior, M. (2017). Organic compounds in hydraulic fracturing fluids and wastewaters: A review. Water Research, 123, 536–548. https://doi.org/10.1016/j.watres.2017.07.012

Malakoff, D. (2014). The gas surge. Scie, 344(6191).

Metcalf, L., Eddy, HP., & Tchobanoglous, G. (1991). Wastewater Engineering, Treatment, Disposal and Reuse (3rd ed.). McGraw Hill .

Morillo, J., Usero, J., Rosado, D., el Bakouri, H., Riaza, A., & Bernaola, F. J. (2014). Comparative study of brine management technologies for desalination plants. Desalination, 336(1), 32–49. https://doi.org/10.1016/j.desal.2013.12.038

Orem, W., Tatu, C., Varonka, M., Lerch, H., Bates, A., Engle, M., Crosby, L., & McIntosh, J. (2014). Organic substances in produced and formation water from unconventional natural gas extraction in coal and shale. International Journal of Coal Geology, 126, 20–31. https://doi.org/10.1016/j.coal.2014.01.003

Pérez-González, A., Urtiaga, A. M., Ibáñez, R., & Ortiz, I. (2012). State of the art and review on the treatment technologies of water reverse osmosis concentrates. Water Research, 46(2), 267–283. https://doi.org/10.1016/j.watres.2011.10.046

Perrin, J. (2019). Horizontally drilled wells dominate U.S. tight formation production. https://www.eia.gov/todayinenergy/detail.php?id=39752

Rosenblum, J. S., Sitterley, K. A., Thurman, E. M., Ferrer, I., & Linden, K. G. (2016). Hydraulic fracturing wastewater treatment by coagulation-adsorption for removal of organic compounds and turbidity. Journal of Environmental Chemical Engineering, 4(2), 1978–1984. https://doi.org/10.1016/j.jece.2016.03.013

Rubinstein, J. (n.d.). Earthquake Hazards. https://www.usgs.gov/natural-hazards/earthquake-hazards/induced-earthquakes?qt-science_support_page_related_con=4#qt-science_support_page_related_con

Sardari, K., Fyfe, P., Lincicome, D., & Ranil Wickramasinghe, S. (2018). Combined electrocoagulation and membrane distillation for treating high salinity produced waters. Journal of Membrane Science, 564, 82–96. https://doi.org/10.1016/j.memsci.2018.06.041

Sardari, K., Fyfe, P., & Ranil Wickramasinghe, S. (2019). Integrated electrocoagulation – Forward osmosis – Membrane distillation for sustainable water recovery from hydraulic fracturing produced water. Journal of Membrane Science, 574, 325–337. https://doi.org/10.1016/j.memsci.2018.12.075

Timmes, T. C., Kim, H. C., & Dempsey, B. A. (2010). Electrocoagulation pretreatment of seawater prior to ultrafiltration: Pilot-scale applications for military water purification systems. Desalination, 250(1), 6–13. https://doi.org/10.1016/j.desal.2009.03.021

Vidic, R. D., Brantley, S. L., Vandenbossche, J. M., Yoxtheimer, D., & Abad, J. D. (2013). Impact of shale gas development on regional water quality. Science, 340(6134). https://doi.org/10.1126/science.1235009

Warpinski, N. R., Mayerhofer, M. J., Vincent, M. C., Cipolla, C. L., & Lolon, E. P. (2008). Stimulating Unconventional Reservoirs : Maximizing Network Growth while Optimizing Fracture Conductivity. SPE International.

Yun, Y., Ma, R., Zhang, W., Fane, A. G., & Li, J. (2006). Direct contact membrane distillation mechanism for high concentration NaCl solutions. Desalination, 188(1–3), 251–262. https://doi.org/10.1016/j.desal.2005.04.123

Image caption: Culture incubations with straw decomposition extract. Photo courtesy of Mary Savin.

Is Rice as Effective as Barley Straw or Hydrogen Peroxide in Inhibiting Cyanobacterial Blooms and Reducing Microcystin Concentrations?

Mary Savin[1]*

[1]Professor, Department of Crop, Soil, and Environmental Sciences (CSES), University of Arkansas, Fayetteville, AR 72701
*Corresponding author, msavin@uark.edu

Abstract: Freshwater harmful algal blooms (HABs) are occurring more frequently and in new locations. The extract from decomposition of rice straw may serve as an effective algal inhibitor because of the production of inhibitory compounds during decomposition. Hydrogen peroxide may be the main inhibitory compound produced. We conducted a series of experiments to compare the effectiveness to inhibit algal growth of rice straw decomposition extract to hydrogen peroxide and barley straw decomposition extract. Hydrogen peroxide added at high concentrations showed immediate and lasting inhibition of algal growth throughout incubation of algal cultures. In *R. subcapitata* cultures after 28 days and in the absence of natural organic matter, decomposition extract filtered from 5.0 g/L rice straw showed 93.4% inhibition compared to the control, followed by 5.0 g/L barley straw (61.8%), whereas 2.5 g/L barley straw (25.2%) and 2.5 g/L rice straw extracts (11.2%) were not significantly different from the control. Phenolic concentrations were 2-3 orders of magnitude greater in hydrogen peroxide compared to straw extract treatments, likely resulting from the large input of hydrogen peroxide. Flavonoid concentrations were detected in straw extract cultures after 1 day, but there was a lag until after day 8 before concentrations increased in the hydrogen peroxide treatments and the control. In lake water, decomposition extract from 5.0 g/L but not 10 g/L rice straw showed delayed growth (at day 28) in *Microcystis aeruginosa* in the absence of bacteria; whereas, *Microcystis aeruginosa* grew in the control only at day 28 when bacteria were retained in the lake water. Results from controlled experiments do not support that inhibitory mechanisms from straw decomposition extracts is driven by hydrogen peroxide generation. Results do support that value can be added to rice straw decomposition extract as a product for algal growth inhibition with further research to specify mechanisms of action. Both the concentration of decomposition extract and the ecology within the lake water are important to understand in order to maximize effectiveness of the use of rice straw decomposition extract to inhibit algal growth in natural waters.

Key Points:

- Large concentrations of hydrogen peroxide showed immediate and lasting inhibition of algal growth throughout incubation of algal cultures and in lake water.
- Filtered extract from decomposition of aqueous 5 g/L rice straw showed greater inhibition of algae using measurements of chlorophyll-a and greater production of flavonoids and polyphenolics than filtered extract from 5 g/L barley straw decomposed under the same conditions.
- Experiments with two algal species and in lake water which has natural organic matter demonstrate the importance of the concentration of rice straw during decomposition in order for the decomposition extract to inhibit algal growth
- Ecology of the algae, and hence results of rice straw decomposition extract to inhibit algal growth, changed if bacteria are present
- Results indicate there is value to continue to investigate rice straw decomposition extract, and the role of polyphenolic compounds produced during decomposition, to inhibit harmful algal blooms in surface waters.

Introduction

Freshwater harmful algal blooms (HABs) are becoming increasingly more common and have been spreading into new locations in recent years. With global climate change, HABs are expected to continue to become more frequent and prevalent. Because cyanobacteria are adaptable organisms, the likelihood of events to predict and the ability to prevent them has been difficult (Pearl, 2017). As a local example, in 2019 the City of Fayetteville announced that there may have been harmful algae in Lake Fayetteville as water was sampled with microcystin concentration greater than 10 µg/L (e.g. http://www.fayetteville-ar.gov/CivicAlerts.aspx?AID=1793&ARC=3303). Arkansas has more than 127,000 farm ponds (Kelly, 2017). Reservoirs are important surface water impoundments in Arkansas. For example, Beaver Lake (encompassing 766,026 acres) is the first in a series of three U.S. Army Corps of Engineers reservoirs on the White River, operates at a capacity of 140 million gallons of water per day, and provides the drinking water for multiple municipalities covering one in seven Arkansans (Ouei and Daniels, 2017). Research continues for models that can accurately predict occurrences and restoration of watershed management approaches that prevent future outbreaks in the face of a changing climate. Meanwhile, use of a simple, ecofriendly approach to control both growth and toxin production of harmful cyanobacteria that does not persist or have non-target effects is imperative. Though Arkansas has not yet experienced catastrophic HABs, the potential for catastrophic HABs in local, freshwater systems makes the necessity of effective treatment approaches imperative.

Cost-effective management approaches should control and prevent outbreaks with minimal risk to people, animals, and the environment. Barley straw has been shown in many lab and field experiments to inhibit algal growth, although experiments have contradicted these results and also shown no response or growth promotion (hUallacháin and Fenton, 2010; Islami and Filizadeh, 2011). Other cereal straws may be as or more effective, depending on specific environmental and biological conditions. Rice straw has been an effective algal inhibitor through the production of multiple inhibitory compounds during decomposition (Park et al., 2006). However, contradictory research has indicated that it may not be as effective an algal inhibitor as barley straw (Ma et al., 2015). Utilization of barley or rice straw depends on production of allelopathic compounds (e.g. phenolic compounds) that are released during aerobic aqueous decomposition of the straw.

Algal population inhibition needs confirmation under controlled laboratory conditions because a field study was inconclusive (Maris et al., 2019). We proposed a series of experiments investigating growth of populations of *Raphidocelis subcapitata* or *Microcystis aeruginosa* in the presence of hydrogen peroxide compared to aqueous extracts of decomposing barley and rice straw to evaluate effectiveness of rice straw extract as an inhibitor of green algae and/or harmful cyanobacteria.

Methods

This study consisted of a series of laboratory-based experiments. Rice straw was obtained from a farmer in central Arkansas and barley straw was purchased from a commercial source. Both straws were washed three times, cut into 2.5-cm pieces, dried (50°C), and stored dry until used in decomposition experiments. Straws (5 g/L) were decomposed aerobically for 30 days in an aquarium at 25°C with aeration controlled using an aquarium pump and light maintained on a 12 hr:12 hr light:dark cycle using cool, white fluorescent tubes. Extracts of decomposing straw were filter-sterilized through a series of filters ending with a 0.45-µm pore size filter. Commercial 3% solution of hydrogen peroxide was filter-sterilized through a 0.45-µm pore size filter and diluted for use in experiments. *Microcystis aeruginosa* and *Raphidocelis subcapitata* were purchased from culture collections and cultures were maintained in Bristol or blue-green (BG-11) and/or media with shaking at 110 rpm, 27°C, and under 12 hr:12 hr light:dark cycle at 100 µmol photons m^{-2} s^{-1} using cool, white fluorescent tubes. Experiments were conducted under these same conditions unless noted elsewhere.

Bioassays for objective 1 (see Table 1) utilized cultures of either *Raphidocelis subcapitata* or *Microcystis aeruginosa* inoculated into sterile culture medium (n = 3) at an initial density approximating 5.8 x 10^5 cells/mL (similar to Hua et al., 2018; USEPA, 2002). Bioassays for objectives 2 and 3 utilized a similar design with lake water collected from northwest Arkansas and filter-sterilized through a 0.45-µm pore-size filter for analysis of growth and toxin production without other organisms but in the presence of natural dissolved organic matter. Lake water filtered through a 5.0-µm pore-size filter for analysis of growth and toxin production in the presence of bacterioplankton was to understand the impact of treatments on both the harmful cyanobacteria in the presence of the bacterial community.

Samples were collected at time 0, 1, 4, and 24 hr for determination of hydrogen peroxide concentration as others have shown rapid decomposition of hydrogen peroxide despite prolonged effects on the algae (Weenink et al., 2015). Chlorophyll-a, pH, dissolved organic carbon (DOC), total phenolics and flavonoids were measured on samples collected on days 0, 1, 4, 8, 15, and 28.

Hydrogen peroxide was analyzed using a cerium sulfate method (Putt and Pugh, 2013). Chlorophyll-a was measured using a fluorometer (Turner Designs, Sunnyvale, CA). Growth inhibition for each algal population added to sterile media was calculated as a percentage of the control to indi-

Table 1: Each chemical (hydrogen peroxide or decomposing straw extract) treatment added to construct microcosms for algal bioassays.

Objective 1 Treatments[1]	Objective 2, 3 Treatments
Control	Pond water control
2.5 g/L H_2O_2	Bacteria control
5.0 g/L H_2O_2	25 mg/L H_2O_2, no bacteria
2.5 g/L BS extract	25 mg/L H_2O_2 with bacteria
5 g/L BS extract	50 mg/L H_2O_2, no bacteria
2.5 g/L RS extract	50 mg/L H_2O_2 with bacteria
5 g/L RS extract	100 mg/L H_2O_2, no bacteria
	100 mg/L H_2O_2, with bacteria
	5 g/L RS extract, no bacteria
	5 g/L RS extract, with bacteria
	10 g/L RS extract, no bacteria
	10 g/L RS extract, with bacteria

[1]BS is barley straw, RS is rice straw, H_2O_2 is hydrogen peroxide

cate inhibition in the presence of each straw or hydrogen peroxide concentration over time. Sample pH was measured using an electrode and calibrated pH meter. Dissolved organic carbon was analyzed on a TOC-V PC-controlled organic C analyzer (Shimadzu, Columbia, MD). Total phenolics (Margraf et al., 2015) and total flavonoid content (Hatamnia et al., 2014) were analyzed by microplate methods. Mean and standard errors were calculated and data were analyzed by repeated measures analysis of variance (ANOVA, $P < 0.05$), with post hoc tests to separate means where appropriate.

Results and Discussion

The main objective of this research was to determine the efficacy of barley and rice straw as algal inhibitors through evaluation of polyphenolic compounds released during decomposition as compared to H_2O_2. Different concentrations of H_2O_2 and aqueous extracts after 30 days of decomposition of rice and barley straw were added to green algae *Raphidocelis subcapitata* and cyanobacterial *Microcystis aeruginosa* cultures. The cultures were sampled for H_2O_2, chlorophyll-a, pH, DOC, and total phenolics and flavonoids. In *R. subcapitata* cultures after 28 days and in the absence of natural organic matter, decomposition extract filtered from 5.0 g/L rice straw showed an inhibitory effect of 93.4%, followed by 5.0 g/L barley straw at 61.8% inhibition (Figure 1). In contrast, decomposition extract filtered from 2.5 g/L barley straw (25.2%), and 2.5 g/L rice straw (11.2%) were not different from the control. Decomposition extract filtered from 2.5 g/L and 5.0 g/L rice straw were effective at inhibiting *Microcystis aeruginosa* growth for 28 days when grown in media (Figure 2). In lake water, decomposition extract from 5.0 g/L but not 10 g/L rice straw showed delayed growth (at day 28) in *Microcystis aeruginosa* in the absence of bacteria; whereas, *Microcystis aeruginosa* grew in the control only at day 28 when bacteria were retained in the lake water (Figure 3). Concentrations initially greater than 5 g/L may be especially important in inhibition of different algal populations in surface waters. The ecology within a lake will also be important to understand better in order for algal control to be achieved.

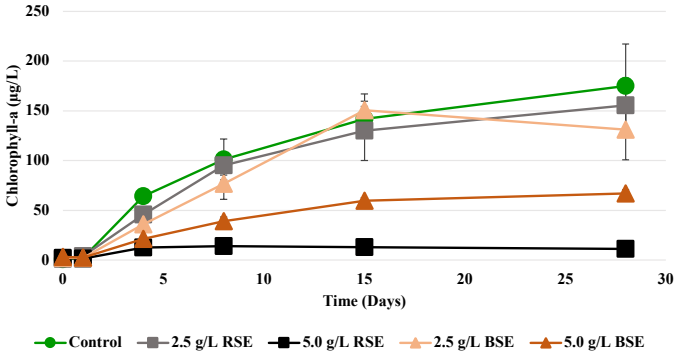

Figure 1: Chlorophyll-a (µg/L) in media based *Raphidocelis subcapitata* cultures for 0 to 28 days following treatment with rice straw extract (RSE), barley straw extract (BSE), or no treatment (control, C) (n=3).

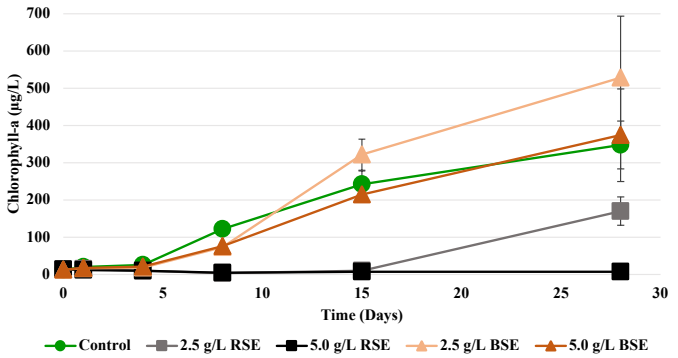

Figure 2: Chlorophyll-a concentrations (µg/L) in media based *Microcystis aeruginosa* cultures for 0 to 28 days following treatment with rice straw extract (RSE), barley straw extract (BSE), or no treatment (control) (n = 3).

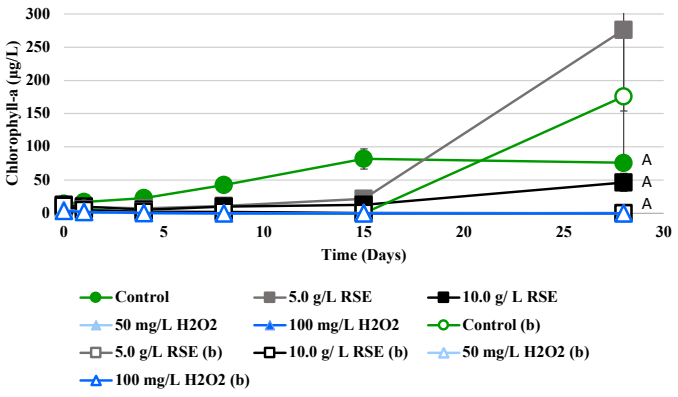

Figure 3: Chlorophyll-a concentrations (µg/L) in lake water based *Microcystis aeruginosa* cultures for 0 to 28 days following treatment with rice straw extract (RSE), hydrogen peroxide (H_2O_2), or no treatment (control) and with bacteria (b) or without bacteria (n = 3). Similar letters represent lack of significant differences between the treatments ($P < 0.05$).

Previous research has indicated that hydrogen peroxide is an effective inhibitory compound and results obtained in these experiments support that conclusion. However, if adding value to rice straw as a product to prevent or inhibit algal blooms is a potential market, there are economic and environmental reasons to continue pursuing mechanistic understanding to explain the inhibitory effect on algae. Results from the rice and barley straw extract treatments do not show appreciable concentrations of hydrogen peroxide produced within 24 hours. Furthermore, the production of polyphenolic compounds is orders of magnitude less than when high concentrations of hydrogen peroxide are applied to water. Thus, it seems that either specific compounds could be produced having an effect on algae, compounds that are produced react chemically before being measured by the experimental analysis, or there are other mechanisms - perhaps more diverse mechanisms – unaccounted for in these experiments. Continuing measurements of the phenolics, flavonoids, DOC, nutrients, and toxin concentrations in the presence of a known lake community composition should provide more insight into potential mechanistic differences contributing to algal inhibition from the decomposition extract of rice straw.

Conclusions

Managers of small aquatic systems may purchase barley straw, guided by the belief that it will prevent HABs (M. Lankford, personal communication). Experimentation on the practical application of using rice straw extract for algal control in Arkansas or the Midsouth is lacking. Experiments utilizing populations in culture media maintained known, controlled conditions to optimize growth while experiments utilizing pond water focus on algal growth under conditions more likely to be present in environmental waters. Results from controlled experiments do not support that inhibitory mechanisms from straw decomposition extracts are driven by hydrogen peroxide generation. Results do support that value can be added to rice straw as an environmental product for algal growth inhibition with further research to specify mechanisms of action. Both the concentration of straw used to produce the decomposition extract and the ecology within the lake water are important variables in order to maximize effectiveness of the use of rice straw decomposition extract to inhibit algal growth in natural waters.

Acknowledgements

This material is based upon work supported by the United States Geological Survey under grant agreement No. G16AP00040 and administered by the Arkansas Water Resources Center. The views and conclusions contained in this document are those of the authors and should not be interpreted as representing the opinions or policies of the U.S. Geological Survey.

References

Hatamnia, A.A., N. Abbaspour, and R. Darvishzadeh. 2014. Antioxidant Activity and Phenolic Profile of Different Parts of Bene (Pistacia atlantica subsp. kurdica) fruits. Food Chemistry. 145:306–311.

Hua, Q. Y.-g. Liu, Z.-l. Yan, G.-m. Zeng, S.-b. Liu, W.-j. Wang, X.-f. Tan, J.-q. Deng, X. Tang, Q.-p. Wang. 2018. Allelopathic Effect of the Rice Straw Aqueous Extract on the Growth of Microcystis aeruginosa. Ecotoxicology and Environmental Safety. 148: 953-959.

hUallacháin, D.Ó., and O. Fenton. 2010. Barley (Hordeum vulgare)-Induced Growth Inhibition of Algae: A Review. Journal of Applied Phycology. 22:651–658. DOI 10.1007/s10811-009-9492-z.

Islami, H.R., and Y. Filizadeh. 2011. Use of Barley Straw to Control Nuisance Freshwater Algae. American Water Works Association Journal. 103(5):111-118.

Kelly, A. 2017. Aquaculture and Fisheries. Cooperative Extension Service, Arkansas Division of Agriculture, Lonoke, AR. Available at https://www.uaex.edu/farm-ranch/special-programs/aquaculture/ (Accessed 8/8/2017).

Lim, B. J., J.H. Park, J.W. Jung, K.S. Hwang, M.S. Son, C.H. Lim, J.E. Na, S.G. Kim, H.M. Chai, K.A. Seo, J.H. Han, S.S. Park, and J.K. Park. 2015. Application of Barley Straw to Dammed River for Algal Control. Desalination and Water Treatment. 54:3728–3736. doi: 10.1080/19443994.2014.923195.

Ma, H., J. Zhang, L. Tonga, and J. Yang. 2015. Photochemical Production of Hydrogen Peroxide from Natural Algicides: Decomposition Organic Matter from Straw. Environmental Science Processes and Impacts. 17:1455–1461.

Margraf, T., A.R. Karnopp, N.D. Rosso, and D. Granato. 2015. Comparison between Folin-Ciocalteu and Prussian Blue Assays to Estimate the Total Phenolic Content of Juices and Teas Using 96-Well Microplates. Journal of Food Science. 80:C2397-C2403.

Maris, J., M. Savin, and L. Wood. 2019. Evaluating Rice Straw as a Substitute for Barley Straw in Inhibiting Algal Growth in Farm Ponds. Discovery: The Student Journal of Dale Bumpers College of Agricultural, Food and Life Sciences. 20:70-79.

Ouei, T., and M. Daniels. 2017. Water Resources of Beaver Lake, FSA9513. Cooperative Extension Service, Arkansas Division of Agriculture, Little Rock, AR. Available at https://www.uaex.edu/publications/pdf/FSA-9513.pdf (Accessed 8/8/2107).

Paerl, H. W. 2017. Controlling Harmful Cyanobacterial Blooms in a Climatically More Extreme World: Management Options and Research Needs. Journal of Plankton Research. 39(5):763–771.

Park, M.-H., M.-S. Han, C.-Y. Ahn, H.-S. Kim, B.-D. Yoon, and H.-M. Oh. 2006. Growth Inhibition of Bloom-Forming Cyanobacterium Microcystis aeruginosa by Rice Straw Extract. Letters in Applied Microbiology. 43:307–312.

Putt K.S., R.B. Pugh. 2013. A high-throughput microtiter plate based method for the determination of peracetic acid and hydrogen peroxide. PLoS One. 8(11): e79218. doi:10.1371/journal.pone.0079218.

United States Environmental Protection Agency (USEPA). 2002. Method 1003.0: Green alga, Selenastrum capricornutum, growth test; chronic toxicity. Short-term Methods for Estimating the Chronic Toxicity of Effluents and Receiving Waters to Freshwater Organisms, 4th edition, EPA-821-R-02-013. Available at https://www.epa.gov/sites/production/files/2015-12/documents/method_1003_2002.pdf.

Weenink, E.F.J., V.M. Luimstra, J.M. Schuurmans, M.J. Van Herk, P.M. Visser, and H.C.P. Matthijs. 2015. Combatting Cyanobacteria with Hydrogen Peroxide: A Laboratory Study on the Consequences for Phytoplankton Community and Diversity. Frontiers in Microbiology 6: doi:10.3389/fmicb.2015.00714.

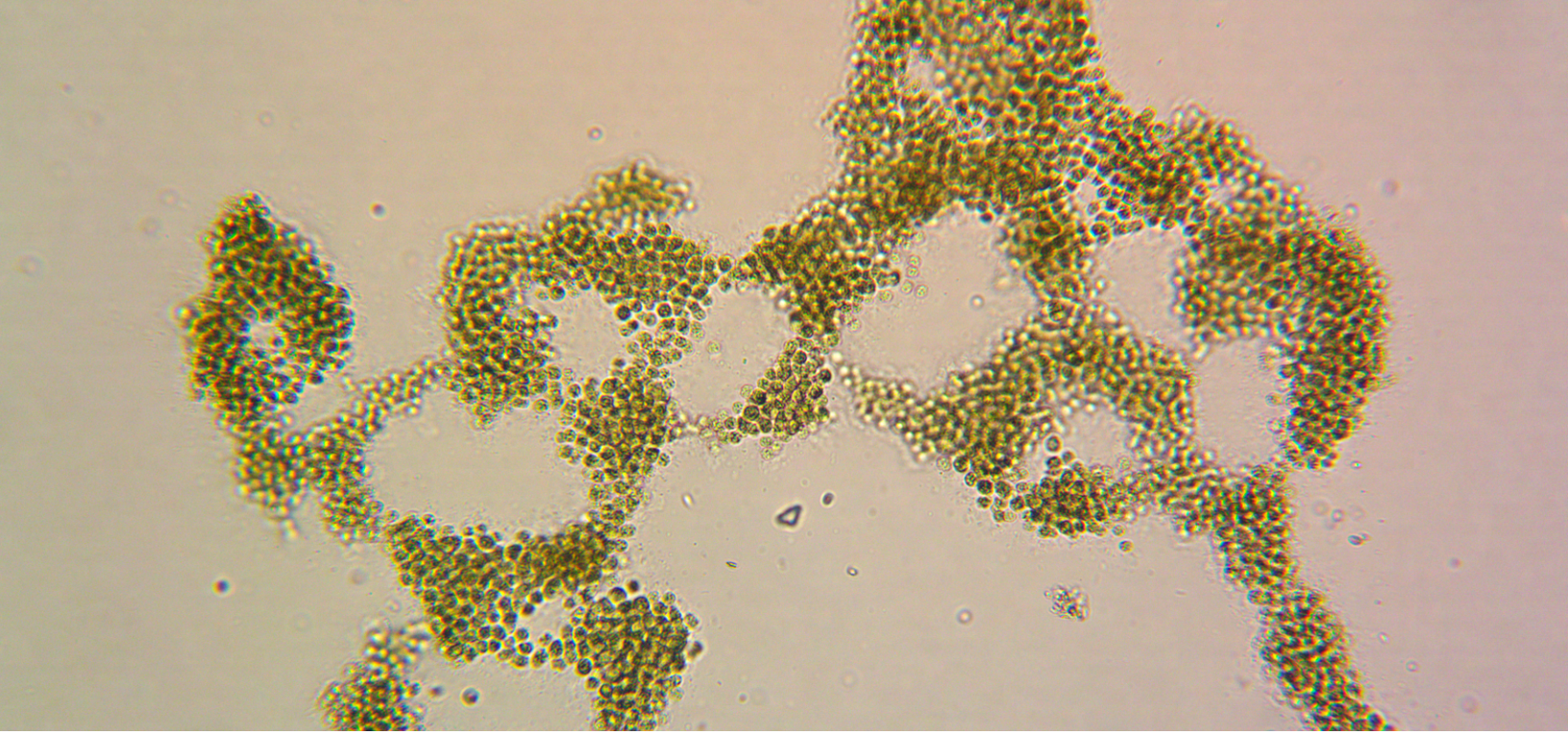

Image caption: *Microcystis aeruginosa* under a microscope, photographed by Brad Austin at the Arkansas Water Resources Center.

Mechanisms, Kinetics and Toxicity of Microcystin-LR Biodegradation by Free and Immobilized Enzymes

Audie Thompson[1]

[1](Former) Assistant Professor, Ralph E. Martin Department of Chemical Engineering, University of Arkansas, Fayetteville, AR 72701

Abstract: Microcystin-LR (MC-LR) is among the most problematic algal toxin in America, with several outbreaks and appearances in fresh water supplies in recent years. We investigated a new strategy for remediation of MC-LR that combines linearization of the toxin using microcystinase A, MlrA, enzyme with rejection of linearized byproducts using membrane filtration. An active MlrA enzyme was produced from a heterologous host, and the enzyme was able to degrade MC-LR and convert it to linearized MC-LR. The linearized MC-LR along with some undegraded cyclic ones were filtered through composite hydrophobic and highly negative membranes made of 95% polysulfone with 5% sulfonated PEEK. We found that a SPEEK membrane could reject or adsorb the vast majority of cyclic MC-LR and virtually all linearized MC-LR. The partial success of modified membranes and reactive processes suggests that a physical barrier membrane with additional functionality (e.g., charge, reactivity) may result in enhanced MC-LR remediation. The PSf/SPEEK membrane was effective at rejecting or adsorbing 97.4% cyclic MC-LR and virtually all linear MC-LR. MC-LR was found to reversibly adsorb to the PSf/SPEEK membranes, with desorption of MC-LR occurring when the membranes were soaked in a methanol/water solution. This is highly advantageous because it provides a method of removing MC-LR from feed waters via reversible adsorption to membranes that can then be cleaned and reused.

Key Points:

- The MlrA enzyme was overexpressed in *Escherichia coli* and purified via a His-tag with 95% purity.
- MlrA was successful at linearizing approximately 86% of the MC-LR over 24 hours.
- Membrane filtration tests showed rejection of 97.4% of cyclic MC-LR and virtually all linearized MC-LR, with adsorption to the membranes being the main rejection mechanism.
- This study demonstrates a novel strategy of remediation of microcystin-tainted water, combining degradation of the toxin with removal by membrane filtration.

Introduction

Enzymatic remediation allows an engineered catalysis system (e.g., enzyme-immobilized catalytic membranes), in comparison to whole-organism bioremediation of cyanotoxins. Our approach is to use enzyme-mediated catalysis to target microcystin degradation and removal from water specifically. The research focuses on proof-of-concept experiments to demonstrate enzyme-driven microcystin-LR (MC-LR) degradation from contaminated synthetic water solutions. The overall goal of this research is to work toward membrane-mediated biocatalysis, an innovative approach where membranes provide structural support and physical separation of contaminants, while enzymes enable catalytic degradation of contaminants.

Methods

MlrA Expression and Experiments

Strain and plasmid construction

Escherichia coli (E. coli) chemically competent BL21 (DE3) was purchased from New England Biolabs Inc. and used as a host to produce targeted recombinant protein. The pET-21a (+) plasmid was purchased from Novagen Life Technologies. A DNA fragment encoding to MlrA was designed and purchased from Integrated DNA Technologies (Coralville, IA). After plasmid construction, recombinant pET-MlrA plasmid was transformed into E. coli Bl-21 cells by heat shock method.

Media, growth, and expression of recombinant MlrA enzyme

Ampicillin contained in Luria-Bertani (LB) broth was used for all plates and seed cultivations. A single colony of E. coli BL21 containing cloned pETmlrA plasmid pick up from agar plate was used to inoculate 10 ml of LB media supplied with 75 μg/mL ampicillin as an initial growth seed culture. The culture was incubated at 37°C with shaking at 200 rpm overnight. This experiment was performed by using 2.5 mL of overnight growth to inoculated 1 L supplemented with 75 μg/mL ampicillin. The growth was incubated at 37°C with 200 rpm shaking speed. Isopropyl β-D-1-thiogalactopyranoside (IPTG) with final concentration of 0.5 mM was used to induce recombinant plasmid at the mid-exponential phase of growth when the optical density 1 reached ~0.6 units (at 600 nm). After 4 hours from induction, cells were harvested to proceed in further experiments.

Cell lysate preparation and Hisx6-tag MlrA purification

After expression was completed, cells were harvested by centrifugation at 4,500 × g for 45 minutes. Cell pellets were resuspended in 10 mM sodium phosphate buffer, pH 7.4 and subjected to sonication on ice with a Qsonica sonicator on a 20 second burst cycle (power 10). The cell homogenate was centrifuged to clarify the cell lysate. Supernatants were collected to proceed in further experiments such as tested for enzyme activity and purification. The Fast Protein Liquid Chromatography system from ÄKTA Amersham Pharmacia Biotech was used to purify the cell lysate. Hisx6-tag is designed to be in the C-terminal of MlrA enzyme to facilitate purification through Immobilized Metal Affinity Chromatography (IMAC). Cobalt loaded HiTrap IMAC FF column (Co-NTA) was used to purify expressed protein. Sodium dodecyl polyacrylamide gel electrophoresis (SDS-PAGE) was used to ensure that the targeted protein expressed and produced properly by the host and to confirm the purity.

Microcystin-LR Degradation Activity of MlrA

The MlrA cyanotoxin degradation activity was tested by incubating MlrA with microcystin-LR. 2 mL solution of 100 μg/L MC-LR and 216 mg/L MlrA in phosphate buffer (5 mM) was incubated in a glass scintillation vial for 24 hours at room temperature. 500 μL samples were taken at 0, 4, and 24 hours after initial mixing and transferred to glass HPLC vials. The reaction in each HPLC vial was stopped by 50 μL of 5% acetic acid. Samples were stored at 4°C until analysis. The linearization of MC-LR was monitored by LC-MS.

LC-MS Methods for Detecting MC-LR

Cyclic and linearized MC-LR were detected using ultra performance liquid chromatography-tandem mass spectrometry (UPLC-MS/MS). A LCMS-8040 Triple Quadrupole Liquid Chromatograph Mass Spectrometer (Shimadzu, Columbia, MD, USA) was used to analyze the samples. A Shimadzu C18 column (2.1 x 50 mm, 1.9 μm particle size) was used for all samples except for those from membrane filtration experiments, for which a Waters Acquity UPLC peptide HSS T3 column (1x100 mm, 1.8 μm particle size) was used. An injection volume of 10 μL was used and the column was held at 40°C. The mobile phases were water with 0.1% formic acid and acetonitrile with 0.1% formic acid. The series of gradients were as follows: the column was initially balanced with 20% acetonitrile for 1 minute, then increased from 20% to 80% acetonitrile over 7 minutes, then held at 80% acetonitrile for 1 minute, then returned to 20% acetonitrile and held for 1 minute.

For mass spectrometry, electrospray ionization was used. Full scans were performed for m/z 400-1200 in positive ion mode. Additionally, for the experiments involving filtration of MC-LR and its degradation products through a membrane, single-ion monitoring was used for m/z 498.5 and 995.7 (2+ and 1+ charge states for the cyclic MC-LR) and for m/z 507.4 and 1013.5 (2+ and 1+ charge states for linear MC-LR).

Membrane Fabrication and Experiments

Sulfonation of SPEEK

The sulfonation procedure was adapted from literature (Eke et al., 2018) and modified as discussed here. In the method, 25 g of PEEK granules were heated in a vacuum oven at 100°C for 24 hours. They were then crushed into fine powder, which was dissolved in concentrated sulfuric acid in a 90:10% (H_2SO_4:PEEK) at room temperature for 48 hours, then precipitated out of the solution using cold deionized water. The precipitant was neutralized and dried overnight in a vacuum oven at 100°C.

Membrane Formation

The membranes were formed via non-solvent induced phase separation. In this method, once the membrane is cast, it is immersed into a non-solvent where a phase transition takes place (Dong et al., 2021). The membrane formed contains a polymer rich surface (active rea) and a polymer poor pore structure suitable for ultrafiltration (Jung et al., 2016; Dong et al., 2021). The non-solvent utilized was water. The dope solution was prepared by dissolving polysulfone (PSf) blended with SPEEK (95:5%) into N-Methyl-2-pyrrolidone solvent to make 79:21% NMP:SPEEK-PSf. The blended dope solution was then spread onto a glass plate using a doctor blade (0.4 mm) and exposed to air for 15 seconds before being immersed in de-ionized water. The formed membrane was then stored in de-ionized water (Eke et al., 2018; Dziga et al., 2019).

Adsorption and Desorption of Microcystin-LR on Membrane

The adsorption and desorption of MC-LR was tested by incubating MC-LR with a PSf/SPEEK membrane to adsorb, then adding methanol to desorb. A ¼ section of a PSf/SPEEK membrane (~4.33 cm^2) was incubated with 100 µg/L MC-LR in phosphate buffer (5 mM) in a glass scintillation vial for 24 hours at room temperature. 500 µL samples were taken at 0, 4, and 24 hours after initial mixing and transferred to glass HPLC vials. Before taking the sample at 24 hours, 667 µL methanol was added to the scintillation vial (bringing the concentration of methanol to 40% by volume and swirled to mix for 5 minutes. Samples were combined with 50 µL of 5% acetic acid to maintain consistency with other tests. Samples were then stored at 4°C and analyzed by LC/MS.

Membrane Filtration

The by-products of enzymatic degradation of MC-LR were filtered through the PSf/SPEEK membranes using a dead-end filtration cell from ®Millipore, MA USA with max operating pressure 5 bar. To provide the required pressure drop for flow, nitrogen gas was employed under a constant pressure of 4.1 bars (60 psi). Pre-compaction of the membrane with D-Ionized water was carried out followed by filtration of the byproducts at the end of the 24-hour degradation study. The filtrate after MC-LR degradation, which was the membrane feed solution, included degradation by-products, potentially MC-LR, methanol, phosphate buffer (containing disodium hydrogen phosphate and potassium phosphate dibasic), acetic acid, and MlrA enzyme solution. The reaction volume was concentrated by four times for all components while maintaining the same reactant concentration ratios. Samples were analyzed by LC/MS.

Results and Discussion

Protein Expression and Inclusion body Formation

E. coli containing cloned pETMlrA plasmid was expressed in a normal condition after optical density 1 reached ~0.6 units (at 600 nm) by using 0.5 mM IPTG. Results shows highly expressed band at ~42 kD (Figure 1, lane 2 and 3), matching the MlrA molecular weight which was designed in this study.

The purity of MlrA eluted in 125 mM imidazole was estimated to be about 95% while less purity of MlrA eluted in 62.5 mM imidazole due to metal weak binding proteins. This purity assessment confirmed by SDS-PAGE as a general detection of total protein. As shown in Figure 1, a single band represents MlrA enzyme in 125 mM was detected. These results prove the full length of MlrA expression and purity.

Microcystin-LR Degradation Activity of MlrA

MC-LR was treated with MlrA in a phosphate buffer (5 mM) solution. LC/MS was used to analyze samples taken

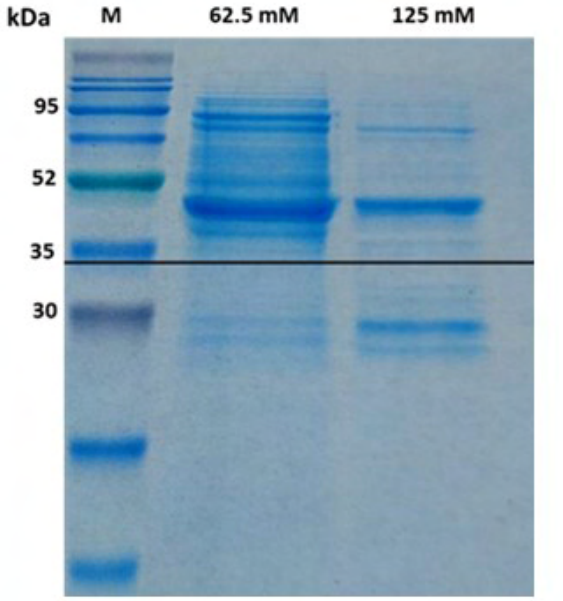

Figure 1: SDS-PAGE stained with Coomassie Brilliant Blue. 1 – molecular weight marker; 2- MlrA eluted with 62.5 mM imidazole; 3- MlrA eluted in 125 mM imidazole

at 0, 4, and 24 hours after initial mixing (Figure 2). At the start of the experiment, all MC-LR is present in the cyclic form (5.03 min). MS detected at peak for the cyclic MC-LR at m/z = 995.6. At 4 hours, the cyclic peak is reduced in height and an additional peak for linear MC-LR is present at 5.17 min. MS detected peaks for the linear MC-LR at m/z = 1013.8 (+1 charge state) (Bourne et al., 1996; Dziga et al., 2012) and m/z = 507.4 (+2 charge state). At 24 hours, the linear MC-LR peak is roughly 6x taller than the cyclic MC-LR peak, indicating that approximately 86% of the MC-LR has been linearized.

Adsorption and Desorption of Microcystin-LR on Membranes

Experiments were performed to determine the adsorption and desorption behavior of MC-LR to a PSf/SPEEK membrane. LC/MS was used to analyze samples taken at 0, 4, and 24 hours after initial mixing (Figure 3). Note that methanol was added just before the sample for 24 hours was taken. At t = 0 h, a cyclic MC-LR peak is visible at 5.06 min. At t = 4 h, the cyclic MC-LR peak is still present, but the height (vs. baseline) is reduced to 20.8% of the starting intensity, indicating that most of the MC-LR has adsorbed to the membrane. At t = 24 h, after methanol addition, the cyclic MC-LR peak height reverts to 73.6% of the starting intensity, indicating that methanol caused most of the adsorbed MC-LR to desorb.

These results are consistent with other studies that found that microcystin adsorbs to various types of plastic, but methanol can reduce adsorption. For example, Altaner et al. found that microcystin congeners dissolved in water adsorbed to polypropylene pipette tips, but methanol (≥ 40%) rectified the adsorption losses (Altaner et al., 2017).

Filtration of MC-LR and Degradation Products Through Membrane

For filtration experiments, MC-LR was incubated with MlrA for 24 hours and the resulting solution was passed through a membrane to determine if MC-LR or any by-products would be adsorbed or rejected by the membrane (Figure 3). For this experiment, a different UPLC column (peptide column) was used than in previously described experiments, so the MC-LR peaks occur at different times from those shown in Figures 2 and 3, where a C18 column

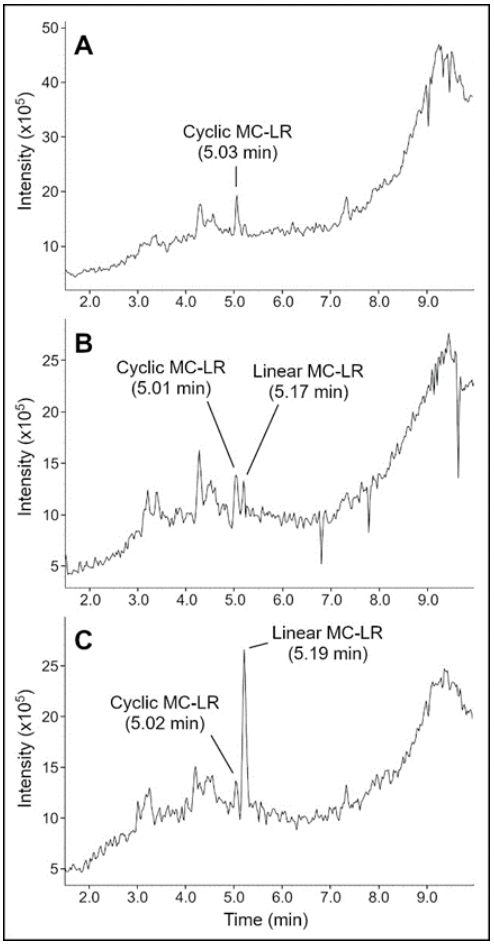

Figure 2: LC/MS analysis of the MC-LR as it is degraded by MlrA in an environment of phosphate buffer (5 mM), for samples taken 0 hours (A), 4 hours (B), and 24 hours (C) after initial mixing.

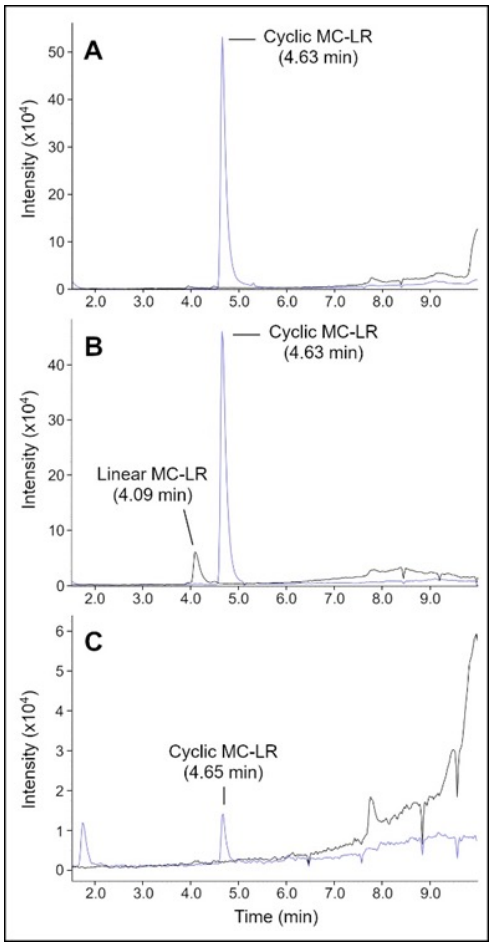

Figure 3: LC/MS analysis of the MC-LR solution incubated with MlrA, for samples taken at 0 hours (A), and 24 hours (B) after initial mixing, and for the solution after 24 hours filtered through a SPEEK membrane (C). Graphs for the cyclic MC-LR region (m/z 498.5) are in blue, while graphs for the linear MC-LR region (m/z 507.4) are in black.

was used. Additionally, single-ion monitoring was used to increase the clarity of the MC-LR peaks.

At t = 0 h (Figure 3A), a cyclic MC-LR peak is visible at 4.63 min. MS detected peaks for the cyclic MC-LR at m/z = 995.6 and 498.5 (+2 ion). At t = 24 h (Figure 3B), a cyclic MC-LR peak is still visible at 4.63 min but there is also a linear MC-LR peak at 4.09 min. MS detected peaks for cyclic MC-LR at m/z = 995.6 and 498.5 (+2 ion) and peaks for linear MC-LR at m/z = 1013.8 and 507.5 (+2 ion). At t = 24 h, the cyclic MC-LR peak is significantly taller than the linear MC-LR peak, indicating that much of the MC-LR was not degraded. This could be because of degradation of the MlrA enzyme over the course of long-term storage. The MlrA was stored at -20°C for approximately two years before being used for this experiment. Loss of MlrA activity can occur over the course of storage. For example, Wu et al. found that MlrA lost approximately 50% of activity at degrading nodularin, a related toxin, after 4 days of storage at 0°C (Wu et al., 2020). MlrA would be expected to lose activity at a slower rate at -20°C, but the loss could still be significant over the course of long-term storage.

For the (partially) degraded MC-LR solution filtered through the SPEEK membrane (Figure 3C), the peak for cyclic MC-LR at 4.65 min is much smaller than it was before filtration (2.6% of original height). Also, the peak for linear MC-LR is no longer visible. The small peak at 1.73 min is likely a contaminant or impurity and the peak was not visible in any other samples. The tall curve that escalades from ~7 min onwards is from the phosphate buffer. This curve is more clearly visible for this sample vs. other samples because the much shorter y-axis scale. In the mass spectrums for this sample, the MC-LR peaks were not distinguishable from background noise due to the significantly reduced concentration of MC-LR.

The LC-MS results of the filtrate indicate that the vast majority (97.4%) of cyclic MC-LR is adsorbed or rejected by the membrane, and virtually all linear MC-LR is adsorbed or rejected. The membrane could be more selective for linear MC-LR than cyclic MC-LR because the larger surface area of linear MC-LR enables stronger adsorption to the membrane. The results from the previous section indicate that the membrane could be soaked in methanol solution to desorb attached MC-LR and regenerate the membrane.

Conclusions

Predicted increases in surface water temperatures, combined with current agricultural practices, is expected to result in the continued expansion of algal blooms containing cyanobacteria, and enhanced public health risk due to algal toxins migrating into potable water. The most common cyanotoxins released during algal blooms are microcystins. Due to MCs cyclic peptide structure, removal via conventional treatment processes remains challenging. Enzymatic remediation allows an engineered catalysis system to potentially destroy these toxins. To investigate enzymatic degradation of MC-LR, MlrA enzyme was used here. In this study, an active MlrA enzyme was produced from a heterologous host, and the enzyme was able to degrade MC-LR and convert it to linearized MC-LR. The linearized MC-LR along with some undegraded cyclic ones were then filtered through composite hydrophobic and highly negative membranes made of 95% polysulfone with 5% sulfonated PEEK. During a dead-end filtration test, we found that a SPEEK membrane could reject or adsorb the vast majority of cyclic MC-LR and virtually all linearized MC-LR. The partial success of modified membranes and reactive processes suggests that a physical barrier membrane with additional functionality (e.g., charge, reactivity) may result in enhanced MC-LR remediation. The PSf/SPEEK membrane was effective at rejecting or adsorbing 97.4% cyclic MC-LR and virtually all linear MC-LR. MC-LR was found to reversibly adsorb to the PSf/SPEEK membranes, with desorption of MC-LR occurring when the membranes were soaked in a methanol/water solution. This is highly advantageous because it provides a method of removing MC-LR from feed waters via reversible adsorption to membranes that can then be cleaned and reused. Algal blooms are becoming more prevalent in the state of Arkansas, specifically Fayetteville. The results are steps toward water treatment in the region and nationally.

Acknowledgements

This material is based upon work supported by the United States Geological Survey under grant agreement No. G16AP00040 and administered by the Arkansas Water Resources Center. The views and conclusions contained in this document are those of the authors and should not be interpreted as representing the opinions or policies of the U.S. Geological Survey.

References

Altaner, S., et al., Adsorption of Ten Microcystin Congeners to Common Laboratory-Ware Is Solvent and Surface Dependent. Toxins, 2017. 9.

Bourne, D.G., et al., Enzymatic pathway for the bacterial degradation of the cyanobacterial cyclic peptide toxin microcystin LR. Applied and Environmental Microbiology, 1996. 62(11): p. 4086-4094.

Dong, X., et al., Polymers and Solvents Used in Membrane Fabrication: A Review Focusing on Sustainable Membrane Development. Membranes, 2021. 11(5): p. 309.

Dziga, D., et al., Heterologous expression and characterisation of microcystinase. Toxicon, 2012. 59(5): p. 578-586.

Dziga, D., et al., The Effect of a Combined Hydrogen Peroxide-MlrA Treatment on the Phytoplankton Community and Microcystin Concentrations in a Mesocosm Experiment in Lake Ludoš. Toxins, 2019. 11(12): p. 725.

Eke, J., K. Elder, and I. Escobar, Self-Cleaning Nanocomposite Membranes with Phosphorene-Based Pore Fillers for Water Treatment. Membranes, 2018. 8(3): p. 79.

Jung, J.T., et al., Understanding the non-solvent induced phase separation (NIPS) effect during the fabrication of microporous PVDF membranes via thermally induced phase separation (TIPS). Journal of Membrane Science, 2016. 514: p. 250-263.

Wu, X., et al., Effect of the immobilized microcystin-LR-degrading enzyme MlrA on nodularin degradation and its immunotoxicity study. Environmental Pollution, 2020. 258: p. 113653.

Image caption: Alyssa Ferri collecting water samples at Lake Fayetteville. Photo courtesy of Brad Austin.

Understanding Microcystin Occurrence and Predictors at Lake Fayetteville

Erin Grantz[1], Brian Haggard[2], Alyssa Ferri[3], Brad Austin[4], and Lillie Haddock[5]

[1]Program Manager, Arkansas Water Resources Center, University of Arkansas, Fayetteville, Arkansas, 73703; [2]Director, Arkansas Water Resources Center, University of Arkansas, Fayetteville, Arkansas, 72703; [3]Former Graduate Student, Crop, Soil, and Environmental Sciences Department, University of Arkansas, Fayetteville, Arkansas, 72701; [4]Research Scientist, Arkansas Water Resources Center, University of Arkansas, Fayetteville, Arkansas, 72703; [5]Program Specialist, Arkansas Water Resources Center, University of Arkansas, Fayetteville Arkansas, 72703
*Corresponding author, haggard@uark.edu

Abstract: Harmful algal blooms (HABs) are widespread and can produce toxins. We wanted to understand if and why algae produce toxins at Lake Fayetteville, a highly productive recreational reservoir in Northwest Arkansas. We collected water samples weekly to monthly from March 2019–December 2021. We measured microcystin (MC), one of the most common algal toxins, and a range of physical, chemical, and biological water quality characteristics. Water quality follows seasonal patterns at Lake Fayetteville that affect MC production. Microcystin levels were sometimes potentially unsafe for human contact (i.e. >8 µg/L). Unsafe conditions were most likely in summer, but also possible in spring and fall. Thresholds in the data can predict when MC is likely to be higher or lower. We analyzed these thresholds across years and for each year individually. We also explored potential secondary thresholds in water quality characteristics after grouping data based on a primary threshold. The top recurring MC predictors were indicators of algal biomass, bioavailable supply nitrogen, and water temperature. Microcystin was greatest at greater algal biomass, especially greater cyanobacterial numbers. We found more MC when supply nitrogen was limited. Microcystin largely occurs when surface water temperature is ≥27°C. Water temperature is a master variable because it strongly affects both algal biomass and nitrogen availability. These themes are a starting point for solving the HABs puzzle at Lake Fayetteville. The observed MC predictors differed between years, however, presenting a challenge for HABs management. We must continue monitoring to understand this interannual variability and recognize patterns across years.

Key Points:

- Many water quality and environmental factors predicted microcystin production by harmful algal blooms at Lake Fayetteville.
- Physical, chemical, and biological characteristics of water quality vary seasonally, and these seasonal differences affect microcystin production.
- The magnitude and timing of microcystin production differed between years (2019 – 2021).
- The predictors for greater microcystin production also differed between years.
- We must continue monitoring to understand this interannual variability in microcystin controls.

Introduction

An algal bloom is considered harmful (HAB) when it produces toxins or other negative effects for human health and ecosystem function. These blooms are frequent and widespread in inland freshwaters and estuaries (Brooks et al., 2016). Their formation is associated with nutrient enrichment in a waterbody and its watershed (Anderson et al., 2002; Paerl et al., 2016; Wurtsbaugh et al., 2019).

Microcystin (MC) is one of the most common toxins and is produced by many types of cyanobacteria, the type of algae that often dominate HABs (Paerl et al., 2001). When MC is found in lakes and reservoirs, other toxins are also often present (Graham et al., 2010). The Environmental Protection Agency (EPA, 2019) has released guidance for states and tribes on what levels of cyanobacterial toxins pose a human health risk. The target for MC is 8 μg L^{-1}.

It is not well understood what causes HABs to produce toxins (Graham et al., 2004). Factors linked to MC production can differ depending on the scale of analysis, global location, and system-specific characteristics. Globally, total nitrogen (TN) is a predictor of MC, while total phosphorus (TP) is not (Buley et al., 2021). But, TP availability affects relative abundance of cyanobacterial biomass (Shan et al., 2020). In general, greater algal biomass coincides with greater MC in lakes (Yuan et al., 2014; Buley et al., 2021; Chaffin et al., 2021). The ratio, or relative availability, of N and P is also a predictor for MC globally (Harris et al., 2014), but may be secondary to large TN concentrations (Scott et al., 2013).

Lake Fayetteville, a recreational lake in Northwest Arkansas, has significant, recurrent algal blooms each year that are dominated by cyanobacteria (Meyer, 1971). We wanted to know if these blooms produce toxins and what the predictors are for toxin production. Our study objectives were: 1) collect a detailed long-term database of MC concentrations and water quality characteristics, and 2) explore relationships between MC and water quality characteristics to discover which factors or combinations of factors are most common when MC occurs at greater or lesser concentrations.

Methods

Study Site and Field Methods

Lake Fayetteville is a small (surface area <1 km^2), shallow (mean depth = 3 m, maximum depth = 10 m), and hypereutrophic reservoir located in Northwest Arkansas (Figure 1). Lake Fayetteville impounds 24 km^2 of the Clear Creek watershed (Hydrologic Unit Code 12 = 111101030201). The reservoir was constructed in 1948 for drinking water supply, but the lake and adjacent public lands now serve as a recre-

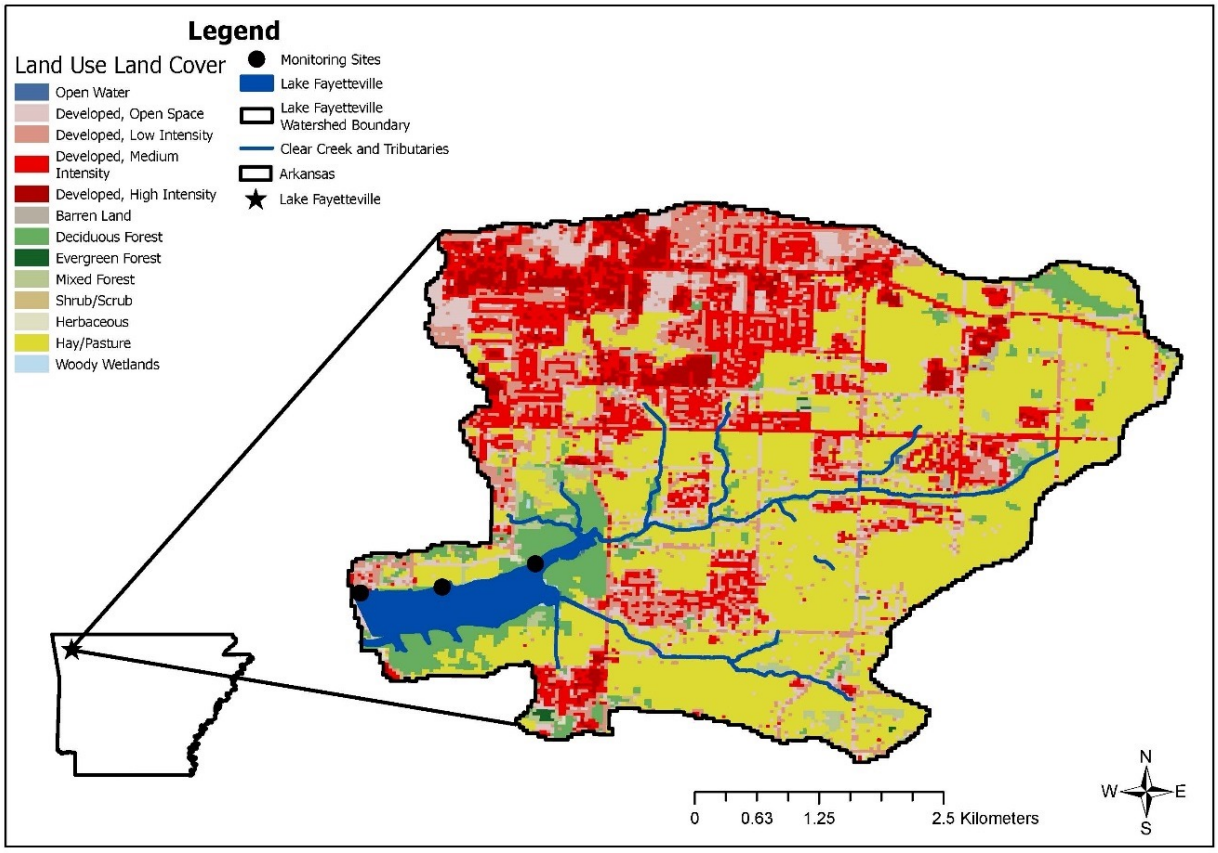

Figure 1: Sampling sites for routine lake monitoring at Lake Fayetteville, Arkansas (March 2019 – December 2021). Watershed land use was estimated using the 2019 National Land Cover Database in Model My Watershed (https://modelmywatershed.org/).

ational area. Primary contact recreation is not permitted, but fishing and boating are common.

We collected water samples weekly to monthly from March 2019 to December 2021 at three public- access sites along the windward side of the reservoir (Figure 1). Samples were collected from just below the water surface (~ 0.15 m) in acid-washed bottles after triple rinsing in the field. Sampling occurred consistently during late morning to afternoon (~11 am – 2 pm). Water temperature, dissolved oxygen, pH, and conductivity were measured on site.

Laboratory Analysis

At the Arkansas Water Resources Center Water Quality Lab (WQL), sample aliquots were processed and stored according to standard methods. All WQL chemical analyses use approved EPA methods, when available (https://awrc.uada.edu/water-quality-lab/). Total N and P were analyzed by colorimetry following pH adjustment (pH < 2) with sulfuric acid (H_2SO_4) and digestion in persulfate. Nitrate+nitrite-nitrogen (NO_x-N), soluble reactive phosphorus (SRP), and ammonium-nitrogen (NH_4-N) were analyzed by colorimetry following filtration through a 0.45 µm membrane and pH adjustment (pH < 2) with H_2SO_4.

Algal biomass was collected on a Whatman GF-F 0.7 µm glass fiber filter and extracted in the freezer in 90% acetone for at least 24 hours. The concentration of the pigment chlorophyll-a (CHL-a) and its degradate pheophytin (PHEO) were then measured by fluorometry. Beginning June 25, 2019, the raw fluorescence units (RFU) of chlorophyll (CHL) and phycocyanin (PC), a pigment in cyanobacteria, was also measured after subtracting the background RFU of filtered (0.45 µm) lake water.

Total microcystin (MC) concentration in raw lake water was measured using enzyme-linked immunosorbent assays after three freeze-thaw cycles to lyse cells and release intracellular microcystin. Before June 2020, we processed 2 mL for MC analysis, but we used 20 mL afterward to reduce method sensitivity to sub-sampling variability (Austin and Haggard, 2022).

Statistical analysis

We calculated several additional variables for statistical analysis. Particulate nitrogen (PN) and phosphorus (PP) fractions are the total fractions of N and P less dissolved "supply" forms (i.e., NO_x-N + NH_4-N and SRP). Molar N:P ratios were calculated for the total, particulate, and supply fractions by dividing the atomic mass of N by P. The PC:CHL ratio equals PC RFU divided by CHL RFU.

Mean MC and predictor variable values were calculated across the three sites on each date as inputs for the statistical analysis. Each date was assigned to a meteorological season (Spring = March 1 – May 31, Summer = June 1 – August 31, Fall = September 1 – November 30, and Winter = December 1 – February 28), as well as to growing season (April 1 – October 31) or off season (November 1 – March 31). We calculated antecedent precipitation (24-hr, 72-hr, and 1-wk) for each date using daily precipitation data from the U.S. Geological Survey gage 071948095 (https://waterdata.usgs.gov/nwis).

We used nonparametric change point analysis (nCPA) to identify differences in mean MC response ($p < 0.05$) at threshold values of nutrients, algal community metrics, physicochemical variables, and antecedent precipitation (King and Richardson, 2003; Qian et al., 2003). We used classification and regression tree (CART) analysis to look for secondary thresholds for MC response (De'Ath and Fabricius, 2000). Months, seasons, and years were included as potential predictors in CART analysis, which is compatible with categorical variables. We pruned our models by requiring a split in the data to increase model complexity by at least 0.05 (out of 1.0) to reduce overfitting.

The nCPA and CART analyses were carried out using all project data across years and separately on data from each calendar year. A minimum of 7 datapoints were required on each side of all thresholds in both nCPA and CART. We used RStudio Desktop (version 2021.09.2+382, RStudio Team, 2021) with the library rpart (Therneau and Atkinson, 2019) for CART analysis.

Results and Discussion

Temporal patterns

Physical, chemical, and biological water quality characteristics followed predictable seasonal patterns at Lake Fayetteville each year (Figure 2). The seasonal cycle of water temperatures shapes the timing of blooms, with the greatest algal biomass, as CHL-a (Kasprzak et al, 2008), in the late spring to early summer. During these blooms, PC:CHL was usually >1, suggesting cyanobacteria dominance (Thomson-Laing et al., 2020). Smaller blooms in the off season tended to have lower PC:CHL.

Water temperature and algal biomass, in turn, shape a seasonal nutrient cycle at Lake Fayetteville (Grantz et al. 2014). Each year, NH_4-N and SRP were consistently near or below reporting limits in surface waters, except immediately after lake mixing in the fall. These compounds accumulate all summer in lower lake layers, then mix with the surface layer in the fall. While also mostly absent during the growing season, NO_x-N concentrations were substantial during the off season each year. Less algal growth allows NO_x-N to build up from NH_4-N transformation and inflows from Clear Creek. Total nutrients also showed weak seasonal cycles. Seasonality in TN was greater than for TP and is driven by NO_x-N.

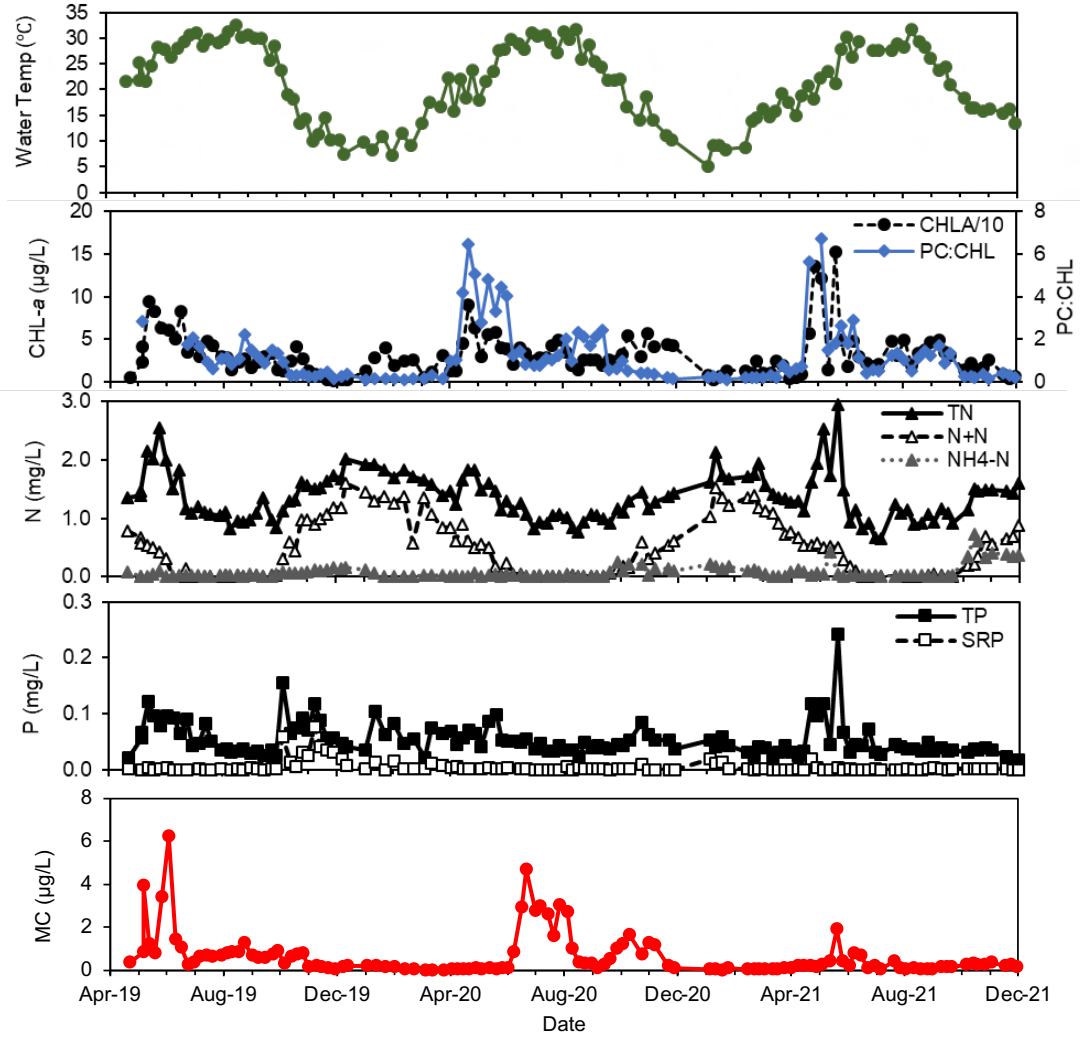

Figure 2: The mean of select physical, chemical, and biological water quality characteristics at Lake Fayetteville shown through time (April 2019 to December 2021).

We can see connections between the timing and magnitude of MC production and water temperature, algal metrics, and nutrients in the timeseries in Figure 2. Peaks in MC occurred throughout the growing season, when water temperatures and algal biomass are greatest and supply nutrients were least. Concentrations in individual samples sometimes exceeded the recreational guideline of 8 µg/L, suggesting water was potentially unsafe for human contact at those sites (data not shown). Maximum MC concentrations occurred earlier in spring in 2019, while 2020 had a more significant fall peak. We observed an interplay between PC:CHL and MC, with peak MC concentrations following peak PC:CHL by approximately a month.

Thresholds in microcystin predictors

We observed MC response thresholds to multiple physical, chemical, and biological water quality characteristics both across and within years at Lake Fayetteville (Table 1). The water quality characteristics with the strongest nCPA thresholds differed between the temporal data groupings, however. The thresholds in Table 1 are ranked from high to low based on R^2, which approximately shows the amount of variability in MC explained by the threshold from 0 – 1.00 (i.e. 0 – 100%).

But, water quality characteristics also recurred as predictors for MC. Water temperature is a master variable that affects cyanobacterial growth (Yang et al., 2020) and nutrient dynamics (Grantz et al., 2014). In 2020 and across years, MC was greater when water temperature was ≥ 27°C. Others have shown increasing MC with increasing water temperature (Brutemark et al., 2015). It is unclear if the relationship is based on greater MC production, or simply greater cyanobacterial biomass (Peng et al., 2018).

Cyanobacterial biomass, as PC RFU, was a top predictor for MC in all years and across years. Thresholds ranged from 1989 – 6909 RFU, showing that more cyanobacteria mean more MC. The ratio of PC to CHL was also a top predictor across years and in 2019 and 2021, though not in 2020.

Table 1: The top five thresholds for MC response to physical, chemical, and biological characteristics of water quality at Lake Fayetteville based on nonparametric change point analysis both across and within years. Thresholds are ranked from high to low based on the R^2, which approximately shows the amount of variability explained by the threshold on a scale of 0 – 1.00. Both DIN and NO_x-N were analyzed as potential MC predictors, but only the threshold with the highest R^2 is shown for each timeframe. Results for these two variables were nearly identical, reflecting that NO_x-N is almost always the dominant component of DIN.

Year	Variable	Units	Threshold	Median	p	R^2	Mean MC < Threshold (µg/L)	Mean MC ≥ Threshold (µg/L)
All Years	PC*	RFU	4530	4530	0.001	0.177	0.234	0.916
	Temp	°C	27.0	27.0	0.001	0.172	0.315	1.062
	NO_3-N	mg/L	0.50	0.50	0.001	0.157	0.844	0.162
	CHL-a	µg/L	23.4	23.4	0.001	0.112	0.252	0.821
	PC:CHL*		0.37	0.37	0.002	0.106	0.154	0.704
2019	PC*	RFU	1989	2348	0.001	0.413	0.176	0.684
	CHL*	RFU	2272	2278	0.001	0.337	0.155	0.649
	PC:CHL*		0.39	0.39	0.001	0.235	0.264	0.647
	PHEO	µg/L	5.18	5.18	0.001	0.208	0.559	1.425
	NO_3-N	mg/L	0.69	0.69	0.004	0.191	0.892	0.187
2020	Temp	°C	27.0	27.0	0.001	0.395	0.354	1.930
	NO_3-N	mg/L	0.32	0.27	0.001	0.287	1.415	0.179
	TN	mg/L	1.37	1.31	0.001	0.259	1.312	0.118
	Supply N:P		84.1	84.1	0.001	0.213	1.406	0.229
	PC	RFU	4524	4524	0.001	0.179	0.265	1.251
2021	72-hr Precip	cm	1.91	1.91	0.001	0.271	0.140	0.452
	PC:CHL		2.39	2.15	0.001	0.237	0.155	0.533
	CHL-a	µg/L	59.1	59.1	0.002	0.214	0.155	0.498
	NO_3-N	mg/L	0.71	0.71	0.003	0.173	0.242	0.056
	PC	RFU	6909	6719	0.003	0.169	0.161	0.496

*Raw fluorescence was added in June 25, 2019, so 2019 and all years had fewer observations for these variables compared to others.

In 2019 and across years, MC was greater on average above PC:CHL ~0.40. This ratio is <1, suggesting even minor cyanobacterial presence may be enough for MC to reach detectable levels. In contrast, the 2021 threshold in PC:CHL >2 associates greater MC with cyanobacterial dominance.

Algal biomass, as CHL-a, was a top threshold across years and in 2021. The threshold across years (CHL-a = 23.4 µg/L) is in range with the transition from productive to highly productive systems (Nuremberg et al., 1996), while the 2021 threshold (CHL-a = 59.1 ug/L) is well over limits suggesting high productivity. Other studies have shown that the probability of exceeding 1 µg L^{-1} MC increases with increasing nutrients and CHL-a (Yuan et al., 2014).

Finally, bioavailable supply nitrogen, as NO_x-N, appeared in the top thresholds across years and in all years. Below thresholds ranging from 0.32 – 0.71 mg/L, MC was greater in all analyses. Prior lab experiments with Lake Fayetteville waters also showed that the magnitude of the supply N affects toxin production (Wagner et al., 2021).

The CART analyses identified secondary thresholds in water quality characteristics. Here, we focus on the most data-rich all-years model. Individual year models are available in Ferri, 2021. The primary threshold in the all-years model was in water temperature, mirroring the nCPA threshold (Figure 3). The greatest MC tended to occur at ≥ 27°C. Samples collected at ≥ 27°C then split by year, where MC in 2020 was greater on average than in 2019 and 2021. For the 2019 and 2021 data, TN was a tertiary predictor, with greater MC when TN ≥ 1.7 mg/L (MC = 2.22 vs. 0.50 µg/L). For 2020, CHL RFU was the tertiary predictor, with greater MC above a threshold of 3570 RFU. Samples with ≥ 3570 RFU further split by TN:TP, where a ratio <59 was associated with in the greater MC (MC = 3.48 vs. 1.9 µg/L).

Conclusions

The driving factors behind HABs formation and toxin production are well known to be highly complex (Graham et al., 2004). No one environmental or water quality factor explained when and why algal blooms produced MC at Lake Fayetteville. Threshold-type analyses identified many physical, chemical, and biological characteristics of water

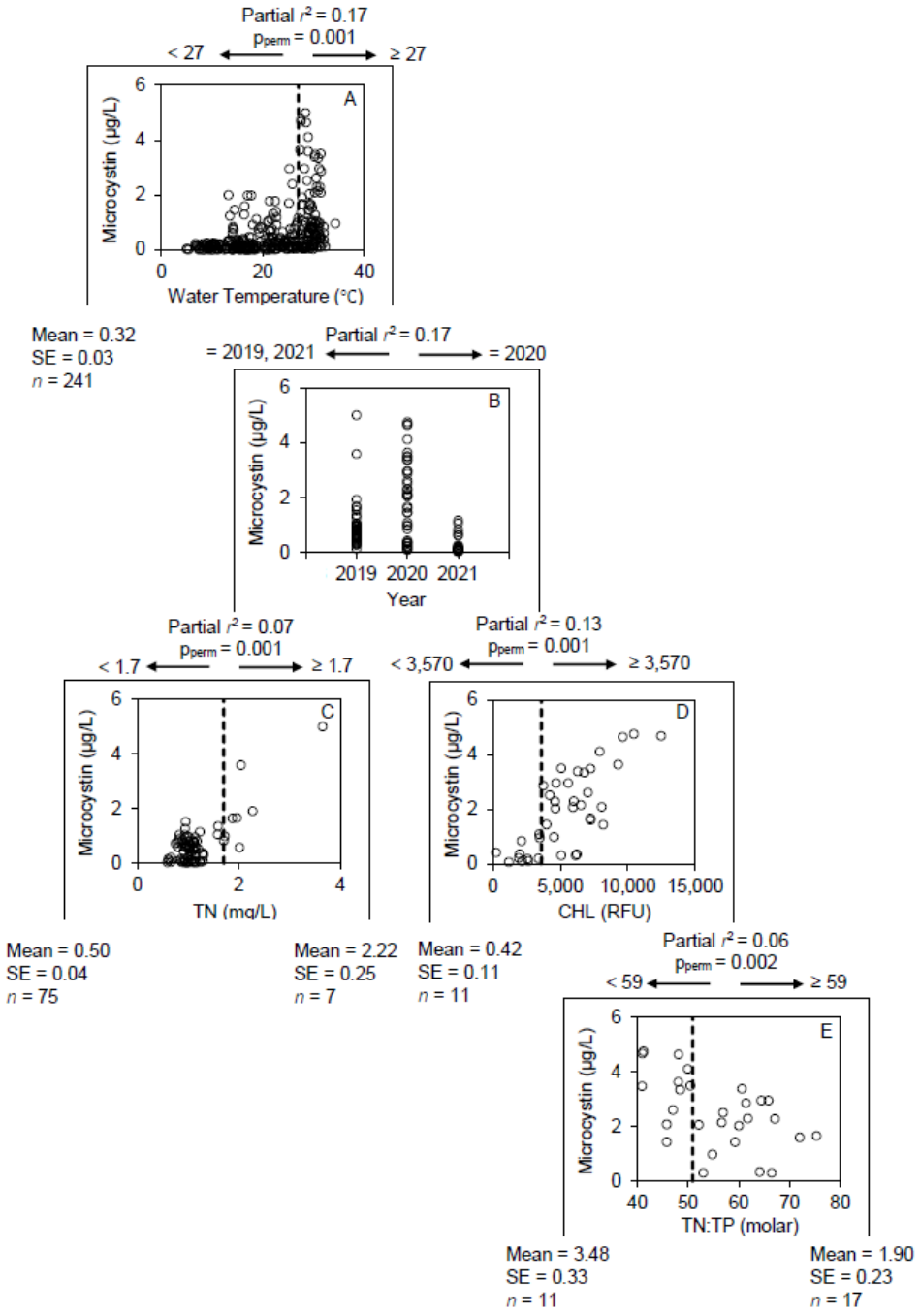

Figure 3: Classification and regression tree model for all years at Lake Fayetteville showing change points (dashed vertical lines) for microcystin response.

quality that predicted greater or less MC. The magnitude and timing of MC production and primary MC predictors differed between years 2019 – 2021. Nevertheless, a suite of interrelated factors is emerging from the multiple timescales of analysis, namely water temperature, algal/cyanobacterial biomass and relative abundance, and supply N availability. These water quality characteristics influence each other over seasonal cycles and appear to influence MC. Continued monitoring is needed to understand this interannual variability in MC levels and predictors in order to solve the HABs puzzle at Lake Fayetteville.

Acknowledgements

This material is based upon work supported by the United States Geological Survey under grant agreement No. G16AP00040 and No. G21AP10581-01, and administered by the Arkansas Water Resources Center. The views and conclusions contained in this document are those of the authors and should not be interpreted as representing the opinions or policies of the U.S. Geological Survey.

References

Anderson, D.M., Glibert, P.M., and Burkholder, J.M. 2002. Harmful algal blooms and eutrophication: nutrient sources, composition, and consequences. Estuaries 25:704–726.

Austin, B.J., Eagle, V., Evans-White, M.A., Scott, J.T., and Haggard, B.E. 2020. Sediment phosphorus release sustains nuisance periphyton growth when nitrogen is not limiting. J. Limnology 79:210–220.

Brooks, B.W., Lazorchak, J.M., Howard, M.D.A., Johnson, M.V., Morton, S.L., Perkins, D.A.K., Reavie, E.D., Scott, G.I., Smith, S.A., and Steevens, J.A. 2015. Are harmful algal blooms becoming the greatest inland water quality threat to public health and aquatic ecosystems? Environ. Toxicology Chem. 35:6–13.

Brutemark, A., Engström-Öst, J., Vehmaa, A., and Gorokhova, E. 2015. Growth, toxicity and oxidative stress of a cultured cyanobacterium (Dolichospermum sp.) under different CO2/pH and temperature conditions. Phycological Research 63:56-63, doi: 10.1111/pre.12075

Buley, R.P., Correia, H.E., Abebe, A., Issa, T.B., and Wilson, A.E. 2021. Predicting microcystin occurrence in freshwater lakes and reservoirs: assessing environmental variables. Inland Waters 11:430-444, doi: 10.1080/20442041.2021.1938491

Chaffin, J.D., Davis, T.W., Smith, D.J., Baer, M.M., and Dick, G.J. 2018. Interactions between nitrogen form, loading rate, and light intensity on Microcystis and Planktothrix growth and microcystin production. Harmful Algae 73:84-97.

De'Ath, G., and Fabricius, K.E. 2000. Classification and regression trees: a powerful yet simple technique for ecological data analysis. Ecology 81:3178–3192.

Environmental Protection Agency (EPA), 2019. Recommended human health recreational ambient water quality criteria or swimming advisories for microcystins and cylindrospermopsin. EPA8222-F-19-001.

Ferri, A. 2022. Cyanobacterial Harmful Algal Blooms Vary Within and Across Years at Lake Fayetteville, Arkansas. Graduate Theses and Dissertations Retrieved from https://scholarworks.uark.edu/etd/4512

Graham, J.L., Jones, J.R., Jones, S.B., Downing, J.A., and Clevenger, T.E. 2004. Environmental factors influencing microcystin distribution and concentration in the Midwestern United States. Water Research 38:4395-4404.

Graham, J.L., Loftin, K.A., Meyer, M.T., and Ziegler, A.C. 2010. Cyanotoxin mixtures and taste-and-odor compounds in cyanobacterial blooms from the Midwestern United States. 44:7361-7368, doi: 10.1021/es1008938

Grantz, E.M., Haggard, B.E., and Scott, T.J. (2014). Stoichiometric imbalance in rates of nitrogen and phosphorus retention, storage, and recycling can perpetuate nitrogen deficiency in highly-productive reservoirs. Limnology and Oceanography, 59(6): 2203-2216.

Harris, T.D., Wilhelm, F.M., Graham, J.L., and Loftin, K.A. 2014. Experimental manipulation of TN:TP ratios suppress cyanobacterial biovolume and microcystin concentration in large scale in situ mesocosms. Lake and Reservoir Management 30:72-83.

Kasprzak, P., Padisák, J., Koshel, R., Krienitz, L, and Gervais, F. 2008. Chlorophyll a concentrations across a trophic gradient of lakes: An estimator of phytoplankton biomass? Limnologica 38:327-338, doi: 10.1016/j.limno.2008.07.002

King, R.S., and Richardson, C.J. 2003. Integrating bioassessment and ecological risk assessment: An approach to developing numerical water-quality criteria. Environ. Manag. 31:795–809

Meyer, R.L. 1971. A study of phytoplankton dynamics in Lake Fayetteville as a means of assessing water quality. Arkansas Water Resources Center Publication Number PUB010A, 69 pp.

Nurmberg, G.K. 1996. Trophic state of clear and colored, soft- and hardwater lakes with special consideration of nutrients, anoxia, phytoplankton and fish. Lake Reservoir and Management 12:432-447.

Paerl, H.W., Fulton, R.S., Moisander, P.H. and Dyble, J. 2001. Harmful freshwater algal blooms, with an emphasis on cyanobacteria. Scientific World 1:76-113.

Paerl, H.W., Gardner, W.S., Havens, K.E., Joyner, A.R., McCarthy, M.J., Newell, S.E., Qin, B. and Scott, J.T. 2016A. Mitigating cyanobacterial harmful algal blooms in aquatic ecosystems impacted by climate change and anthropogenic nutrients. Harmful Algae 54: 213–222.

Peng, G., Martin, R.M., Dearth, S.P., Sun, X., Boyer, G.L., Campagna, S.R., Lin, S. and Wilhelm, S.W. Seasonally relevant cool temperatures interact with N chemistry to increase microcystins produced in lab cultures of Microcystis aeruginosa NIES-843. Environmental Science and Technology 52:4127-4136, doi: 10.1021/acs.est.7b06532

Qian, S.S., King, R.S., and Richardson, C.J. 2003. Two methods for the detection of environmental thresholds. Ecological Model 166:87–97.

RStudio Team. 2021. Rstudio: Integrated development for R. RStudio, PBC, Boston, MA, hhttp://www.rstudio.com

Scott, J.T., McCarthy, M.J., Otten, T.G., Steffen, M.M., Baker, B.C., Grantz, E.M., Wilhelm, S.W., and Paerl, H.W. 2013. Comment: An alternative interpretation of the relationship between TN:TP and microcystins in Canadian lakes. Canadian Journal of Fisheries and Aquatic Sciences 70:1265-1268.

Shan, K., Wang, X., Yang, H., Zhou, B., Song, L., and Shang, M. (2020). Use statistical machine learning to detect nutrient thresholds in Microcystis blooms and microcystin management. Harmful algae 94:101807.

Therneau, T. and Atkinson, B. 2019. rpart: Recursive Partitioning and Regression Trees. R Package version 4.1-15. https://CRAN.R-project.org/package=rpart

Thomson-Laing, G., Puddick, J., and Wood, S.A. 2020. Predicting cyanobacterial biovolumes from phycocyanin fluorescence using a handheld fluorometer in the field. Harmful Algae 97:101869.

Wagner, N.D., Quach, E., Buscho, S., Ricciardelli, A., Kannan, A., Naung, S.W., Phillip, G., Sheppard, B., Ferguson, L., Allen, A., Sharon, C., Duke, J.R., Taylor, R.B., Austin, B.J., Stovall, J.K., Haggard, B.E., Chambliss, C.K., Brooks, B.W., and Scott, J.T. 2021. Nitrogen form, concentration, and micronutrient availability affect microcystin production in cyanobacterial blooms. Harmful Algae 103:102002

Wurtsbaugh, W.A., Paerl, H.W., and Dodds, W.K. 2019. Nutrients, eutrophication and harmful algal blooms along the freshwater to marine continuum. WIREs Water 6:e1373.

Yang, Z., Zhang, M., Yang, Y., and Shi, X. 2020. Temperature triggers the annual cycle of Microcystis, comparable results from the laboratory and a large shallow lake. Chemosphere 260:12753

Yuan, L.L., Pollard, A.I., Pather, S., Oliver, J.L., and D'Anglada, L. (2014). Managing microcystin: identifying national-scale thresholds for total nitrogen and chlorophyll a. Freshwater Biology 59:1970–1981. https://doi.org/10.1111/fwb.12400.

Arkansas Bulletin of Water Research

A publication of the Arkansas Water Resources Center

Brian E. Haggard
Director

Erin Grantz
Program Manager

Lillie Haddock
Program Specialist

University of Arkansas
Don Tyson Center for Agricultural Sciences
1371 W. Altheimer Drive
Room 106
Fayetteville, AR 72704

phone: 479-502-9854
email: egrantz@uark.edu

Visit our website: awrc.uada.edu

Call for Papers

Share your research results in a citable publication

To submit, go to awrc.uada.edu to view author instructions.

Partners

DIVISION OF AGRICULTURE
RESEARCH & EXTENSION
University of Arkansas System

The National Institutes for Water Resources

USGS
science for a changing world